NTNU

Norwegian University of
Science and Technology

Submerged Towing and Upending of TLP Thethers

Numerical Simulations and Assessment of
Operational Limits

Petter Andre Tvedt

Marine Technology (2-year)
Submission date: June 2016
Supervisor: Kjell Larsen, IMT

Norwegian University of Science and Technology
Department of Marine Technology

NTNU Trondheim
Norges teknisk-naturvitenskapelige universitet
Institutt for marin teknikk

MASTER THESIS SPRING 2016
for

Stud. tech. Petter Andre Tvedt

Submerged Towing and Upending of TLP Tethers- Numerical Simulations and Assessment of Operational Limits

Installasjon av strekkstag – numeriske simuleringer og kartlegging av operasjonsgrenser

Background

In order to be able to design, install and operate a subsea oil and gas factory, a cost-effective installation method is crucial. Present capital expenditure of the marine operations for a subsea production system in 300-500m water depth is for some cases in the range 15-30% of the total capital invested.

Installation of long slender elements such as TLP tethers and risers bundles are often performed by submerged or surface towing to site followed by upending.

Important parts of the risk understanding of such operations are the global behavior of the tow (tugs and towed structure) and the local load effects in the slender structure. In many cases, the ultimate load effects and a large part of the fatigue damage are experienced during the tow-out and upending operation due to the direct wave loads and imposed dynamic loads by the vessels involved. This is particularly the case for TLP tethers where the tether is welded onshore and then towed to site in one long piece; usually by a near-surface towing method. The concept considered in this thesis shall be the tethers of the Heidrun TLP.

Scope of Work

1) Describe the theory involved in numerical simulation of the load effect in TLP tethers during near surface towing and upending. The description shall be limited to the wave-frequency (WF) response and the load effects due to ocean current. The theory of RIFLEX shall be briefly described.

2) Further develop and describe the numerical simulation model established during the project work (autumn 2015). Perform a parameter study in order to increase the understanding of the response of the tether during the near surface towing operation. The location of the most loaded locations and hot-spots along the tether shall be determined.

3) Establish operational limits in terms of significant waveheight (Hs) and peak period (Tp) based on time domain simulations of ultimate loads. The variability of extreme load effects during towing in different realizations of the seastates shall be assessed. Parameters selected shall be agreed with the supervisor.

4) Propose an efficient way of upending the tether at site. The proposal shall be based on assessment and numerical simulations of the tether behavior during the upending operation. Assess and conclude on the importance of load effects due to ocean current vs wave loads.

5) Conclusions and recommendations for further work.

General information

This thesis shall build on the project work reported in "Assessment of methods for marine installation of slender structures by towing and upending".

The work scope may change or prove to be larger than initially anticipated. Subject to approval from the supervisor, topics may be changed or reduced in extent.

In the project the candidate shall present her's/his personal contribution to the resolution of problems within the scope of work.

Theories and conclusions should be based on mathematical derivations and/or logic reasoning identifying the various steps in the deduction.

The candidates should utilise the existing possibilities for obtaining relevant literature.

Thesis format

The thesis report shall be organised in a rational manner to give a clear exposition of results, assessments, and conclusions. The text should be brief and to the point, with a clear language. Telegraphic language should be avoided.

The report shall be written in English and edited as a research report including literature survey, description of relevant mathematical models together with numerical simulation results, discussion, conclusions and proposal for further work. List of symbols and acronyms, references and (optional) appendices shall also be included. All figures, tables and equations shall be numerated.

The original contribution of the candidate and material taken from other sources shall be clearly defined. Work from other sources shall be properly referenced using an acknowledged referencing system.

The report shall be submitted in two copies:

- Signed by the candidate
- The text defining the scope included
- In bound volume(s)
- Drawings and/or computer prints which cannot be bound should be organised in a separate folder.

Ownership
NTNU has according to the present rules the ownership of the project results. Any use of the project results has to be approved by NTNU (or external partner when this applies). The department has the right to use the results as if the work was carried out by a NTNU employee, if nothing else has been agreed in advance.

Thesis supervisor**:**
Prof. II Kjell Larsen, NTNU/Statoil

Deadline: June 10th, 2016

Trondheim, June 6th, 2016

Kjell Larsen (signature):

Petter Andre Tvedt (signature):

Preface

This master's thesis is written by Stud. tech. Petter Andre Tvedt spring of 2016, for the Norwegian University of Science and Technology (NTNU) - department of marine technology. The thesis work is conducted in cooperation with supervisor Prof. II Kjell Larsen and Statoil. The topic and title of this thesis is "Submerged Towing and Upending of TLP Tethers - Numerical Simulations and Assessment of Operational Limits". The thesis work build on the project work done by the student in a pre-project of autumn 2015. The thesis itself is independent of the pre-project report.

The thesis includes a case study for the transportation and installation of 16 replacement steel tethers for the Heidrun tension-leg platform. The platform was the first ever concrete TLP, installed in 1995 and run by Statoil. Much of the case relevant data and recommendations are given by thesis supervisor Prof. II Kjell Larsen (Statiol/NTNU).

Credit is due to thesis supervisor Prof. II Kjell Larsen for helping me throughout the work of this thesis and the preliminary specialization project of autumn 2015.

Summary

In the event of transport, installation and operation of subsea oil and gas factories, marine operations are often a huge part of the total capital expenditure. As a result of this, oil and gas companies are looking for new or improved methods for transport and installation of offshore installations in order to reduce cost and minimize risk. The focus of this thesis is a study of the challenges related to transport and installation of long slender structures such as risers and TLP tethers.

The scope of this thesis is to evaluate a submerged tow operation of replacement tethers for Heidrun TLP and propose an efficient method to conduct the upending at site. The thesis work include a further development of Riflex simulation models for numerical simulations of a tow and upending operation. Time domain model simulations are used to conduct parametric study in order to study the behaviour of the system, evaluate the importance of different load effects, establish operational limitations and compare different solutions for the tow and upending.

The simulation results indicate that the limiting factor for the tow operation will be with respect to fatigue damage in tether welds. With a operational limit of maximum 10% total fatigue utilization, the results indicate that the tow solution is not feasible for any of the simulated conditions. This suggests an operation weather forecast limit of $OP_{wf} = H_S < 1.8$m. The main contribution to both ultimate stress and fatigue damage are identified as bending stress and dynamic loading from the vessel motions. It is recommended that measurements should be taken in order to increase operability.

Based on simulation comparison of four possible upending solutions, the study suggest a free-drop upending method, with clamp-on weights still attached. The solution appeared to be the most efficient of the simulated cases. The tether seemed to behave in a stable manner and with induced stress well within the operational ULS limit for the simulated weather conditions. The results suggests that the effect of currents is negligible compared to the effect of wave and vessel motion induced loads.

Sammendrag

For de totale utgiftene av transport, installasjon og drift av offshore olje og gass anlegg, vil kosnader relater til ulike marine operasjoner ofte utgjøre en betydelig andel. Som et resultat av dette er olje og gass selskaper stadig ute etter ny eller forbedrete metoder for offshore transport og instalasjon, både med tanke på kostader men også sikkerhet. Fokuset for denne masteroppgaven er å studere de ulike utfordringene som er relatert til transport og installasjon av lange slanke konstruksjoner som for eksemple stigerør eller strekkstag til strekkstagplattformer.

Arbeid utført i denne masteroppgaven vil omhandle evaluering av en neddynket taueopperasjon av nye strekkstag til Heidrun plattformen og utarbeiding av et forslag til utføringen av installasjonen. Arbeidet inkluderer videreutvikling av en Riflex simuleringsmodell for numeriske simuleringer av taue- og installasjons opeasjonen. Simuleringer utført i tidsdomene er brukt til å utføre parametriske studier for analysere oppførselen til systemet, effekten av ulike laster, foreslå operasjonsgrenser og for å sammenligne ulike installasjons løsninger.

Simulerings resultatene indikerer at den operasjonelle grensen av taueoperasjonen vil være relatert opp mot utmattingsskader. Med en grense på maksimum 10% utnyttelse av strekkstagets totale utmattingslevetid, indikerer resultatene at operasjonen ikke er gjennomførbar i noen av værkondisjonene som er simulert. Dette tilsier en operasjonsgrense relatert til værmeldinger $OP_{wf} = H_S < 1.8$m. Lastene som bidrar mest til både de største lastene og til utmattingsskade er identifisert til dynamiske momentlaster knyttet opp mot store skipsbevegelser. Det er anbefalt at tiltak må vurderes for å minske utmatingssskadene og øke operabiliteten til operasjonen.

Bassert på sammenligning av fire ulike løsninger for installasjonsoperasjonen er en frislipp vertikaloppretting av strekkstaget, med tillgeggsvekter i endene, anbefalt som en mulig god løsning. Denne løsningen viste seg å være den mest effektive av de simulerte løsningene. Strekkstaget viste til å oppføre seg stabilt under hele operasjonen, hvor de induserte lestene er godt innenfor de tillatte grensene. Analysene indikerte også at effekten av strøm vil være neglisjerbare sammenlignet med effekten av bølger og skipsbevegelser.

Table of Contents

List of Figures

List of Tables

Symbols

α	=	Angle
α	=	Alpha factor
ε	=	Phase shift
λ	=	Wave length
ν	=	Kinematic viscosity
ξ	=	Damping ratio
$\zeta(t)$	=	Wave elevation
ζ_a	=	Wave amplitude
ρ	=	Density (Seawater density if not otherwise specified)
ρ_{SW}	=	Seawater density
ω	=	Wave period (radians)
ω_0	=	Natural period / Undamped eigenfrequency
ω_d	=	Natural period / Damped eigenfrequency
ω_m	=	Natural period / Frequency of maximum responce
ω_n	=	Natural period / Eigenfrequency
ω_s	=	Shedding frequency (Vortex shedding)
γ_m	=	Material factor
γ_f	=	Load factor
γ_g	=	Load factor permanent loads
γ_e	=	Load factor environmental loads
σ	=	Standard deviation
η	=	Deflection distance
$\dot{\eta}$	=	Velocity
$\ddot{\eta}$	=	Acceleration

A	=	Area
C_A	=	Added mass coefficient
C_{crit}	=	Critical damping
C_D	=	Drag coefficient
D	=	Diameter
D_i	=	Inner diameter (Pipe)
D_o	=	Outer diameter (Pipe)
E	=	Elasticity
F_x	=	Force in x-direction
H_H	=	Hydrodynamic transfer function
H_M	=	Mechanical transfer function
H_s	=	Significant wave height

H_x	=	Response transfer function
I	=	Second moment area
KC	=	Keulegan-Carpenter number
M	=	Mass
M	=	Moment
OP_{lim}	=	Operation limitation
OP_{wf}	=	Operational weather forecast limitation
R	=	Center radius
R_d	=	Designed resistance
R_k	=	Characteristic resistance
R_n	=	Reynols number
$S_x(\omega)$	=	Response spectrum
$S_\zeta(\omega)$	=	Wave spectrum
S	=	Stress
S_A	=	Axial stress
S_{as}	=	Resultant axial stress
S_B	=	Bending stress
S_d	=	Design stress
S_e	=	Effective stress
S_H	=	Hoop stress
S_i	=	Internal surface area
S_x	=	Response spectrum
St	=	Strouhal's number
T	=	Period (Wave period)
T_C	=	Contingency period
T_e	=	Effective tension
T_P	=	Peak period
T_{POP}	=	Planed operation period
T_R	=	Reference period
T_{TW}	=	True wall tension
W	=	Weight

f_n	=	Natural frequency / Eigenfrequency
f_v	=	Shedding frequency (Vortex shedding)
k	=	Wave number
l	=	Length
m	=	Mass
nm	=	Nautical miles
p_e	=	External pressure
p_i	=	Inner pressure
r	=	Radius
t	=	Thickness

AHP	=	Active Heave Compensator
CDF	=	Cumulative Distribution Function
CDT	=	Controlled Depth Tow
DLF	=	Dynamic Load Factor
DNV	=	Det Norske Veritas - Norwegian veritas (Clasification company)
DNVGL	=	Same as DNV, new name (GL = Germanischer Lloyd)
DOF/dof	=	Degree of freedom
FE	=	Fininte element
FLS	=	Fatigue Limit State
KTL	=	*Offshore supplier of mooring and towlines*
LRFD	=	Load Resistance Factor Design
MBL	=	Minimum Break Load
MPM	=	Most Probable Maximum
OS	=	Offshore Standard
PDF	=	Probability Distribution Function
PSV	=	Platform Supply Vessel
RP	=	Recommended Practice
TLP	=	Tension-Leg Platform
ULS	=	Ultimate Limit State
VIV	=	Vortex Induced Vibrations

Introduction

In today's oil and gas marked, with a saturated market and highly varying oil prices, the production companies have had and increased focus on reducing cost. One of the greatest capital expenditures for a new oil- or gas project, with a big potential of improvement, are the costs of various marine operations like transport and installation of marine structures. For some case of a subsea production system at 300-500 meter water depth the total cost of the marine operations may be as high 15 - 30% of the total capital investment.

This thesis will focus on the challenges related to the transportation and installation of long slender structures such as riser bundles and TLP tethers. The preferred installation method of these structures is often a surface- or submerged tow to installation site followed by an upending.

During phases of the transportation and installation of long slender structures the equipment and the structure itself will be subjected to harsh environmental loads. The structure will in many cases experience it's ultimate load effect and also a significant fatigue damage during these two phases. In order to asses the risk of a tow operation and minimize the damage, it is important to map the global behaviour of the system and the effect of local loads.

The scope of this thesis is to evaluate a submerged tow operation of the tethers of the Heidrun TLP and propose an efficient way to conduct the upending at site. Numerical simulations are carried out using SIMA/Riflex, a simulation and analysis software tool for marine operations and floating systems, in order to investigate the effect of different load effects. Parametric studies are preformed in order to improve the tow- and upending solution, and also establish operational limitations in terms of significant wave height and peak period.

Chapter 1

Theory

The scope of this thesis is to analyse a submerged tow and upending operation of a TLP tether in order to better understand the risks involved in these operations. In order to do so, numerical simulations of a predetermined case are conducted in order to study the global behaviour of the coupled system and the local load effect in the slender structure. During this first chapter, an introduction to the theory regarding planing of marine tow operations and numerical simulation will be presented. The introduction will include following topics:

- Submerged towing operations, in particular near surface/control depth tow
- Submerged upending operations
- Planning of marine operations
- Dynamic properties for a floating coupled system
- Important load factors related to both the tow and upending operation
- Calculation of stress
- Load and response statistics
- Numerical simulations

1.1 Submerged towing

Parts of this section are taken from pre-project report

Towing is one of the most common marine operations, as most offshore projects involve one or several towing operations. Towing is often the preferred transportation method for large or long slender structures as it do not require large transportation vessels. An additional advantage by towing is that it in many cases simplifies the offshore installation as it replaces complicated offshore lifting operations. This mean reducing the required crane capacity and eliminating problems related to lifting trough splash zones.

Towing of long slender structures such as spools, pipelines, riser bundles and TLP tethers are usually preformed by one of the three following towing methods:

- Surface or near surface tow
- Deeply submerged or Controlled Depth Tow (CDT)
- Off-bottom tow

A modified illustration of the towing methods taken from DNV 2014a:

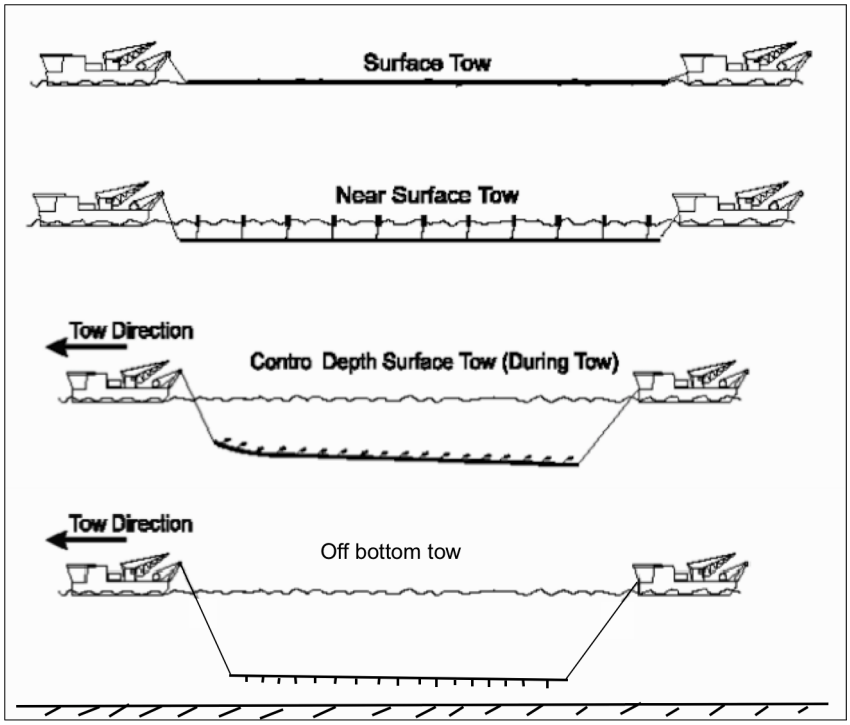

Figure 1.1: Towing methods for long slender structures (DNV 2014a) (modified)

These towing methods all include the usage of a leading and a tailing tug, two tow lines of either steel chain or fibre rope and the structure itself, towed at a given depth. The trailing tug will normally sail with reduced or negative thrust in order to keep the tow arrangement in tension. The use of a tailing tug will also increase manoeuvrability and provide better control of the motions of the towing system. The slender structure may also be equipped with either temporary buoyancy elements or clamp-on weights in order to change the properties of the system.

Even though these methods may look quite similar they all have different properties. Choosing a tow configuration may in many cases be crucial to the success of the tow operation. This thesis will focus on the dynamic behaviour and structural response during a near surface/control depth tow. A more detailed description of the different towing methods as well, as an evaluation regarding the advantages, disadvantages, important load factors and the application of these methods was previously presented in the pre-project thesis. This will therefore not be discussed further during this thesis. The conclusion drawn from the project thesis suggests that all three methods are very promising and that the ideal method of choice will strongly be dependent of the environment and the towed object of the operation. The controlled depth tow method was evaluated to be the most versatile method, as it has a large flexibility regarding the arrangement (tow lines, towed depth, weights/buoyancy elements, etc.).

1.1.1 Near surface / Control depth tow

A control depth tow method (CDT) may be used for transport of long slender structures over a short or longer distance. The structure is towed at a predetermined depth in order to avoid large oscillating loading from waves and current near the surface. A control depth tow where the structure is located relatively close to the surface, not penetrating the surface during waves, is often referred to as a near surface tow.

Determining the tow depth is crucial for the operation, as it will affect the magnitude of the forces acting on the structure as well as the response characteristics of the system. How the tow depth, amongst several other parameters will affect the operation is a complex coupled problem which will be explained in the following chapters. The most important parameters to take into consideration when designing a control depth tow is the towline properties, the hold-back tension, buoyancy, ballast, tow speed as well as the environment and weather conditions.

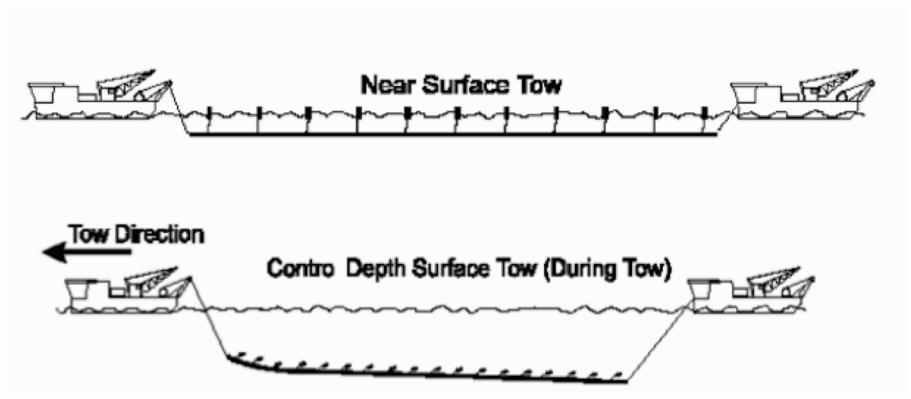

Figure 1.2: Tow-Arrangements: Near surface and Control depth tow (DNV 2014a) (modified)

Temporary buoyancy and weight elements

During the tow, long slender structures are often equipped with temporary buoyancy and/or weight elements in order to alter the properties of the tow system.

Temporary clamp-on weights are added in order to lower the body to towing depth if the submerged weight of the structure alone is not sufficient or when a large hold-back tension is applied. The clamp-on weights may be applied either evenly distributed over the length of the body or only at the ends.

The structure may alternatively be equipped with buoyancy elements during the tow. This in order to make the structure self-floating or as a measurement to reduce stress in the member from the static weight of the structure. An additional utilization of buoyancy elements is making the body self-floating. This will mean that the structure is not dependent on towlines connected to the towing vessels and thus reducing the risk of loosing the structure in the event of a towline failure. Added buoyancy elements are particularity common for near surface tows. The elements may be applied evenly distributed over the length of the body or only at the ends.

It is also possible to use a combination of weight and buoyancy elements in order to make a combination of the upper mentioned properties.

Advantages

The advantage of a submerged tow is a reduced effect from oscillating surface wave- and current loads. This will in many cases result in a significant reduction of fatigue loading. Extreme value loading during tow operations may also be reduced for cases where direct surface wave and current loads contribute with large part of the total loading. How these forces vary with the depth is described in section 1.4.

Having a tow configuration with long towlines may reduces the response loads in the structure induced by vessel motions. This will be due to the elasticity in the towline absorbing some of the forces.

One of the advantages of a near surface towing arrangement is a good system manoeuvrability compared to a deeper tow.

Having the structure near to the surface means that the current variation, as a function of depth, do not have to be taken into consideration during the transportation. The downward current profile is often not known in the planing of a marine transportation and can be difficult to determine. This variation and the uncertainties this brings is unfavourable for any operation. More theory about currents are described in chapter 1.4.

Having the option of altering arrangement parameters, like tow depth, and ability to use temporary buoyancy/weight elements makes the controlled depth towing method very flexible. The operation designer do thereby have the ability to strongly affect the properties of the tow in the most favourable manner.

Disadvantages

A challenges when designing a CDT relates to accurate determination of the behaviour and response of the towed structure as this is a coupled and rather complex problem.

Towing the structure at deeper tow depths leads to difficulties in determining the current depth profile which both will affect the slender structure and the towlines. The behaviour of the towlines may in relation to this be significant to the behaviour of the member and will be hard to predict. Towing at a large depth will also reduce the manoeuvrability of the tow.

The main challenge of a CTD tow close to the surface is related to the large oscillating forces from surface waves and currents. This means large dynamic forces on the structure and possibly also large fatigue damage.

During a CDT, the towed structure will also be subjected to loading induced by the motion of the towing vessels. This loading will in situations where large ship motions are transferred down to the member lead to a significant damage to the structure.

Good applications

A controlled depth tow method is a good solution for offshore transportation of long slender structures where significant wave and currents forces are expected. It may especially be applicable for transportation of structures sensitive to fatigue damage.

A near surface towing solution is well suited for short or longer tow operations where large wave or surface current loads are not expected. This solution will apply well for inshore tow operation requiring high manoeuvrability.

A CTD/near surface tow solution utilizing evenly distributed buoyancy elements is well suited for transport of long slender structures where the submerged weight of the structure may lead to a big bending moment in the structure.

The near surface tow method is also well suited for operations where water depths are limited.

1.2 Upending

Parts of the theory of upending operations are based on DNV 2013

For horizontal oriented transportation of structures installed at a vertical position, an upending operation will usually follow the transport operation. Typical examples of structures being installed in this manner are installation of jackets, risers and TLP tethers. For this thesis, the theory will be limited to installation of TLP tether. The theory may however be adapted to other slender structures like risers or similar.

In general, there are three main methods conducting an upending operation:

- Towline assisted upending
- Free drop upending
- Buoyancy/ballasting/de-ballasting upending

An illustration of the different upending methods are presented below:

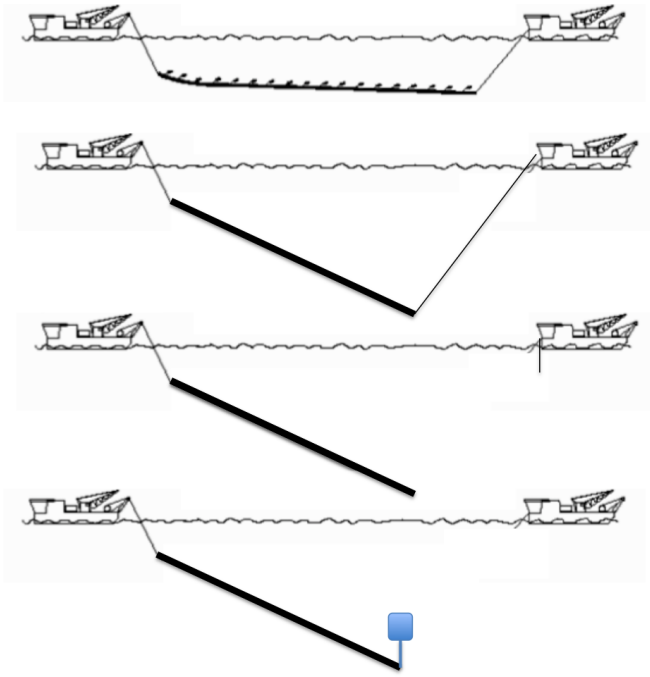

Figure 1.3: Upending methods (Adapted from DNV 2014a)

Conducting an upending operation using a towline assisted method, towline of either steel chain, guy wire or synthetic fibre rope are fed out from either a vessel mounted winch or crane. The tailing towline for this method is used to regulate the upending speed as well as increasing control of the structure. The operation may be conducted in one sequence with a constant line feed rate, or be divided into several intervals. In order to reduce the effect of vessel motions, the winch may be equipped with an active heave compensator (AHC).

For the free drop method, the towline in one of the structure ends is released while the other end is still attached. The free drop method will in general be the most time efficient method, but are without the ability of reducing the upending speed or otherwise control the bottom end of the structure. It is therefore crucial for these operation that the upending speed and structural response are thoroughly assessed in advance of the operation.

The third upending method utilize either added buoyancy or ballast elements attached to the structure during the upending. The upending speed of this method is controlled by eight adding or reducing ballast/buoyancy to the elements. The solution does not, however give the option of otherwise control the bottom end of the structure during the upending phase.

As all upending methods have different advantages and disadvantages, the method of choice have to be determined by a case-to-case evaluation.

1.3 Planing of marine operations

All major marine operation have to be carefully designed and planed in order to ensure the safety of personnel, equipment and environment. Unfortunately there are several examples of poorly designed and/or planed operations which have lead to damage or loss of equipment, economical loss and even personnel injury. As a result of this, there's been developed several procedures, regulations and standards in order to minimize the risks of operations. During the design and planing phase, it is recommended to adopt the following steps (Nielsen 2007):

- Identify relevant rules, regulations and standards
- Identify the physical limitations
- Develop an overall plan of the operation (concept, available equipment, economical limits, etc.)
- Create a deign basis, describing physical limitations and environmental conditions
- Conduct engineering and design analysis
- Develop a detailed step-by-step plan of the operation

Standards are made in order to ensure that marine operations are preformed within clear and recognized level of safety. There are several of these standards, the most utilized of them are DNV-OS-H101 (DNV 2011a) and GL Noble Denton. During this thesis only the key elements from DNV 2011a will be discussed.

1.3.1 Reference period

The duration of any operation or sub-operation shall be defined by an operational reference period T_R. The reference period consists of a planed period T_{POP} and an additional contingency period T_C.

$$T_R = T_{POP} + T_C \tag{1.1}$$

The planed operation period T_{POP} shall be defined based on experience and a detailed scheduled for the operation or sub-operation.

The contingency period is added in order to compensate for general uncertainty in the duration of the operation, as well as possible situations leading to contingency. The contingency period may for instance include time waiting for calm weather before initiating a more weather sensitive sub-operation. The duration of the contingency period should normally not be taken less than the planed operation period. However for some cases a T_C duration equal to 50% of T_{POP} can be accepted. This is for operations where T_{POP} has been accurately defined and the operator has extensive experience with the actual or similar operation. A reduced T_C value may also be accepted for tow operations with a properly assessed towing speed and where extra tugs are used.

1.3.2 Operational limitations

For a marine operation there are several factors that will set different limitations to the operation. The operational limitations (OP_{lim}) are defined for the operation as the first of these limiting factor. Operational limitations may also be defined for each sub-operation. Examples of limiting factors are as following:

- Physical limitations
- Owner/contractor defined limitations
- Limitation for safe working condition
- Concept limitations
- Equipment limitations
- Any limitations related to identified hazards
- Environmental design criteria
- Limitations regarding repression handling

Typical physical limitations related to a tow-operation of a long slender structure are collisions and structural limitations for both ultimate loading (ULS) and fatigue loading (FLS). DNV offshore standard covering marine operations (DNV-OS-H101) is made based on the principle of ensuring a probability for structural failure during an operation less than 1/10 000.

In addition to the physical limitations, the owner/contractor may also have limitations to for instance how much fatigue damage the structure is allowed during the transportation.

When concept and equipment for the operation is decided upon, there are in general also limitations related to these. Example of a concept limitation for a CDT may for instance be related to the towed structure not penetrating the water surface during waves. Equipment limitations may be related to structural limitations of the tow-lines, maximum winch capacity or operational limitations for the towing vessels.

Most of the limitations that are described till now relates to a system response of either structural loading or in form of induced motion. The external forces inducing system response for a tow configuration (vessels, towlines and slender structure) are in general environmental forces. The most important environmental forces are related to wind, waves, current and tides. The next step in the planing and design phase are establishing the relationship between the environmental forces and the induced response. Following, the results are compared with the defined operational limitations in order to establish an environmental design criteria for the operation. For a tow operation, these design criteria are typically linked to significant wave height H_S, peak period T_P and current velocity V_C.

When defining the environmental design criteria DNV classifies marine operations as either "weather restricted" or as "weather unrestricted" based on the duration of the operation.

Weather unrestricted operations

Operations with a planed operation period T_{POP} longer than 74 hours and reference period T_R less than 96 hours are classified as weather unrestricted. These operations shall be designed for environmental extreme value conditions based on long-term statistics for the actual site. Seasonal variation may be taken into consideration for operations of moderate duration.

A further description of planing and design of weather unrestricted operations can be found in DNV 2011a. This process will not be further elaborated as most of the relevant operations to this thesis are assumed to have a operation period less than 72 hrs.

Weather restricted operations

Operations with a planed operation period less than 72 hours are classified as weather restricted. The environmental design condition for these operations can be determined independent of statistical data. These operations are normally designed using a characteristic weather condition for the area and season. The feasibility of operation executions are then evaluated based on weather forecasts.

An α-factor is introduced when evaluating the weather-window for the operation in order to correct for the uncertainty that lays in the weather forecast. It is important to notice that the α-factor is selected using T_{POP} while the weather window is evaluated for the whole reference period T_R.

$$OP_{wf} = \alpha \cdot OP_{lim} \tag{1.2}$$

Where:

- OP_{lim} Operational limitation
- OP_{wf} Forecast operational criteria
- α α-factor correcting for uncertainty in weather forecast

DNV introduces two α-factors, one for significant wave height H_S and one for mean wind speed. Values for the α-factor related to wind speed will not be discussed in this thesis, but can be found in DNV 2011a. The α-factor related to H_S is a function of H_S, the planed operation period T_{POP} and the sensitivity of the operation.

Uncertainty in environmental weather forecasts and α-factors related to significant wave height are analysed and discussed in detail in Natskaar, Moan, and Alvær 2015.

Table 1.1 is taken from DNV 2011a and shows values of α for normal marine operations.

Table 1.1: Values for α-factor related to significant wave height (DNV 2011a)

Table 4-1 α-factor for waves, base case							
Operational Period [h]	*Design Wave Height [m]*						
	$H_s = 1$	$1 < H_s < 2$	$H_s = 2 = 2$	$2 < H_s < 4$	$H_s = 4$	$4 < H_s < 6$	$H_s \geq 6$
$T_{POP} \leq 12$	0.65	Linear Interpolation	0.76	Linear Interpolation	0.79	Linear Interpolation	0.80
$T_{POP} \leq 24$	0.63		0.73		0.76		0.78
$T_{POP} \leq 36$	0.62		0.71		0.73		0.76
$T_{POP} \leq 48$	0.60		0.68		0.71		0.74
$T_{POP} \leq 72$	0.55		0.63		0.68		0.72

Some operations are how ever more sensitive to wave forces or certain wave periods. Therefore, DNV also classifies the weather forecast level to how sensitive the operation is.

Major marine operations sensitive to environmental conditions are classified as level A. These operations also requires a meteorologist to supervise during the operation. Upending and other offshore installation operations will normally be classified as level A.

Operations where the importance of the weather sensitivity is significant is classified as level B. A tow-out operation may be classified as either level A or level B, dependent on how sensitive it is to for instance wave loads.

For operations classified as either level A or B the α-factor is taken from tables specified for these levels. Level B operations will have more conservative values of the α-factor, as these operations do not require meteorologist surveillance.

Values for the α-factor for operations classified as level A and B are presented in table 1.2 and 1.3.

Table 1.2: Values for α-factor related to significant wave height for weather forecast level A (DNV 2011a)

Table 4-3 α-factor for waves, Level A with meteorologist at site							
Operational Period [h]	*Design Wave Height [m]*						
	$H_s = 1$	$1 < H_s < 2$	$H_s = 2$	$2 < H_s < 4$	$H_s = 4$	$4 < H_s < 6$	$H_s \geq 6$
$T_{POP} \leq 12$	0.72	Linear Interpolation	0.84	Linear Interpolation	0.87	Linear Interpolation	0.88
$T_{POP} \leq 24$	0.69		0.80		0.84		0.86
$T_{POP} \leq 36$	0.68		0.78		0.80		0.84
$T_{POP} \leq 48$	0.66		0.75		0.78		0.81
$T_{POP} \leq 72$	0.61		0.69		0.75		0.79

Table 1.3: Values for α-factor related to significant wave height for weather forecast level B (DNV 2011a)

Table 4-2 α-factor for waves, Level B highest forecast							
Operational Period [h]	*Design Wave Height [m]*						
	$H_s = 1$	$1 < H_s < 2$	$H_s = 2$	$2 < H_s < 4$	$H_s = 4$	$4 < H_s < 6$	$H_s \geq 6$
$T_{POP} \leq 12$	0.68	Linear Interpolation	0.80	Linear Interpolation	0.83	Linear Interpolation	0.84
$T_{POP} \leq 24$	0.66		0.77		0.80		0.82
$T_{POP} \leq 36$	0.65		0.75		0.77		0.80
$T_{POP} \leq 48$	0.63		0.71		0.75		0.78
$T_{POP} \leq 72$	0.58		0.66		0.71		0.76

Evaluating a weather forecast prior to the execution of a marine operation, a weather window where the weather forecast are continuously below the operation weather cast limit (OP_{WF}), for the extent of the operation reference period (T_R) is required.

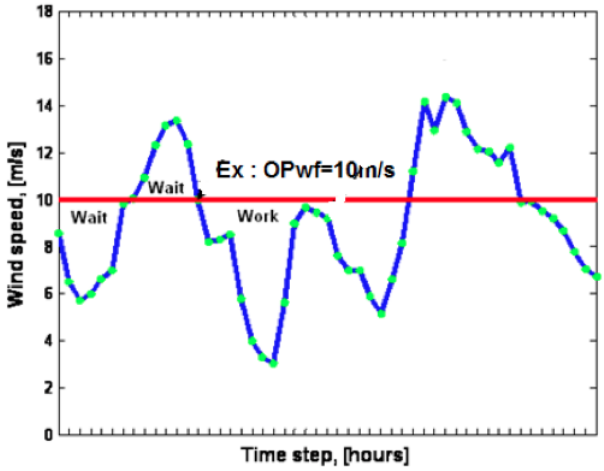

Figure 1.4: Example: Weather forecast evaluation (Larsen 2015)

1.3.3 Failure modes

The failure modes that have to be taken into consideration related to a towing and installation operation are as following (DNV 2012):

- Structural collapse
- Loss of hydrostatic and hydrodynamic stability, related to VIV
- Buckling (local and global)
- Fatigue loading

1.4 Important load factors

In order to analyse and plan an operation it is important to determine which forces are involved and understand their properties. After the loads are determined it is possible to analyse the contribution from different load effects and improve the solution. In general, loads can be classified as one of five load categories:

- Permanent loads (P)
- Live loads (L)
- Deformation loads (D)
- Environmental loads (E)
- Accidental loads (A)

Where:

Permanent loads are static, predictable loads such as gravity force.

Live loads are external, non-environmental, loads that vary with time.

Deformation loads occur as a result of structural deformation. These deformations could represent fabrication error or deformations that has occurred later on.

Environmental loads are forces from wind, waves and currents.

Accidental loads are loads from for instance collisions, fire or explosions.

For the case of designing a transportation and installation method for a towed structure it is mainly the permanent and environmental loads that are of interest. The permanent loads in form of the structure's own submerged weight, and the environmental loads from mainly waves and currents.

The effects of environmental loads which will be described in this thesis are:

- Direct, first order wave loads on the structure
- Current loads
- Vortex induced vibrations (VIV)
- Loading as a result of motion of the towing vessels (and coupled system behaviour)

In addition to these forces the operation will also be subjected to higher order effects from (ref. MARINTEK):

- Geometric stiffness
- Non-linear material properties
- Second order hydrodynamic loading

1.4.1 Static load

The static loads generally relates to gravity, buoyancy and hydrostatic forces. For the case of a tow and upending operation the static forces will be the structural weight and buoyancy of towlines, towed structure and the potential added weights and buoyancy elements.

The weight of the different elements are often given as mass per unit length, kg/m, and material depends on the shape and material of the element.

Gravity and buoyancy forces will act as an evenly distributed load, resulting in both axial- and bending stress.

Calculating static forces in a slender hollow cylinder, hydrostatic and internal pressure will also contribute.

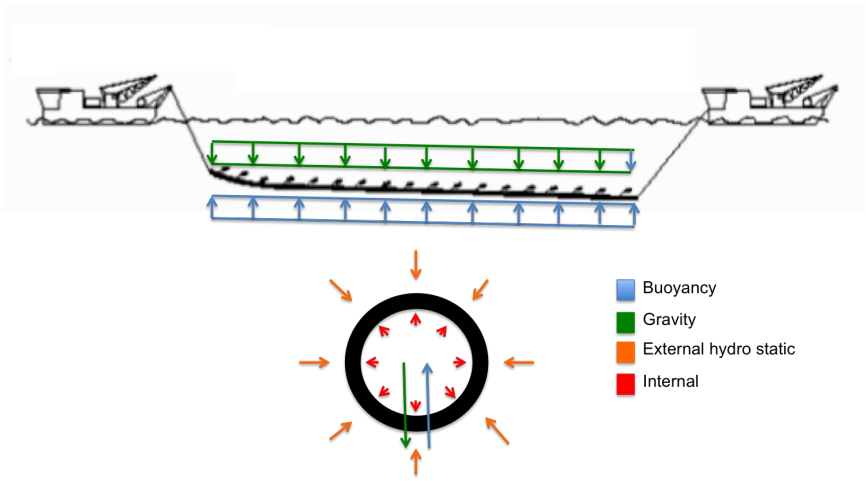

Figure 1.5: Static forces on a submerge towed pipe structure (DNV 2014a) (adapted)

1.4.2 Load estimation on slender structures

Strip theory

An estimate of the hydrodynamic forces acting on a slender structure may be establish by calculating the forces on a small part of the structure dL, and adding all contributions along the structure. This method is called strip theory.

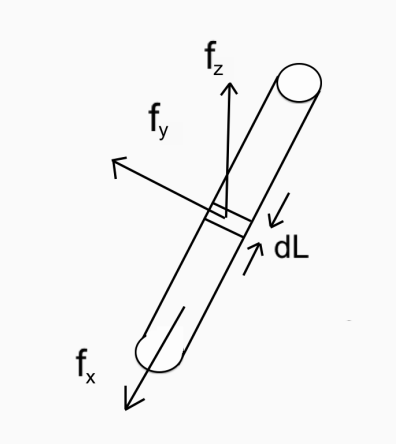

Figure 1.6: Force estimation using strip theory

Classification of wave forces

The hydrodynamic forces from irregular sea states can be obtained by linearly superimposing the forces from regular, sinusoidal wave components. This can be done by first assuming a steady state condition, meaning there's no transient effects due to initial conditions. By these assumptions one can further assume that the structure will harmonically oscillate with the same frequency as the wave components. These are the first order forces and responses. The hydrodynamic response problem can now be split in to two sub problems:

- **Diffraction problem:** Forces from regular waves, acting on structure retained from motions. These force can be split into Froude-Kriloff and diffraction forces. The resulting forces for this problem are wave excitation.

- **Radiation problem:** These are forces obtained from a structure in forced motion, with no incident waves. The resulting forces for this problem are related to added mass, damping and restoring.

The added mass force relates to acceleration of the surrounding water and is linearly dependent on the object acceleration. Damping forces will for a small volume structure mostly consist of viscous damping. The damping forces will be proportional to the velocity of the structure.

The importance of each force contribution is illustrated for a fixed vertical cylinder in regular waves in deep water. Even though it can be hard to precisely determine the magnitude of each contribution, the figure below gives an indication of which forces that dominate.

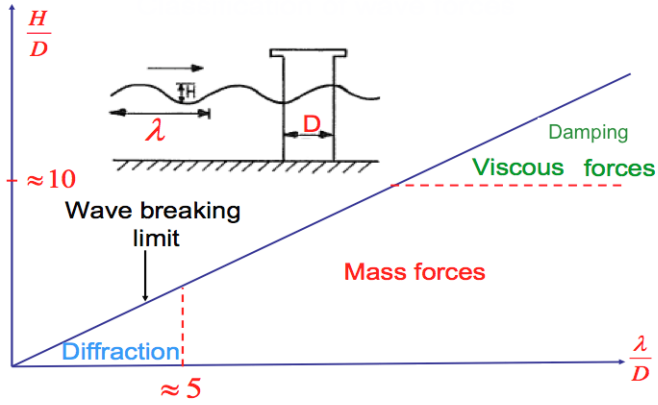

Figure 1.7: Classification of wave forces (Greco 2012)

Structures where $\frac{\lambda}{D} \lesssim 5$, where the diffraction forces are dominating are classified as large volume structures.

Similarly, structures where $\frac{\lambda}{D} \gtrsim 5$ are classified as small volume structures. The forces acting on small volume structures of circular cross-section are often estimated using Morison's equation.

Morison's equation

Morison's equation is applicable for force estimation on structures of circular cross-section in wave conditions $\frac{\lambda}{D} \gtrsim 5$. Morison's equation calculates the force on a cylinder strip, not taking end effects in to consideration, as:

$$f_N(t) = \rho A C_M \dot{u}_n + \frac{1}{2}\rho C_D u_n |u_n| \tag{1.3}$$

Where:

- ρ Water density (1025 kg/m^3)
- D Diameter od the cylinder
- A Cross sectional area
- u_n Water particle velocity normal to the cylinder
- $\dot{u}_n$ Water particle acceleration normal to the cylinder
- C_M Mass coefficient
- C_D Drag coefficient

The first part of the equation represent mass and added mass forces, while the second part represent drag forces.

The drag- and mass coefficients are dimensionless and defined ass:

$$C_M = \frac{f_{Mass}}{\rho A \dot{u}_n} \tag{1.4}$$

$$C_D = \frac{f_{drag}}{\frac{1}{2}\rho D u_n^2} \tag{1.5}$$

As the total mass force is a product of both mass- and added mass, the mass coefficient can be split into two parts.

$$C_M = 1 + C_A \tag{1.6}$$

The main challenge of using Morison's equation is accurately determine the values of C_A, C_D, v and $\dot{v}$ for irregular waves. In order to make an estimate, conservative simplifications and assumptions often have to be made.

The value of both C_A and C_D can be found for different shapes, either by experiments or from empirical data. Coefficients are dependent on factors like relative velocity, wave frequency, surface roughness (μ), Reynold's number (R_n) and Keulegan-Carpenter's number (KC). Several of these factors are time dependent like velocity and Keulegan-Carpenter's number, further complicating the problem. The effect of these parameters on drag- and added mass coefficients were discussed in detail in the pre-project (autumn 2015), and will not be discussed further in this thesis. For the majority of relevant cases, the coefficients for a circular cross-section in infinite water may be taken as constant values defined in DNV 2014b:

$C_A = 1$
$C_D = 1$

In the case of a near surface or off bottom tow, the drag coefficient will also be a function of the distance to the surface/bottom.

Additional forces due to added weights or buoyancy elements has to be taken into consideration. The approach method for these calculations are described in DNV 2014b.

For a moving cylinder in waves and current, Morison's equation can be written to account for relative velocity and acceleration (DNV 2014b):

$$f_N(t) = -\rho A C_A \ddot{r} + \rho(1 + C_A) A \dot{u} + \frac{1}{2}\rho C_D u_r |u_r| \tag{1.7}$$

$$f_N(t) = \rho A C_A a + \rho C_A A a_r + \frac{1}{2}\rho C_D u_r |u_r| \tag{1.8}$$

Where:

- $\dot{r}$ Structure's velocity
- $\ddot{r}$ Structure's acceleration
- a = $\dot{u}$ The fluids acceleration
- $u_r = u - \dot{r}$ Relative velocity
- $a_r = \dot{u} - \ddot{r}$ Relative acceleration

1.4.3 Direct wave loads

Direct wave loads on a slender structure consist of mainly mass- and drag forces, calculated using Morison's equation. In order to calculate these forces the velocity potential ϕ of the water particles acting on the member has to be determined. For marine applications there are mainly two alternative methods for calculating wave potentials

- Airly linear wave theory
- Stoke's 5th order wave theory

Airly linear wave theory is utilized for this thesis. Stoke's 5th order wave theory will not be described.

The profile of a regular wave propagating in the positive x-direction is described as:

$$\zeta = \zeta_a sin(\omega t - kx) \tag{1.9}$$

Where:

- ζ Wave elevation at a given time and location
- ζ_a Wave amplitude

The wave potential (ϕ) for regular waves in deep water, according to Airly linear wave theory is described as:

$$\phi = \frac{g}{\omega}\zeta_a e^{kz} cos(\omega t - kx) \tag{1.10}$$

Where:

- ϕ Velocity potential
- ω Wave frequency
- ζ_a Wave amplitude
- k Wave number
- z Z-coordinate

- x X-coordinate

$$k = \frac{\omega^2}{g} \tag{1.11}$$

From this the x- and z-component of velocity and acceleration are derived:

$$u = \omega\zeta_a e^{kz} sin(\omega t - kx) \tag{1.12a}$$

$$w = \omega\zeta_a e^{kz} cos(\omega t - kx) \tag{1.12b}$$

$$a_x = \omega^2\zeta_a e^{kz} cos(\omega t - kx) \tag{1.12c}$$

$$a_z = \omega^2\zeta_a e^{kz} sin(\omega t - kx) \tag{1.12d}$$

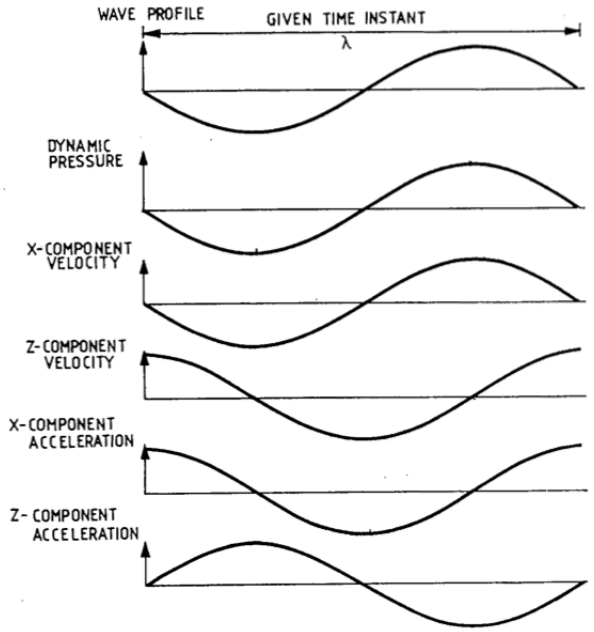

Figure 1.8: Wave elevation, pressure, velocity and acceleration profiles (Faltinsen 1999)

As mentioned earlier, viscous drag forces are related to the water particle velocities and the mass/inertia forces are linearly proportional to the accelerations.

As seen from formula 1.12, the velocity and acceleration potential decreases exponentially with the water depth. At water depth $\frac{\lambda}{2}$ the potential wave energy is effectively reduced by 96%. This decay in potential is illustrated by:

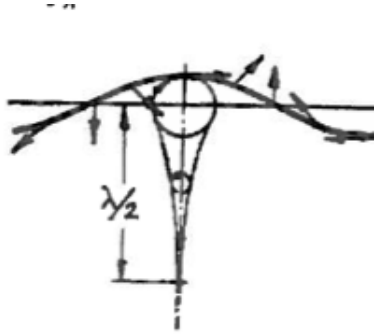

Figure 1.9: Wave energy potential decreasing with water depth (Pettersen 2007)

There are several ways to deal with the wave potential close to the surface, as described by ref. MARINTEK. The method of choice will affect the result for structure close to the surface, given that the wave loads are of importance in the first place.

- 1. Integration to mean water level
- 2. Deformation of potential by stretching and compressing
- 3. Parallel move of potential

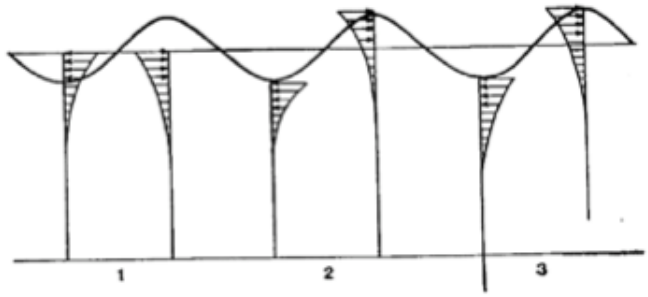

Figure 1.10: Methods for use of wave potential close to surface ref. (MARINTEK)

For a horizontally oriented slander structure in head seas, the different forces contributions will vary over the length of the structure. This is illustrated using a CDT-configuration:

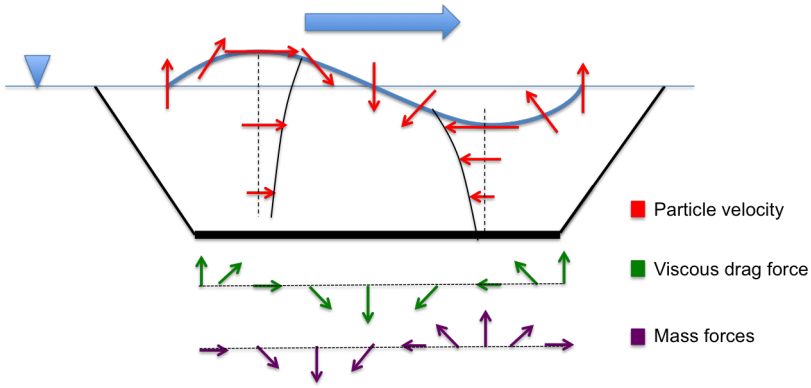

Figure 1.11: Varying wave forces on a CDT-configuration

1.4.4 Current

When estimating the hydrodynamic forces using Morison's equation, the current loads also have to be taken into consideration. As most currents are mainly steady, the load will primarily be related to the current velocity, contributing with viscous drag forces.

In addition to the drag forces, currents will in some cases also give rise other loads like: slow drift forces, lift force, loads related to a combination of waves and strong currents (change in wave height and wave period), and as will be discussed in the next subsection vortex induced vibrations (VIV).

The current velocity may either be in the same direction as the wave induced velocities or they can be oriented in a different direction. Using Morison's equation, the "u" velocity, normal to the cylinder will be a sum of the different wave and current velocities and directions

Ocean currents are divided into different categories. The most common ones are:

- Tidal currents
- Wind generated
- Circulation currents (Ocean or local geographic)
- Long shore currents
- Water density difference
- Stokes drift

The total current velocity (u_c) is defined as:

$$u_c = u_{tidal} + u_{Wind} + u_{circulation} + ... \tag{1.13}$$

Determining the magnitude of each current component may be difficult as they vary with both time, location and depth, conservative estimations are therefore made.

Tidal currents

Tidal currents are often the most predictable and easiest to determine of the current contributions. The tidal currents are dependent of the position of the moon and are usually found from weather forecasts.

Wind generated current

The wind generated currents are in general based on statistical data. If these data are not available the magnitude can be estimated using data from DNV 2014b:

$$u_{wind}(0) = k \cdot u_{1hr,10m} \tag{1.14}$$

Where:

- $u_{wind}(0)$ Wind generated current velocity at the surface
- $u_{1hr,10m}$ Wind speed of one hour return period, 10m above surface
- $k = 0.015 - 0.03$

Current profile

Determining a downward current profile is challenging as the current typically consists of several components, each varying with time, depth and direction. The downward change in pattern may be especially important for vertically orientated long structures and during a potential upending operation.

The downward variation of the surface wind generated currents are expressed by DNV 2014b as:

$$u_{wind}(z) = u_{wind}(0)\frac{d_0 + \mathbf{z}}{d_0} \tag{1.15}$$

Where:

- $\mathbf{z}$ Water depth
- d_0 Reference depth equal to 50m

1.4.5 Vortex Induced Vibrations

The following section is part of the pre-project rapport

Vortex induces vibrations (VIV), vortex induced oscillations (VIO) or vortex induced motion (VIM) are all different names describing the same viscous phenomenon. VIV is a structural response phenomena due to oscillating forces from vortex shedding of a flow passing around a structure. The flow may represent a steady current, wave drift or a relative velocity between structure and fluid particles. Induced forces due to vortex shedding has to be investigated as they may in some cases contribute significantly to the total force acting on the structure and lead to resonant lock-in effects. An extensive description of procedures to calculate these forces is found in section 9 in DNV-RP-C205 (DNV 2014b). In the following chapter an introductory description of the phenomenon and how to estimate the forces/structural response is presented.

Important parameters when describing and/or doing calculations on VIV are:

- KC Keulegan-Carpenter number
- R_e Reynold's number
- St Strouhal number
- m^* Mass ratio
- ζ Damping ratio
- f_0 Natural frequency
- V_r Reduced velocity
- f_v Vortex shedding frequency

$$R_e = \frac{uD}{\nu} \tag{1.16}$$

$$St = \frac{f_v D}{u} \tag{1.17}$$

$$m^* = m(0.25\pi\rho D^2) \tag{1.18}$$

$$V_r = \frac{u}{f_n D} \tag{1.19}$$

Vortex shedding

Flow passing around a circular cylinder will start to separate from the cylinder due to viscous boundary layer effects and create vortex shedding behind the cylinder. The shedding

pattern behind the cylinder will strongly depend on Reynold s number and Keulegan-Carpenter number.

For sufficiently high Re and KC numbers the vortex shedding will start to oscillate, altering from side to side. The altering shedding induce oscillating lift and drag forces on the cylinder:

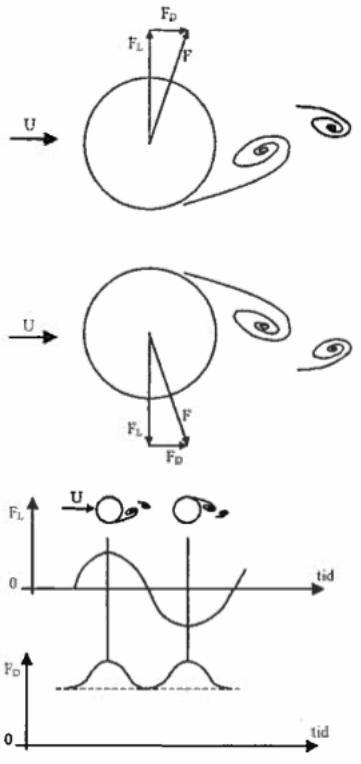

Figure 1.12: Altering vortex shedding (Pettersen 2007)

In the situation of large oscillating lift- and drag forces, vortex shedding could lead to significant fatigue damage on the structure. Large forces could also induce large motions which could cause collisions. It is therefore important to take these forces into consideration, both magnitude and frequency.

Shedding frequency

The Czech physicist Strouhal studied the phenomenon of vortex shedding and established the relation between the shedding frequency as a function of Strohal's number, this relation is expressed by equation 29. The Strouhal number is a function of Reynold s number, but as we can see from figure 14, equal to approximately 0.2 for a large area of the subcritical flow.

$$St = \frac{f_v D}{u} \tag{1.20}$$

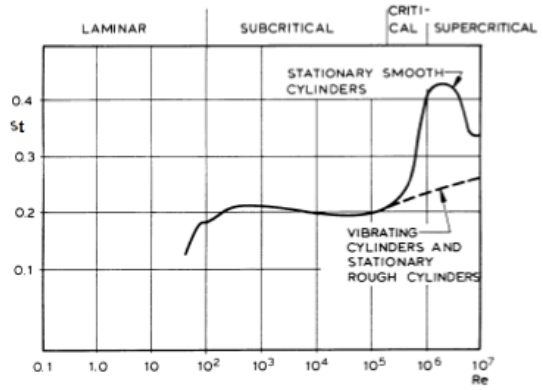

Figure 1.13: Strouhald number as a function of R_e (DNV 2014b)

Drag force

The total drag forces on a slender cylinder in steady flow may be calculated as:

$$f_D = \frac{1}{2}\rho A u^2 (C_D + \tilde{C_D}) \tag{1.21}$$

Where $\tilde{C_D}$ is vortex added drag coefficient. The additional drag coefficient may be difficult to establish accurately, as it is dependent on the amplitude of the cross flow vibration.

Vortex induced drag forces will oscillate around the initial drag force, with twice the frequency of the shedding frequency 1.14.

Lift forces

The lift forces may be estimated as (Faltinsen 1999):

$$f_L(t) = |f_L|(cos(2\pi f_v t) + \alpha) \tag{1.22}$$

Where:

- $|f_L|$ Lift force without vortex shedding
- f_v Vortex shedding frequency [Hz]
- α Phase angle

Lift force on a cylinder will oscillate around zero, with the same frequency as the vortex shedding:

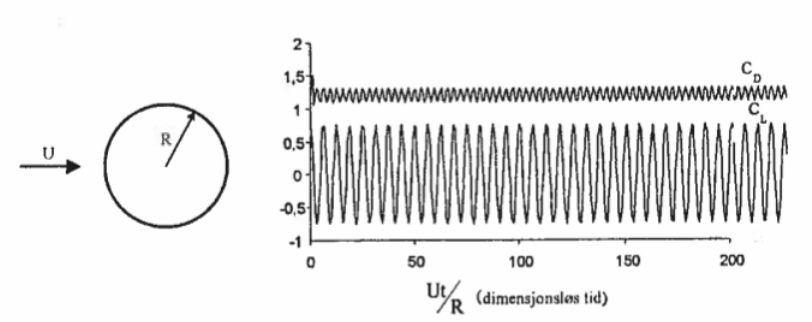

Figure 1.14: Oscillating drag and lift forces due to vortex shedding (Pettersen 2007)

Lock-in

Equation 1.20 indicate a linear relation between the flow velocity u and the shedding frequency f_v. However, as the shedding frequency coincides with the natural frequency of the cylinder, the shedding frequency will lock itself to this frequency (figure 1.15), this is called the lock-in phenomenon. Vortex shedding lock-in effects may cause large resonant motion behaviour of the cylinder which often are related to large induced stress.

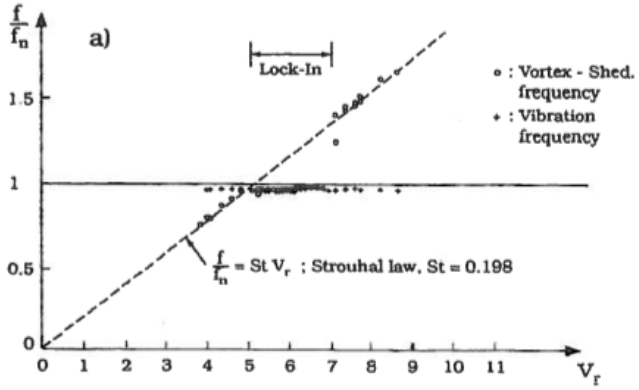

Figure 1.15: VIV lock.in (Pettersen 2012)

VIV related to towing and upending

For the case of a submerged tow and upending operation, the occurrence of VIV during any phase of the operation are undesirable. The critical phases during the operation, with

respect to VIV are believed to be during towing in beam sea and during upending. VIV can occur in the tether as well as in the towlines.

As wave induced water particle velocity alters over the course of each wave, resonant lock-in effects are not expected during a tow relatively close to the sea surface.

The calculation method for determining the eigenfrequencies are described in section 1.5.2.

1.4.6 Ship motion

For a marine operations like submerged tow and upending operations, forces acting on the vessels involved will in some cases be as important as the hydrodynamic forces acting on the structure being transported. Wave induced motion of the ships will be transmitted trough the towlines to the point of attachment on the structure. This results in a forced motion and induced loading in the towlines and the slender structure. These loads may be of importance during both the tow and upending phase of the operation.

When planing a marine operation involving transport vessels, the type of vessel will often be predetermined or limited to a few alternative vessels. The response characteristics of the vessels are usually known in form of a response amplitude operator (RAO) curve. These curves describes the linear relationship between the wave amplitude and the amplitude of the ship motion for different wave frequencies.

A freely floating ship will have six degrees of freedom, three translations and three rotations. Additionally, there are coupling effects between the different motions. A ship will have an RAO curve for each degree of freedom and also for different wave directions and loading conditions.

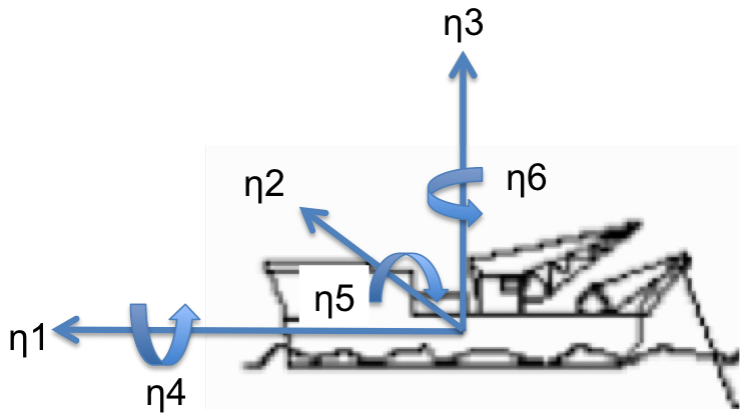

Figure 1.16: Six degrees of freedom

Where:

- η_1 Surge motion
- η_2 Sway motion
- η_3 Heave motion
- η_4 Roll
- η_5 Pitch
- η_6 Yaw

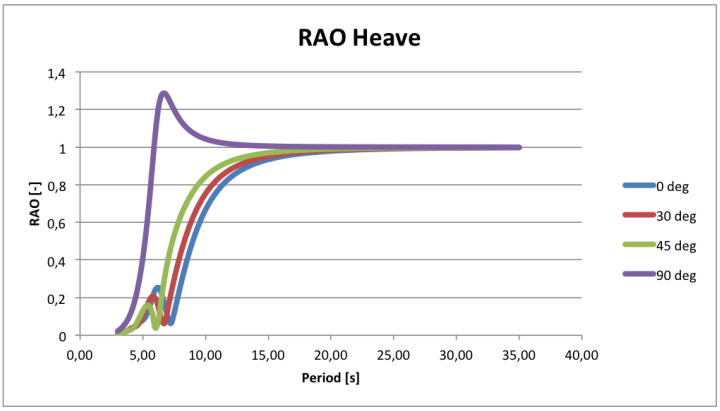

Figure 1.17: Example of RAO curve in heave direction

In order to calculate local motions, knowing the phase angle (ε) between the waves and response motion are equally important as knowing the relation between the wave- and ship-amplitudes. This phase angle will also be known for the different degrees of freedom and wave frequencies. The motion of the centre of gravity can then be expressed as:

$$\eta = \eta_{max} \cdot cos(\omega t + \varepsilon) \tag{1.23}$$

Knowing the RAO at centre of gravity of a vessel, an equivalent RAO curve can be established local for a point on the vessel. For a CDT configuration, it is of interest to establish RAO curves, describing the motions of the towline attachment point. These points will for the case illustrated in figure 1.18 be at the back of the leading vessel and at the front of the tailing vessel.

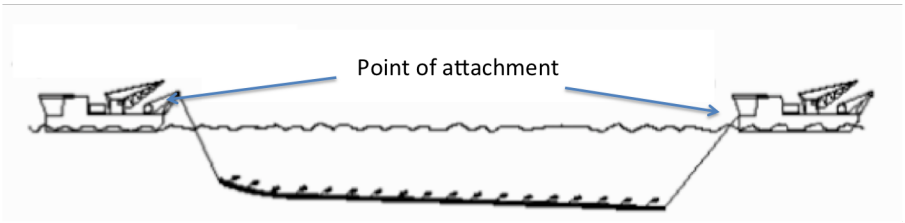

Figure 1.18: Point of attachment on a CDT configuration (Adapted fromDNV 2014a)

The total coupled motion of a point on the vessel can be expressed as:

$$S = (\eta_1 + z\eta_5 - y\eta_6)\mathbf{i} + (\eta_2 - z\eta_4 + x\eta_6)\mathbf{j} + (\eta_3 + y\eta_4 - x\eta_5)\mathbf{k} \tag{1.24}$$

Where i, j, k indicate direction in x-, y- and z-direction, respectively.

By combining equation 1.23 and 1.24 the response amplitude and phase angle at a given point can be calculated.

1.5 Dynamic properties

When analysing the dynamic behaviour of a linear oscillating system it is common to describe the system as a set of mass, damping and spring elements. The simplest way to explain this principle is to look at a simple one-DOF oscillating system as shown in fig. 1.19.

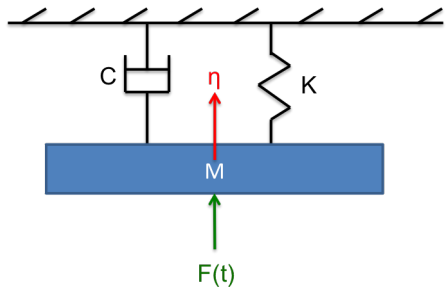

Figure 1.19: Oscillating mass, damper, spring system

The mass element will provide the system inertia, the spring restoring forces and the damper with damping forces. The motion of the object can be described by equation 1.25 based on Newtons 2nd law.

$$\sum F = -M\ddot{\eta} - C\dot{\eta} - K\eta + F_{ex} \tag{1.25}$$

Where:

- F — All forces
- M — Mass coefficient
- C — Damping coefficient
- K — Stiffness coefficient
- F(ex) — Excitation force

- η — Deflection distance
- $\dot{\eta}$ — Velocity
- $\ddot{\eta}$ — Acceleration

- $M\ddot{\eta}$ — Inertia force
- $D\dot{\eta}$ — Damping force
- $K\eta$ — Spring force

It is the external forces F(t) that will excite the system to move, while the damping, mass and spring force will act against the external force, breaking the motions and restoring the system to equilibrium.

1.5.1 Coupled system

Describing compete coupled problem in three dimensions, each body can have as many as six independent motions giving them six degrees of freedom (fig. 1.20). In general there will also be a coupling between these degrees of freedom.

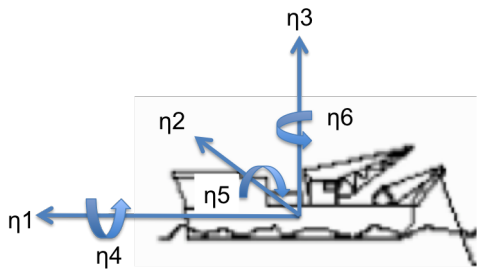

Figure 1.20: Six degrees of freedom

Looking at a submerged tow configuration consisting of three bodies, each having six degrees of freedom, the system will in total have 18 degrees of freedom (fig. 1.21).

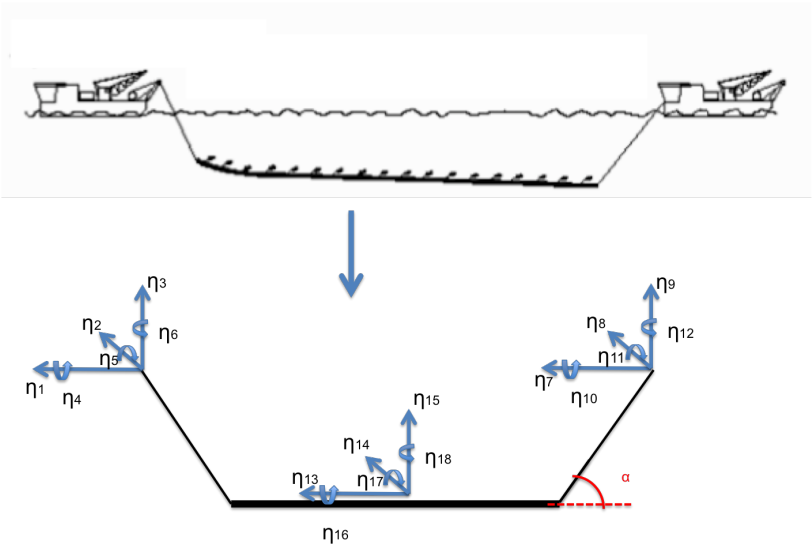

Figure 1.21: Tow arrangement with 18 DOF (DNV 2014a) (modified)

The dynamic behaviour of a coupled system with several degrees of freedom can be described using several components of mass, damping and spring elements. Relating to a submerged tow, and looking at the heave motion of the towed structure exclusively, the system may be described by two spring-, one mass- and an evenly distributed damping element as illustrated in fig. 1.22.

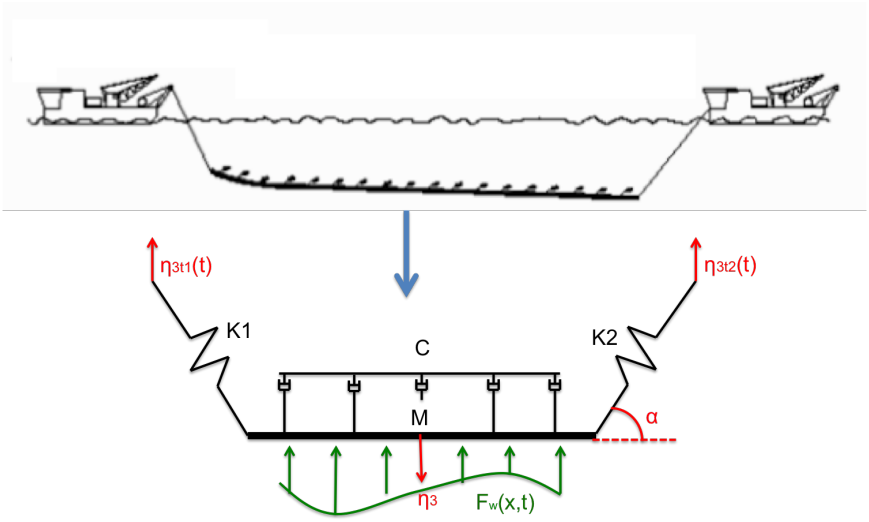

Figure 1.22: Tow arrangement as an oscillating mass, damper, spring system (DNV 2014a) (modified)

Where:

- η_{3t1}, η_{3t2} are heave motion of the tow vessels connected to the towlines.
- F_w is the environmental and other external forces acting on the system. This force will be a function of time, location, waves, current, shape of the structure and water depth. What these forces are, and how we can calculate them is described in section 1.4.
- M is the mass of the towed structure as well as added mass.
- C is the damping acting on the system, which in this case would mostly be viscous damping.
- K is the stiffness of the coupling towlines. These elements can be decomposed, knowing the vertical tow angle α, in order analyse the motion of one single direction.

In general, the added mass and damping term will be dependent of the frequency of the excitation force. This is further described in the following subsection 1.4.

The stiffness K from the towlines will be dependent on the length of the line and the elasticity of the material. The towline may also consist of several segments with different properties. The structural stiffness of a tight towline segment can be calculated using eq. 1.26:

$$K_S = \frac{EA}{L} \tag{1.26}$$

Where:

- K_S Structural stiffness (axial)
- E Elasticity of the material
- A Cross section area
- L Length of the line

In addition to structural stiffness, a geometric stiffness K_G and bending stiffness K_B may also contribute to the total stiffness of the system. A geometric stiffness will be a result of tightening a slack or otherwise non-straight line (change in geometry). The bending stiffness will be a function of material properties, geometric cross-section properties and potentially also pre-tension in the line.

The total stiffness can be calculated as:

$$\frac{1}{K_{tot}} = \frac{1}{K_S} + \frac{1}{K_G} + \frac{1}{K_B} \tag{1.27}$$

One can also develop the model further to include mass and damping elements from the towlines for cases where these effects will affect the results.

1.5.2 Eigenfrequencies

By determining the values of mass, spring and damping coefficients, one can analyse the response behaviour of the system. A characteristic property related to the response study is the system eigenfrequency, also called natural frequency. The eigenfrequency is the frequency the system will oscillate without external forces. A system can also have several eigenfrequencies. An external force with a frequency close or equal to one of the system's eigenfrequencies will lead to a large dynamic response and large stress. It is therefore important to determine the eigenfrequencies in order to make sure non of the predicted forces coincide with the eigenfrequencies.

Important frequencies

For a oscillating system there are three frequencies that are of particular interest:

- Undamped eigenfrequency, ω_0
- Damped eigenfrequency, ω_d
- Frequency of maximum response, ω_m

What these frequencies represent will be explained by looking at a simple mass, spring damper system, oscillating in one dof, as previously illustrated in fig. 1.19.

Undamped eigenfrequency is the frequency a undamped system will naturally oscillate with. The behaviour of the system will be sinusoidal as illustrated in fig. 1.23.

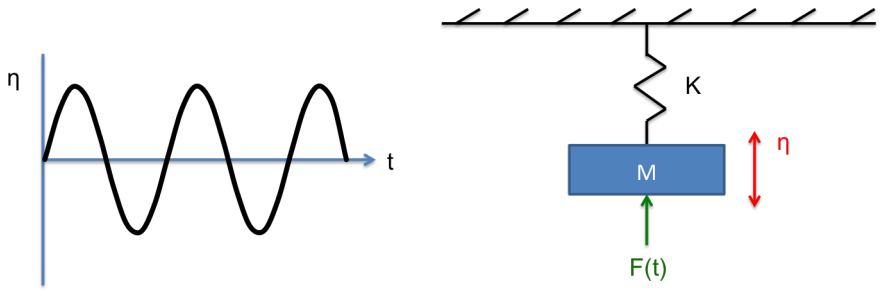

Figure 1.23: Naturally oscillating undamped system

The motion of the system can be described as:

$$\eta_3 = U_0 \cdot sin(\omega_0 t) \tag{1.28}$$

Where U_0 represent the amplitude.

The undamped eigenfrequency can be calculated by:

$$\omega_0 = \sqrt{\frac{k}{m}} \tag{1.29}$$

All eigenfrequency calculations originate from the equation of the undamped eigenfrequency. k and m in this case represent different types of stiffness and mass (e.g. structural-, modal- or system stiffness and mass coefficients).

Damped eigenfrequency are the frequency a damped system will oscillate with. As the system is damped, the amplitude will decrease with time. An oscillating damped system is illustrated in fig. 1.24

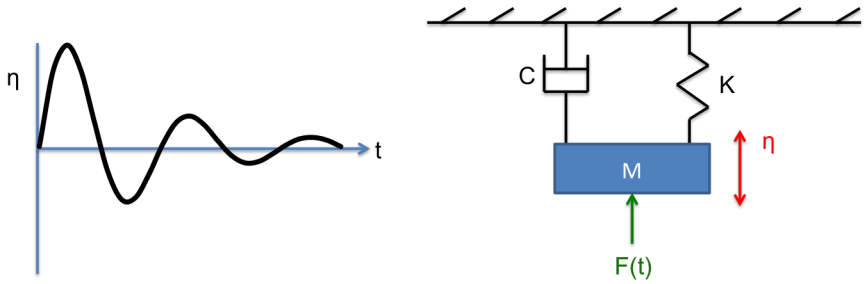

Figure 1.24: Naturally oscillating damped system

The motion of a damped system can be described as:

$$\eta_3 = U_0 \cdot sin(\omega_d t) \cdot e^{-\frac{c}{2m} \cdot t} \tag{1.30}$$

The $e^{-\frac{c}{2m}}$ part of the equation contributes with the amplitude decrease.

The damped eigenfrequency ω_d can be determined by:

$$\omega_d = \omega_0 \sqrt{1 - \frac{c^2}{4m^2\omega_0^2}} = \sqrt{\frac{k}{m} - \frac{c^2}{4m^2}} \tag{1.31}$$

By introduce a term for critical damping C_{crit} and critical damping ratio ξ as:

$$C_{crit} = 2\sqrt{mk} \tag{1.32}$$

$$\xi = \frac{C}{C_{crit}} \tag{1.33}$$

The formula for damped eigenfrequency, eq. 1.31, can be rewritten as:

$$\omega_d = \omega_0 \sqrt{1 - \xi^2} \tag{1.34}$$

Frequency of maximum response , ω_m is the external force frequency which will induce a maximum response. This frequency is in general slightly higher than the eigenfrequency for marine applications. The frequency is best illustrated in a graph for dynamic load factor (DLF), fig. 1.25. The dynamic load factor represent the relation between the load and response amplitude and will be further described in the following sections.

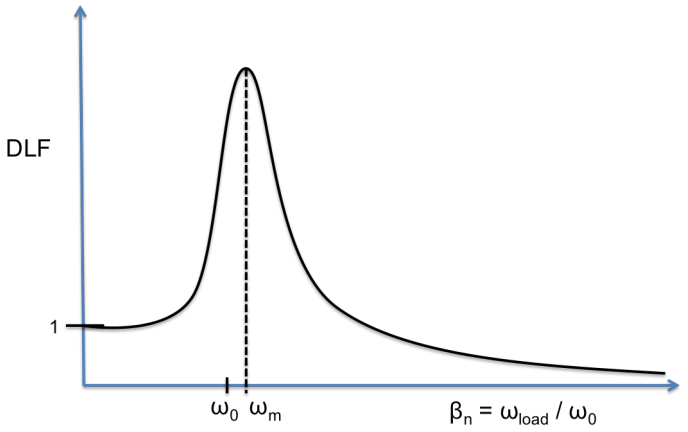

Figure 1.25: Frequency of maximum response

The frequency of maximum response can be calculated as:

$$\omega_m = \omega_0 \sqrt{1 - 2\xi^2} \tag{1.35}$$

All of the upper mentioned frequencies, ω_0, ω_d and ω_m, will all be slightly different. A load in any of these frequencies will in general induce a large system response.

Resonance is a phenomenon where a oscillating force with constant amplitude in the right frequency, close or equal to the natural frequency results in response of large amplitudes.

Eigenmodes

An explanation of how system can have several eigenfrequencies will now be presented by first looking at the response of a vibrating beam. Theoretically, all possible deformations patterns of a beam can be described as the sum of several sinuously deformation patterns, or mode shapes. The different sinus pattern may be of various amplitudes and frequencies, generally occurring with a phase angle relative to each other. Each of these mode shapes will then be related to a eigenfrequency.

The five first mode shapes of a freely supported beam are illustrated in figure 1.26. A ”beam” structure in a marine application may represent a slender structure e.g. a riser or a tether (Larsen 2014).

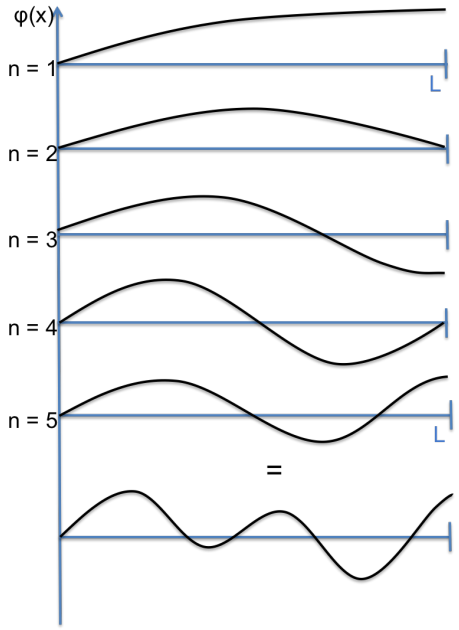

Figure 1.26: Five first mode shapes of a beam

Where $\phi(x)$ is the deflection along the beam. The shape function for a freely supported beam can be described as:

$$\phi(x) = \phi_0 sin(\frac{n\pi}{L}x), n = 1, 2, 3, ... \tag{1.36}$$

Where:

- $\phi(x)$ Shape function
- ϕ_0 Undetermined deflection amplitude
- n Mode shape number
- L Length of the beam

The eigenfrequencies of a beam in tension can be calculated as the result of two stiffness contributions; structural stiffness (K_s) and axial tension in the beam.

The eigenfrequency related to axial tension is the same as the eigenfrequency for a straight string or cable with relatively low or no structural bending stiffness, and can be calculated as (ref. Larsen 2014):

$$\omega_{0,t} = \frac{n\pi}{L}\sqrt{\frac{T}{m}}, n = 1, 2, 3, ... \tag{1.37}$$

Where:

- n Mode shape number
- L Length of the beam
- T Tension - representing a stiffness, K_t
- m Mass per unit length [kg/m]

The second contribution is the eigenfrequency for a beam without tension and can be calculated as (ref. Larsen 2014):

$$\omega_{0,s} = \frac{n^2\pi^2}{L^2}\sqrt{\frac{EI}{m}}, n = 1, 2, 3, ... \tag{1.38}$$

$$EI = K_s \tag{1.39}$$

Where:

- E Structural elasticity
- I Second area moment
- EI Structural bending stiffness, K_s

By combining the two contributions one can determine a total system stiffness K_{tot}:

$$K_{tot} = T + K_s \tag{1.40}$$

And a total modal eigenfrequency for the different modes:

$$\omega_0 = \sqrt{\omega_{0,t}^2 + \omega_{0,s}^2} = \frac{n\pi}{L}\sqrt{\frac{T}{m} + \frac{n^2\pi^2}{L^2} \cdot \frac{EI}{m}} \tag{1.41}$$

The calculation formula change with different boundary conditions. How to calculate eigenfrequencies for other boundary conditions will not be discussed in this thesis, as most tow operations of slender structures may be related to a simply supported problem.

The number of possible modes are almost infinite as $n \to \infty$ and the structures ability to have deflection in several directions. Even though there are almost infinite number of eigenfrequencies, one for each mode, it is in general the lowest frequencies that will be of most interest. From equation 1.41 one can see that for increasing n, the frequencies will rapidly increase. Higher frequencies will in general carry lower energy and will not be as important as the lower frequencies.

For most marine related problems environmental loads at sea rarely occurs in a single harmonic frequency, and the induced response will consist of several mode shapes. By preforming a modal superpositioning of the response, one can look at the contribution of each mode and force frequency.

Analysing the response of a system or structure, the determination of relevant mode shapes is at as important as determining the eigenfrequency.

The first natural frequency of a simply supported beam may according to DNV 2014a be calculated as:

$$f_1 = 1.57\sqrt{\frac{EI}{m'L^4}[1 + 0.8(\frac{\delta}{D})^2]} \tag{1.42}$$

Where:

- m' Total mass per unit length
- δ Static deflection

$$\delta = \frac{5}{384}\frac{qL^4}{EI} \tag{1.43}$$

Where q is the sectional current drag force.

$$\omega_0 = 2\pi \cdot f_0 \tag{1.44}$$

Coupled continuous systems

For a coupled continuous system consisting of several components, moving in several coupled motions, the problem quickly becomes more complicated. There are several different methods to handle such problems. Generally, the calculation of eigenfrequencies and mode shapes for complex systems are calculated by computer programs (FE-program).

By relating the theory described to the submerged tow configuration in figure 1.21 and 1.22, the eigenmodes for vertical motion will look like figure 1.27:

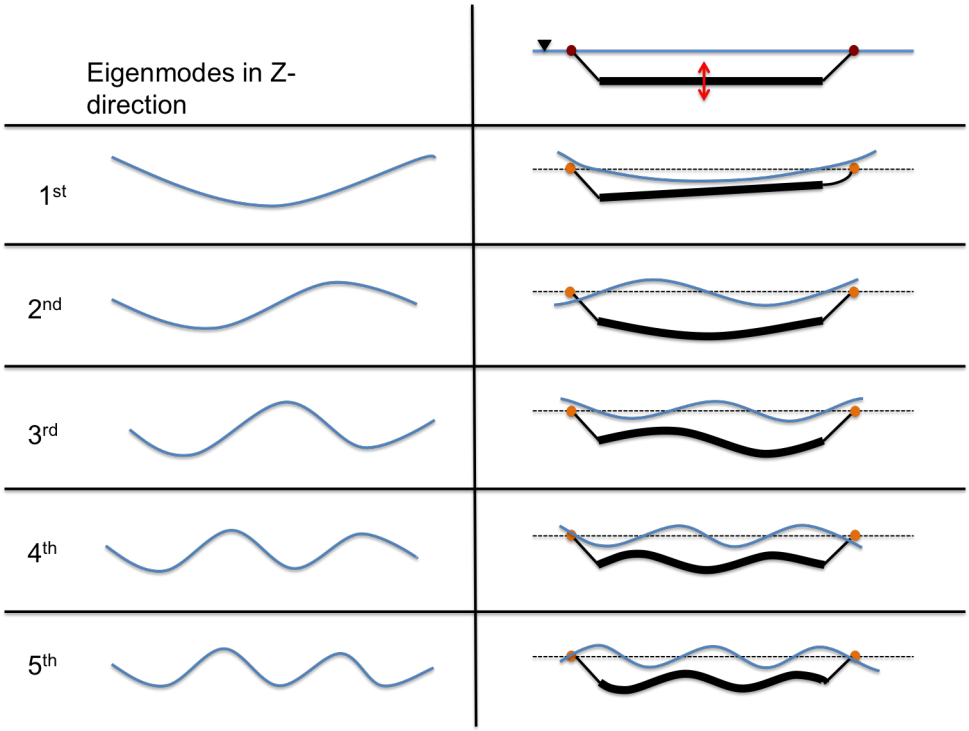

Figure 1.27: System mode shapes in z-direction for a tow arrangement

After determining the eigenfrequencies and mode shapes, the results have to be compared with the expected loading in order to evaluate if the towing configuration is feasible or not.

1.5.3 Stiffness-, resonance- and inertia dominated systems

When all the coefficients for the system are determined, it is possible to draw a curve illustrating the dynamic amplification of different load frequencies. That is the relation between the load frequency and the undamped eigenfrequancy. This relation is expressed by the dynamic load factor (DLF), which is expressed as:

$$DLF = \frac{1}{\sqrt{[1 - \frac{\omega^2}{\omega_0^2}]^2 + \omega^2 \frac{c^2}{k^2}}} \tag{1.45}$$

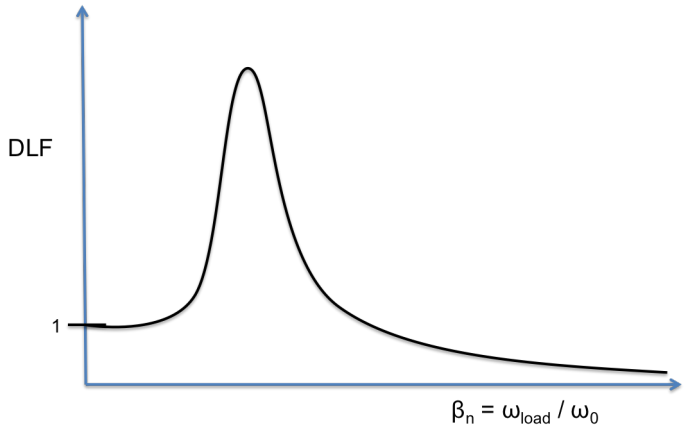

Figure 1.28: Dynamic load factor (DLF)

Where β_n is the relation between the load frequency and the undamped eigenfrequency.

Dependent on the β_n value, the response behaviour of a system can be classified as either stiffness-, resonance- or inertia dominated. The different sections are illustrated below:

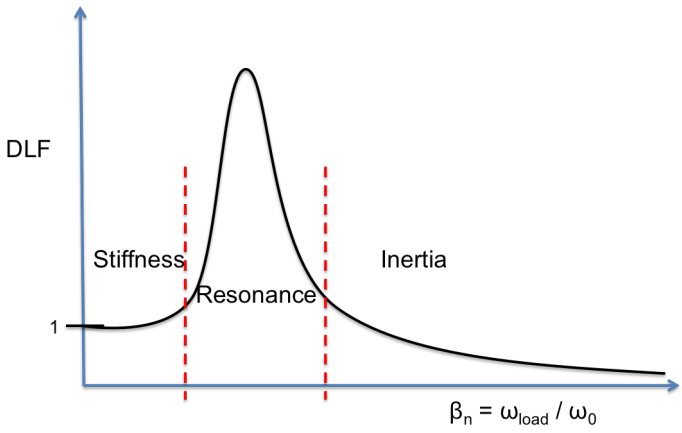

Figure 1.29: Stiffness-, resonance- and inertia dominated systems

Stiffness dominates systems: The load frequancy is significantly lower than the eigen-frequancy, $\omega < \omega_0$. The external force are slowly varying, inducing a response of small acceleration. The structure or system is acting quasi static with a dynamic load factor approximately equal to one.

Resonance dominated systems: The load frequency is close to, or equal to the eigen-frequency, inducing a large responce, $\omega \approx \omega_0$. For marine operations, loads within this area is in general unwanted as they often cause large motions and stress.

Inertia dominated systems: The load frequancy is significantly higher than the eigen-frequancy, $\omega > \omega_0$. The system has too high inertia for any large large stiffness forces to be induced. The response of the system will in general have a small response relative to the force amplitude (Larsen 2014).

1.6 Stress and fatigue calculations

In order to evaluate the feasibility of an operation with respect to structural limitations, the total stress in each section have to be determined. This section gives an introduction of how to calculate different stresses in a tow configuration and also describes how to evaluate them with respect to ultimate limit state (ULS) and fatigue limit state (FLS).

1.6.1 Stress calculations

Different structures are vulnerable to different types of stress. Looking at a tow and installation of a slender pipe, the methods for calculating stresses in the towlines and in a pipe will be described in this section.

Stress in towlines

A towline, consisting of either chain or fibre rope, will for many cases have relatively low bending stiffness. By neglecting bending stiffness, only stress contribution in the lowlines will be axial stress, S_A (or tension). The axial stress will be dependent on the axial force (F_A) acting on the towline and the cross-section area (A):

$$S_A = \frac{F_A}{A} \tag{1.46}$$

The stress capacity of the towline depends on the material and other structural properties of the towline. The capacity is generally given for the towlines in form of ”minimum breaking load” (MBL).

The feasibility of neglecting bending stiffness have to be evaluated from case to case.

Pipe stress

For a circular cylinder there are mainly three stress contributions to the total stress: axial-, bending- (S_B) and hoop stress (S_H). In addition there may also be torsional stress, which for a freely supported tow configuration will be ignored.

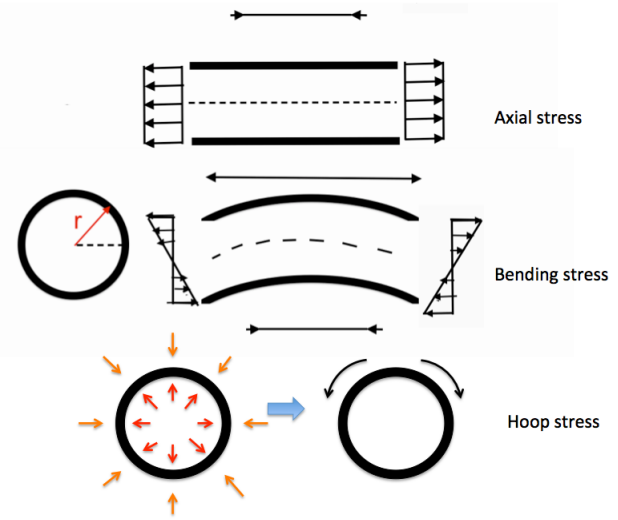

Figure 1.30: Pipe stress contributions

$$S_B = \frac{M}{I} r_{max} \tag{1.47}$$

$$S_H = \frac{R(p_i - p_e)}{2t}, R = \frac{1}{2}(D_o - t) \tag{1.48}$$

Where:

- M Bending moment [Nm]
- I Second area moment
- r_{max} Radius to outer wall, where the stress is largest
- R Center radius
- p_i Internal pressure $[N/m^2]$
- p_e External pressure $[N/m^2]$
- t Wall thickness
- D_o Outer diameter

The resultant axial stress can be calculated as:

$$S_{as} = S_A + S_B + S_H \tag{1.49}$$

Stress concentration factor

Analysing the induced stress in a structure, some critical areas will experience higher intensity of stress than others. These critical areas, also called ”hot-spots”, occur in general in relation to joints, cracks, welds and critical geometric shapes. In order to account for the increased stress in these ares, the stress are multiplied with a ”stress concentration factor” (SCF). The stress concentration factor for different welds, shapes and geometries are determined from DNV 2011b.

1.6.2 Fatigue calculations

Equally important as determining the largest stress with regard to ULS is calculating the fatigue damage. A large fatigue damage during transportation will lead to a reduction in the installed fatigue lifetime. Fatigue damages are in particular important for welded structures.

The fatigue damage is estimated using Miner's sum:

$$D = \sum \frac{n_i(S_i)}{N_i(S_i)} \tag{1.50}$$

Where:

- D — Fatigue damage where D = 1 equals fatigue structural collapse
- S_i — Stress range
- n_i — Number of stress cycles with stress range S_i
- N_i — Total number of stress cycles to failure for stress range S_i

Typical, the contractor of a marine transportation will sett a limit for fatigue damage during the operation, e.g. 10% of the total fatigue lifetime D = 0.1.

The total numbers to failure N_i for a given stress range S_i will be determined from a SN-curve. SN-curves are found in DNV 2011b and will be dependent on the properties of the structure and welds. Figure 1.31 is taken from DNV 2011b and shows different SN-curves for structures in seawater with cathodic protection.

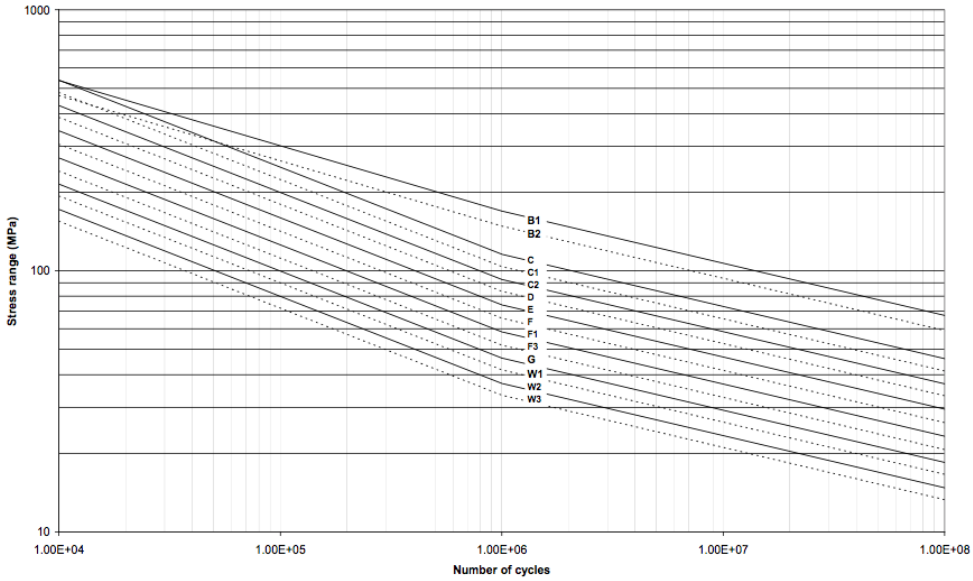

Figure 1.31: SN curves in seawater with cathodic protection (DNV 2011b)

The total fatigue damage on a structure is dependent on the full loading history where both large and small stress cycles will contribute. The most frequently used method for counting stress cycles, accounting for small ”internal cycles” is the rainfall counting method.

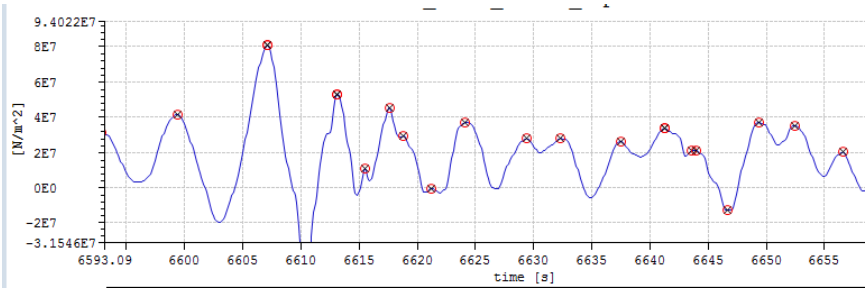

Figure 1.32: Irregular stress series

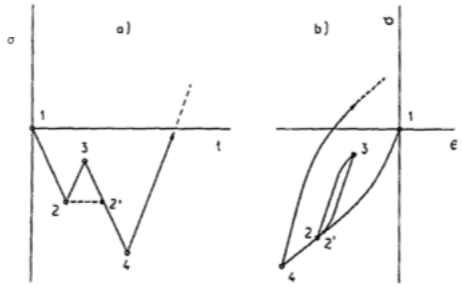

Figure 1.33: Rainflow counting (Berge 2006)

1.6.3 Load resistance factor design (LRFD)

One of the most frequently used structural design method is the load resistance factor design (LRFD) which is described in DNVGL 2015a. The principle behind the method is that the sum of all stresses (S) shall always be less than a designed resistance capacity (R) of the structure, while accounting for proper material and load factors.

$$S_d < R_d \tag{1.51}$$

Where:

- S_d Design stress
- R_d Design resistance

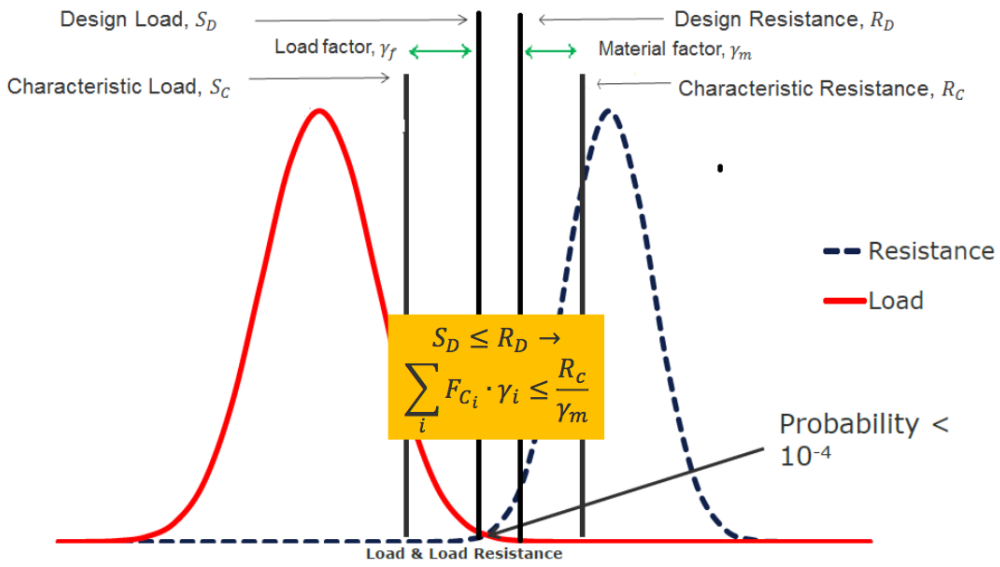

Figure 1.34: Design load and resistance (Larsen 2015)

The design stress and resistance are determined by (for linear load - stress relations):

$$S_d = \sum(\gamma_{fi} S_{fi}) \tag{1.52}$$

$$R_d = \frac{R_k}{\gamma_m} \tag{1.53}$$

Where:

- S_{fi} Characteristic load effect
- R_k Characteristic resistance
- γ_{fi} Load factor
- γ_m Material factor

The characteristic resistance is dependent on structural parameters such as material and geometry.

Design loads are dependent on the type of loading and load effects defined in DNVGL 2015a as:

Table 1.4: Load factor (DNVGL 2015a)

Combination of design loads	*Load categories*			
	G	*Q*	*E*	*D*
a)	1.3	1.3	0.7	1.0
b)	1.0	1.0	1.3	1.0
Load categories are: G = permanent load Q = variable functional load E = environmental load D = deformation load For description of load categories see Sec.2.				

The value of the material factor vary with the different limit state and can be taken as:

Table 1.5: Material factor (DNVGL 2015a)

Table 5-2 Material resistance factor, γ_m		
Limit state category[1)]	*SLS/ULS/ALS*	*FLS*
γ_m	1.15	1.00
1) The limit states (SLS, ULS, ALS and FLS) are defined in D.		

1.7 Load and response statistics

Understanding and being able to describe the dynamic response of a marine system is an important part of analysing and evaluating a marine operation. Also, as sea loads vary with time, and generally are not regular, it is important also to be able to describe the statistical properties of the loads and dynamic response. The statistical variability is divided into short term (20 min - 3 hrs) and long term statistics (3+ hrs - years).

Statistics are used in order to describe the variability of both different load components and dynamic response in form of deformations and stress. The statistical data are typically presented in form of a force/response spectrum. The statistical data are used for structural design and also during planing of different operations. The procedure for a stochastic analysis of a marine structure/operation are in general:

- Establish environmental statistics
- Calculate hydrodynamic forces
- Calculate dynamic response
- Response statistics
- Structural dimensioning/operational design

The following section contains description of how the statistical data are established, the relation between load and response statistics and how to use the statistics in planing and designing a marine operation.

1.7.1 Wave statistics

Wave statistics are divided into short term- and long term wave statistics. Short term statistics describe how the surface elevation varies with time and are described with constant statistical values like significant wave height (H_S) and peak period (T_P). The long term statistics describe how these environmental parameters varies over longer periods.

Short term statistics

An observation of the sea surface elevation will show that the wave series consists of a number of irregular waves. It can be shown that the irregular time series can be described by a sum of different regular waves with different wave heights, periods and phase shifts. By measuring a time series and using super-positioning in order to look at the individual regular wave series, a spectrum in the frequency domain is made. The spectrum describes the distribution of the different regular waves. The super-positioning is mathematically done by a Fouirer (or fast Fouirer-) transformation. Characteristic statistical data in form of H_S and T_P are also calculated.

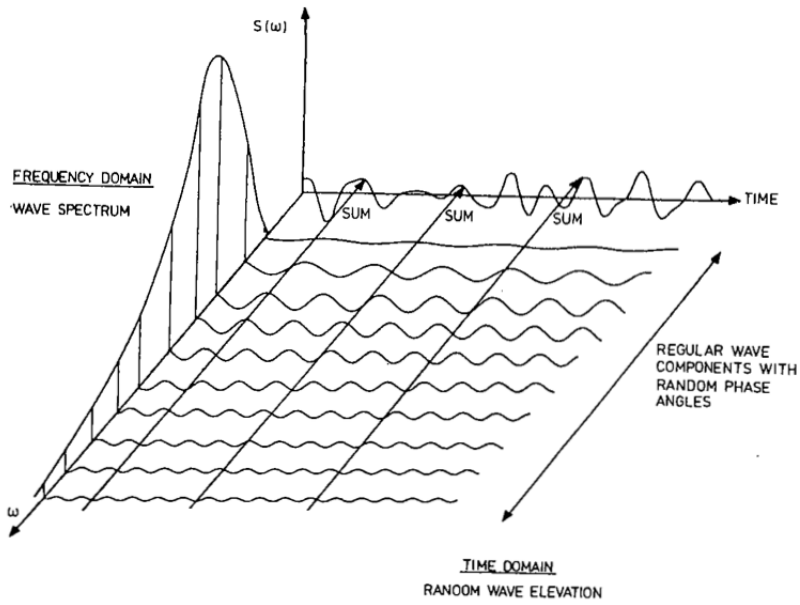

Figure 1.35: Irregular wave spectrum (Faltinsen 1999)

A spectrum will carry the statistical properties of a process such as standard deviation, zero crossing periods and also extreme values.

Gathering sufficient short time statistics is a both time consuming and expensive task, at the same time there's been a lot of research at the area. Therefore there's been developed several standardized wave spectrums which can be adapted to different areas and cases. One of these standardized spectra is the JONSWAP wave spectre which is based on a large range of statistical data from the southern part of the North sea.

For a given wave spectrum it is possible to make a short term time realization of a stochastic wave proses by an inverse Fouirer transformation:

$$\zeta(t) = \sum \zeta_{ai} sin(\omega_i t + \varepsilon_i) \tag{1.54}$$

$$\zeta_i = \sqrt{2 S_\zeta(\omega_i) \Delta\omega_i} \tag{1.55}$$

Where:

- $\zeta(t)$ Instantaneous surface elevation
- ζ_{ai} Wave amplitude of wave "i"
- ω_i Wave frequency of wave "i"
- ε_i Random phase shift

Using a sett of random phase angles ε_i will give a unique realization of the spectrum, using different phase angles will give a totally different realization. Even though the different time realizations will be unique, they all have the same (or almost the same) statistical properties in form of mean value and standard deviation. A computer program will make time realizations using pseudo-random number series for ε, each series defined by a "seed number". Each seed number will generate a specific time realization which can be regenerated.

Characteristic most probable maximum wave height for a JONSWAP wave spectre are defined in DNV 2014b as:

$$\frac{H_{Max}}{H_S} = \sqrt{\frac{1}{2} ln(N)} \tag{1.56}$$

Long term statistics

The long term statistics describes how the statistical parameters, like H_S and T_P, vary over a longer period of time. Long term wave statistics are usually presented as a scatter diagram. The scatter diagram for a specific area shows the number of occurrences for different combinations of H_S and T_P. From the diagram one can calculate the probability for a particular sea state or the cumulative probability for a sea state.

1.7.2 Response statistics

The same way as the wave loads can be described by a statistical spectrum, the response may be presented in form of a response spectrum. The response spectrum is established based on short term wave statistics. The procedure from a wave spectrum to a response spectrum will now be explained.

In section 1.4 the calculation method for estimating environmental forces was explained. The relation between a characteristic environmental property and the related forces can in general be presented as the following:

$$F_0(\omega) = H_H(\omega) \cdot \zeta_0(\omega) \tag{1.57}$$

Where H_H is a hydrodynamic transfer function related to Morison's equation. The equation is valid given the relation between wave and wave load is linear.

In the same manner it is possible to describe the relation between a load and response. The response can either represent a stress or an induced motion. The relation can be written as:

$$x_0(\omega) = H_M(\omega) \cdot F_0(\omega) \tag{1.58}$$

H_M is here a mechanical transfer function.

By combining the two equations 1.59 and 1.58 the response can be written in form of:

$$x_0(\omega) = H_M(\omega) \cdot H_H(\omega) \cdot \zeta_0(\omega) = H_x(\omega) \cdot \zeta(\omega) \tag{1.59}$$

Where H_x is the total transfer function, describing the linear relation between wave amplitude and response (Larsen 2014).

Further it can be shown (Larsen 2014) that the relation between the wave- and response spectrum can be expressed as:

$$S_x(\omega) = H_X^2(\omega) \cdot S_\zeta(\omega) \tag{1.60}$$

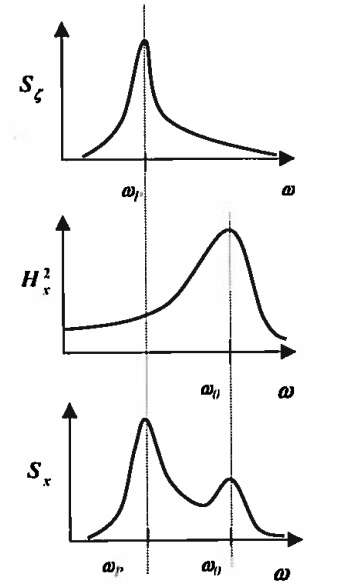

Figure 1.36: Wave- to response spectre (Larsen 2014)

From figure 1.36 one can see that both the wave spectral peak period ω_P and the system eigenfrequency ω_0 will be represented in the response spectre.

The response spectrum may also be obtained from a response time series, similar to the wave elevation previously described. Distribution of time series symmetric about the mean value is called a normal, or Gaussian distribution. Characteristic values to describe the response spectrum are mean value and standard deviation σ. The standard deviation is an indication of how much the time series values vary from the mean, where most of the individual response values will lay within the boundaries of the standard deviation. The time series may be obtained from numerical time integrations as described in the next section.

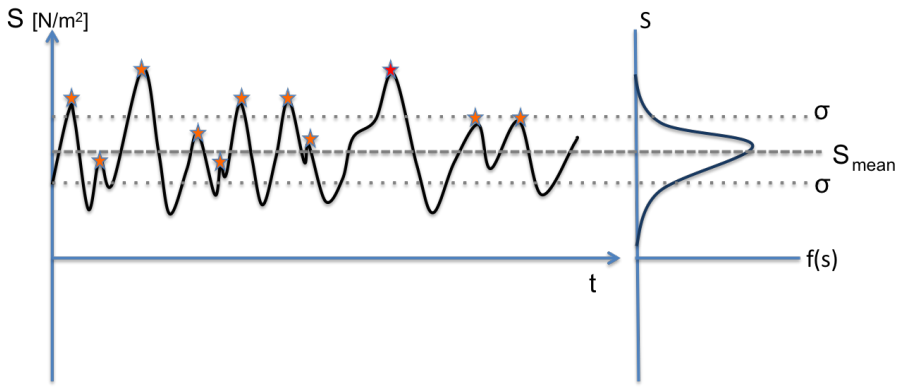

Figure 1.37: Response spectre from time series

Logging the individual peaks in the time series, a peak spectrum may be obtained ($f_{peak}(S)$), describing the probability of individual response peaks. Analysing the maximum value from several time series, a distribution of the extreme values may be obtained ($f_{MAXpeak}(S)$).

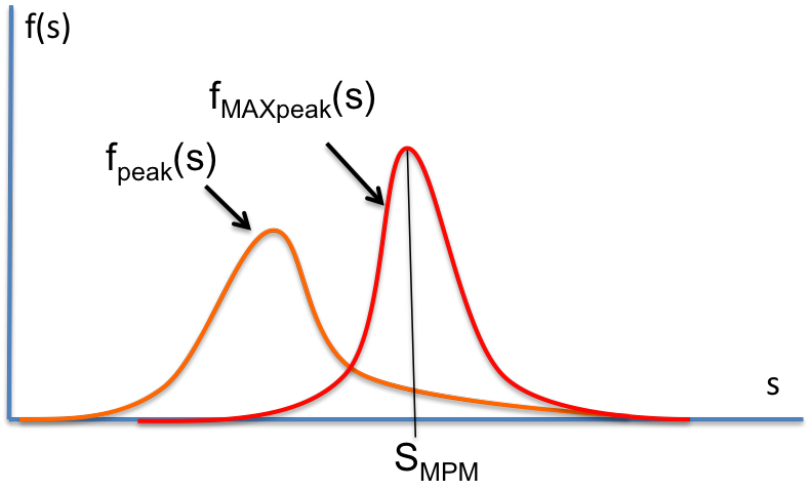

Figure 1.38: Response peak and extreme value spectre

The top of the extreme value distribution describes the most probable maxima (MPM) and may for a Gaussian distribution be calculated as:

$$S_{MPM} = \sigma\sqrt{2ln(N)} \tag{1.61}$$

Where :

- S_{MPM} Most probable maximum response
- σ Standard deviation
- N Number of individual peaks

1.8 Numerical simulations

Large parts of this section are taken from the pre-project report

Computer aided numerical simulation analysis are a useful engineering tool used more and more frequently. Numerical simulations provides the opportunity to study the behaviour of systems whose mathematical models otherwise are too complex to solve. The application areas for numerical simulations are many, some of the most common are:

- Verification of new concepts
- Verification or design of solutions/operations
- Sensitivity analysis of different design or load parameters
- Analysis of coupled system or non-linear behaviour
- Establishment of operational criteria/limitations for a solution/operation
- Analysis of fatigue damage

Numerical simulations are conducted in either time- or frequency domain, depending on the simulation model and load effects.

1.8.1 Frequency domain

In frequency domain simulations a harmonic load with a fixed load amplitude and frequency is applied to a system in order to determine the response of the system. By preforming several simulations for different frequencies a response spectrum or a transfer function can be established for the system. The transfer function describe the relation between a load and response amplitude. Solutions in the frequency domain are normally obtained for large structures in order to establish a response spectrum or in order to identify natural frequencies in a system. Frequency domain analysis are usually used for fatigue analysis or for moderate environmental conditions. A frequency domain analysis may also be used in order to conduct parametric studies and to generate quick estimates. The advantage of using frequency domain is that the computation is relatively simple and efficient compared to time domain.

1.8.2 Time domain

Time domain simulations are required in order to capture non-linear load or response effects and will give a more realistic result than a frequency domain simulation. A time domain simulation will be the preferred method in cases where non-linear loading are of importance, and for multi body coupled systems with non-linear dynamic response. A time domain simulation is therefore the preferred for the case of a tow operation.

A time domain simulation will generate a time varying realization of the environmental forces, as described in section 1.7, and calculate the response for each time increment. The response is calculated using setts of mass- damping- and restoring matrices which is updated between each time step. The dynamic response will be dependent on the instantaneous force, behaviour of previous time step as well as the dynamic properties of the system (section 1.5).

Internal structural response in form of deformations and forces/stress are calculated for each body using finite element method (FEM). FEM analysis divide the body into several elements and connecting nodes. The internal forces are then calculated for each time step in all nodes/elements.

The result of a time domain simulation is a time series of the different response parameters, such as position, velocity, acceleration and stress. The result will be a complete representation of the response, including non-linear effects. Further, the time series may also be transformed into a response spectre though a Fourier transformation.

The duration of a time domain simulation is recommended to be at least 3 hours for irregular sea states, in order to provide sufficient statistics (DNV 2014a).

Chapter 2

Heidrun tension-leg platform

Heidrun is a tension leg platform (TLP) located at the northern part of Haltenbaken, approximately 190 kilometres of the western coast of Norway at 345 meters depth. The platform was the world's first concrete TLP developed by Conoco Norway, installed in 1995 and is now run by Statoil (Conoco Norway Inc 1994) (Statoil).

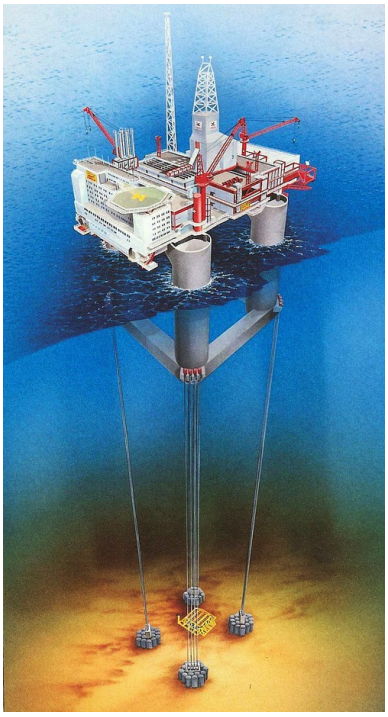

(a) Heidrin TLP (oljemuseum 2015)

(b) Location of Heidrun TLP (Google maps)

Figure 2.1: Heidrun TLP

The platform has a total of 16 tethers that are scheduled to be replaced within the next following years. The tethers consists of pipe-sections of 22 meters each, which will be welded together at a location at Gullvika, Namsos. From there, each tether will be towed in one piece to installation site. The towing method of choice is a control depth-/near surface tow configuration as illustrated in figure 1.2.

During the initial installation of the Heidrun TLP in 1995, the 16 tethers was transported individually from a location outside of Trondheim by a in-surface tow method. A few hours into the second tow, large vessel motions due to port-side waves were reported. Measurements were taken accordingly and the tow operation proceeded. Some hours later into the operation the foremost buoyancy element detached itself which ultimately resulted in loss of the tether. The tow operations were designed to withstand a sea-state of H_S = 5 meters T_P = 11.5, still the weather conditions of the incident was reported to be significantly less with H_S = 2.5 meters, T_P = 6 sec.

After the incident, measurements were taken, and the remaining tethers as well as a spare tether was successfully installed. The incident did not lead to any serious delays, and the installation of the TLP was completed the same year (Berge 2006) (Norwegian Contractors 1995).

2.1 Tow route

The 16 replacement tethers for the Heidrun TLP is planed to be transported from the location Gullvika, Namsos out to the Heidrun TLP. The Heidrun field is located in the northern part of Haltenbak in the Norwegian sea, approximately 190 km of the west coast of Norway.

The total travelling distance is approximately 218 kilometres, or around 117 nautical miles. The first 21 nautical miles of the route will consist of navigating through the deep and narrow fjords, from Namsos out to open waters. The last part of the of the route is a 96 nm stretch over the open waters of the Norwegian sea.

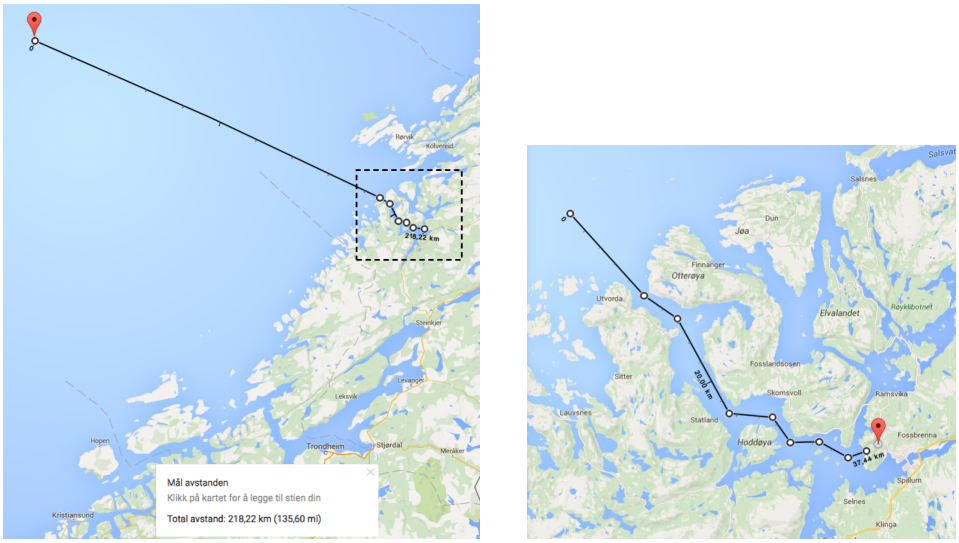

(a) Location of Heidrun TLP (Google maps)

(b) Inshore route

Figure 2.2: Transport route

2.2 Equipment

2.2.1 Tether

The following tether specifications are given by Statoil in ref.Statoil. Segment length and weld type given by supervisor Prof. II Kjell Larsen.

As the tether consists of welded tether-segments, hot-spot stress has to be evaluated according to DNV 2011b.

Table 2.1: Specifications for Heidrun tether

Heidrun tethers	
Number of tethers	16
Tether length	263 $[m]$
Tether segment length	22 $[m]$
Outer diameter	1.118 $[m]$
Wall thickness	0.038 $[m]$
Cross-section area	0.12898 $[m^2]$
Axial stiffness ($\frac{EA}{L}$)	105 $[MN/m]$
Yield tension	480 $[MPa]$
Maximum ULS design load	47.7 $[MN]$
Material	High tensile steel
Material density, ρ	7850 $[kg/m]$
Segment weld type	One side butt weld
Tether sealed, containing air at atmospheric pressure	

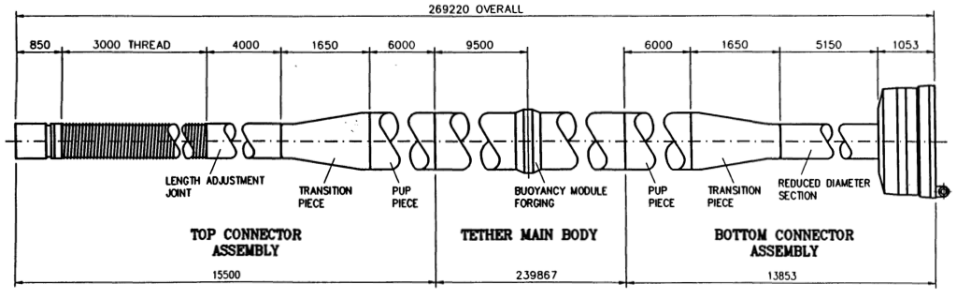

Figure 2.3: Tether assembly (Norwegian Contractors 1991)

2.2.2 Vessel

The tow and installation operation is planed to be preformed by the use of two platform supply vessels (PSV). The vessel data are taken from case specific hand-out from Prof. II Kjell Larsen. Vessel RAOs are given in appendix A.

Table 2.2: Vessel specifications for PSV

PSV data for tow operation	
Length, L_{PP}	84 $[m]$
Beam, B	20 $[m]$
Draught, D	5.8 $[m]$

The ship RAOs are established by Statoil, from analysis using Wamit software program. The result RAOs shows a heave eigenperiod of around 6 - 7 seconds and a very large roll eigenperiod around 11 seconds. The most critical direction for both eigenfrequencies are beam sea.

Related to a tow operation, a beam sea condition with frequencies around the heave eigenperiod of 6 seconds will lead to large induced ship motions. For a tow configuration sensitive to vessel motion induced loads this will mean a large undesirable response. The RAO curve in heave also show a far less vessel response in sea headings less than 90 degrees.

Environmental loading in the region of roll eigenfrequency equal to 11 seconds will in general not significantly affect the tow system, but will be undesirable due to crew safety and comfort.

2.2.3 Tow lines

The most utilized towlines for transport of marine constructions consists of either chain, wire, synthetic fibre (polyester or nylon) or in some cases, a combination of these. The most important towline properties to considerer when choosing towline are (**Larsen2015**):

- Breaking load
- Stiffness
- Handling
- Weight
- Damping properties
- Wear and corrosion

For the case analysis of this thesis, two towline types are considered, one of studded chain and one of synthetic nylon fibres. The line properties for this study are taken from KTL.

Table 2.3: Spesifications for studded chain lines KTL

Table Of Minimum Breaking Load: Anchor & Chafe Chain

Chain Diameter	Approximate Weight per metre	Minimum Breaking Load (metric tons)	
(mm)	(kg/m)	Grade 2 U2	Grade 3 U3
48	53	129	185
52	62	151	215
54	66	162	231
58	77	185	265
60	82	198	282
64	93	223	319
68	105	250	357
70	112	263	376
73	121	284	407
76	132	307	438

Table 2.4: Spesifications for nylon fibre lines KTL

Table of Minimum Breaking Load: Single & Double Part Nylon Towing Stretchers

Nylon Body (Single part) Size		Approximate Weight (kg/m)		*Minimum Breaking Load (metric tons)	
Diameter (mm)	Circle (inches)	Single Stretcher	Double Stretcher	Single Stretcher	Double Stretcher
80	10	3.85	7.70	110	220
96	12	5.45	10.90	152	304
112	14	7.50	15.00	189	378
120	15	8.00	16.00	230	461
130	16	8.89	17.78	270	540

*Splicing efficiency already taken into consideration

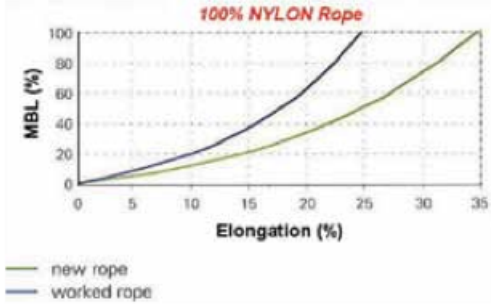

Table 2.5: Line elongation for nylon fibre lines KTL

Choosing a synthetic fibre rope, one also have to be aware that all fibre ropes change propertied with time and load history. The change in properties will in general not be of any significant magnitude during a tow operation, but in cases where the lines have been used in previous operations one have to be aware that the properties may not be the same.

2.3 Environment

Environmental data for the Heidrun field are provided by supervisor in form of MetOcean data (Nygaard 2004). The data include long term weather statistics of wind, waves and current as well as a general guidance to the modelling of the environment.

2.3.1 Waves

The following plots taken from Nygaard 2004 illustrates the cumulative probability distribution of different significant wave heights (fig. 2.4) and conditional scatter diagram of significant wave height and peak period (fig. 2.5).

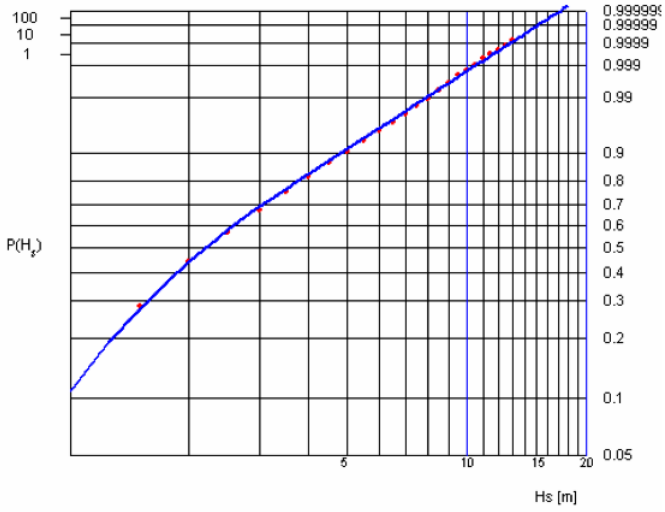

Figure 2.4: Cumulative probability distribution of H_S at the Heidrun field (Nygaard 2004)

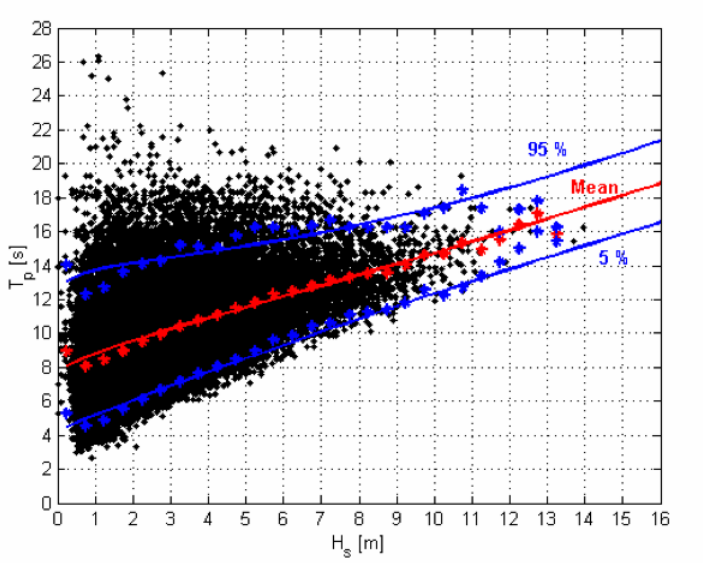

Figure 2.5: Scatter diagram of H_S and T_P at the Heidrun field (Nygaard 2004)

The total wave pattern will in reality be a product of both wind- and swell generated waves. The two wave contributions will for most cases have a different directional propagation. However it will in general be conservative to assume that these contributions propagate in the same direction.

For a wave realization model based on an arbitrary combination of H_S and T_P Nygaard 2004 recommend the Torsethaugen spectral model. This spectrum represents both wind- and swell generated waves and is essentially a combination of two JONSWAP like spectra. The Torsethaugen spectrum defines a boundary T_{pb} between a wind dominated and a swell dominated region in equation 2.1. For response calculations with critical conditions close to this boundary, a simple spectral model like the JONSWAP spectrum will be sufficient.

$$T_{pb} = 6.6 H_S^{0.333} \tag{2.1}$$

2.3.2 Current

The Metocean data basin (Nygaard 2004) do not provide data for currents at depths less than 50 meters. For the purpose of this thesis, the current velocity and current profile will be established based on the theory of wind generated currents, described in section 1.4, and typical values of tidal currents.

Typical value of tidal current are discussed with supervisor Prof.II Kjell Larsen and for this thesis taken as 0.25 m/s.

The wind velocity $u_{1hr,10m}$, used to calculate the wind induced current in equation 1.14 will be based on statistical wind data given in Nygaard 2004. The value of $k = 0.02$ in equation 1.14 will be used. The wind velocity for a given wave condition defined by H_S and T_P is selected using figures 2.4 and 2.6 and assuming $P(H_S) = P(Windspeed)$. The profile of the depth varying wind currents is established using equation 1.15.

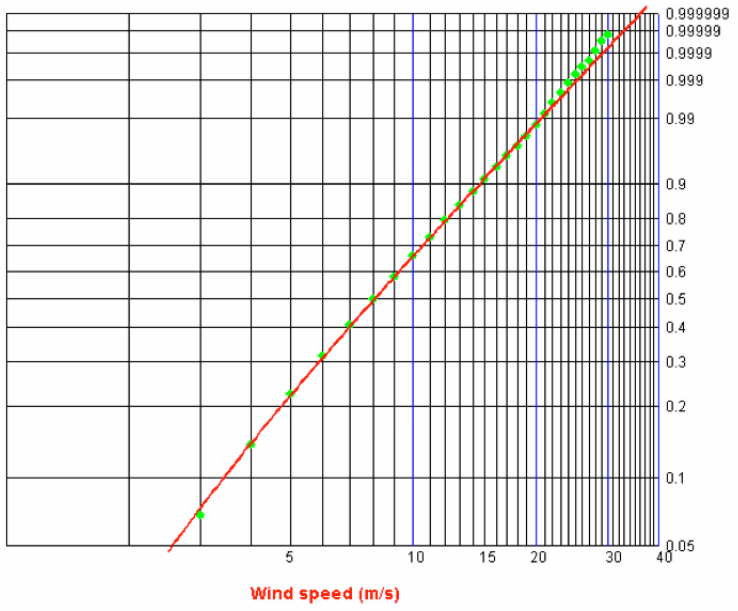

Figure 2.6: Probability curve of wind speed (Nygaard 2004)

Chapter 3

SIMA simulations

In order to study the effect of different environmental loads and establish operational limitations of a submerged tow and installation operation numerical simulations have been conducted. The simulations are preformed using MARINTEK's SIMA and RIFLEX software programs. The simulations are based on time domain theory in order to analyse effect of non-linear loads and behaviour of the coupled system. The establishment of operational limitations will be based on fatigue calculations as well as extreme value statistics and "hot-spot" stress related to ULS.

The particular case that's been studied are a near surface/control depth tow and upending of a tether for the Heidrun TLP. The simulation model for the towing operation was developed during the pre-project (autumn 2015) and further developed and improved during the work of this present thesis. The model used in simulations of the upending operation has further been adapted from the towing model.

3.1 SIMA

Section taken from pre-project report, based on fact sheet for SIMA software

The SIMA workbench is an engineering software and analysing tool for marine operations and floating systems developed by MARINTEK. The software is a great tool for simulations of non-linear time domain analysis of large and complex systems. 2D and 3D graphics from the simulations makes it easy to understand the result and also identify possible challenges.

Typical simulation analysis preformed using SIMA are lifting operations, installations, transportation, station keeping, analysis of riser systems, wind turbines and more.

Using SIMA allows the user to model a complex system of multiple bodies. Examples of

different model elements in SIMA are vessels, cranes, winches, finite elements of slender structures, coupling elements and thrusters. Environmental conditions are modelled by a selection of wave, wind and current models. While modelling in SIMA a graphic model of the system is continuously updated in order to make the modelling process as easy as possible for the user.

After a system model is prepared the SIMA workbench can be used to preform static, non-linear time domain, fully coupled, eigenvalue and VIV analysis. The workbench also includes a post-processor feature and a workflow engine in order to make the post processing of the simulation data from one or several simulations as simple as possible. A workflow engine also makes it easy to conduct, and compare the results from several different conditions. SIMA also include the ability to interact with external programs.

3.2 Riflex

Large parts of this section is taken from the pre-project

Riflex software is a program system implemented into SIMA workbench, tailor-made for static and dynamic analysis of slender marine structures. The Riflex program system is developed by MARINTEK and is also a part of SESAMs DeepC package for coupled analysis of mooring and riser systems.

RIFLEX conducts simulations in the time domain with the option of implementing several different irregular environmental loadings. The program is developed for analysis of mainly slender structures and slender structure systems, calculating forces based on Morrison's equation as previously described in this thesis

As part of the SIMA workbench the Riflex application can be used to analyse both structural and hydrodynamic analysis of slender structures in irregular waves and currents.

3.2.1 RIFLEX limitations

RIEFLEX is a great engineering tool for estimating loads and response. In order to properly evaluate the results it is important to understand the limitations of the program. The main limitations related to the simulation results from RIEFLEX will be presented in this section.

As Riflex uses Morison's equation to calculate the hydrodynamic forces the accuracy of the results provided by Riflex are limited by the accuracy of the underlying theory. Several limitations to the Morison's equation may be discussed, even though the equation is widely accepted a good method for estimating hydrodynamic forces on slender structures.

Based on Morisons equation, Riflex do not take into account the effect of hydrodynamic pressure variation over the structure induced by waves (diffraction forces), as these are neglected using Morison. This simplification is justified by the wave force theory where

diffraction forces on a slender in wave conditions $\frac{\lambda}{D} \gtrsim 5$ are negligible compared to the inertia- and viscous damping forces.

The drag and mass coefficients used to calculate the forces using Morison's equation in RIFLEX are user defined and will be constant throughout the simulation. A good estimate of these coefficients are therefore crucial in order to get a good estimate of the response. Conservative estimated of C_D and C_A has to be made, as these value will be constant during the simulation. In reality these values will vary with time and be dependent on a number of factors.

The wave forces are modelled in RIFLEX based on a stochastic time realization of a user defined wave spectre. In order to make a good prediction of the extreme value statistics, several simulations with different wave seeds (see 1.7) are required.

The simulation results will also be dependent on the time integration step defined by the user. An accurate presentation of internal structural response will be limited to the number of elements and the element types, also user defined.

Riflex is based on the theory of Morisons equation, which is based of some simplifications. Therefor Riflex is not suited for the study of complex or detailed hydrodynamic effects. This would have to be done using CFD software.

Using Riflex, the motion of the support vessels are calculated RAOs for the vessels. The motion of the vessel will affect the slender system (given they are connected) but the forces acting on the slender structure will not affect the motions of the vessel using Riflex.

Using Riflex alone, a study of VIV and VIV lock-in phenomena is not possible . In order to ensure that the system out of risk of lock-in, a VIV lock-in check has to be conducted separate. This check may be preformed by either compare the system eigenfrequencies to hand-calculations of the vortex shedding frequency, or by other computational methods. VIVANA by MARINTEK is separate software program in the SIMA workbench well suited for the VIV studies analysis. SIMA also offers the ability for coupled RIFLEX-VIVANA simulations in order to account for VIV (will not be discussed further).

Riflex cannot simulate forward moving systems, making it hard to analyse the effects of encountering waves for a moving system. Conservative measurements has to be made accordingly.

3.3 Simulation model

Two Riflex models have been made in order to preform simulation analysis on both the tow operation and the upending operation for the Heidrun TLP tethers. The model of the tow configuration was made in the pre-project (autumn 2015), and further developed during the work of this master's thesis (spring 2016). The model for simulation of the upending operation have later been adapted from the tow model.

The models are based on the case and equipment earlier described for the Heidrun platform, consisting of two towing vessels, two towlines and the transported tether.

Both models are made to be easily adaptable to simulate different configurations and conditions. The parameter variables for both models are as following:

- H_S [m] Significant wave height
- T_P [s] Peak period
- $DirWave$ [deg] Wave direction
- $DirCurrent$ [deg] Current direction
- Vcw [m/s] Velocity of wind induced current (at surface)
- C_d [-] Tether drag coefficient (relative velocity formulation of Morison)
- h [m] Tow depth
- L_{tl} [m] Length of towlines
- D_{tl} [m] Diameter of towlines
- $Mass_{tl}$ [kg/m] Mass of towlines
- K_{tl} [N] Towline stiffness (EA)
- MBL_{tl} [N] Minimum breaking load of towlines
- W_{rel} [-] Relative submerged weight of towlines
- V_S [m/s] Forward vessel speed
- T_{tug} [kg] Horizontal tug hold-back tension

3.3.1 Towing model

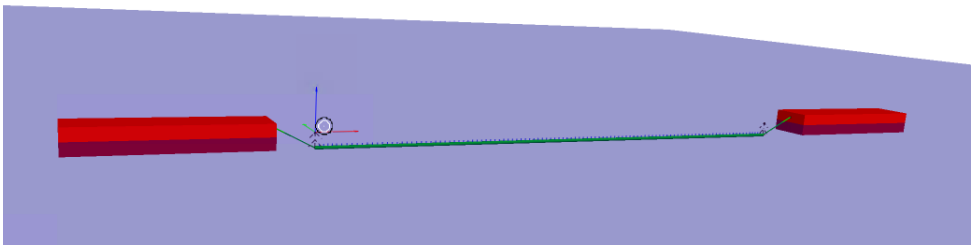

Figure 3.1: SIMA simulation model, tow operation

Model

The model for the towing simulations consists of three elements, vessels, towlines and tether. The different elements are connected by supernodes sett free to rotate.

Tow vessels

The towing vessels are based on the PSV hand-out data described previously. The response of the vessels are defined by an input-file containing ROA data. The ships are visualized by a simple box, with the main dimensions given i table 2.2, and a height of 11.6 meters.

Towlines

For the simulations of this thesis two different types of towlines are modelled, one representing a studded chain towline and one representing a synthetic nylon rope. The two line types have different properties regarding weight, stiffness, dimensions and load capacity. The towline data are based on lines found in ref. KTL.

Both line types are modelled as axisymmetric pipe-sections. The cross-section is defined as bar-elements having axial stiffness and axial deformations only. This is a simplification, justified by the fact that chains and nylon ropes have a relative low bending stiffness.

The properties defining the towlines are:

- Mass coefficient [kg/m]
- External area [m^2]
- Axial stiffness (EA) [N]
- Hydrodynamic diameter [m]
- Quadratic drag coefficient in x- and y-direction C_D [-]
- Added mass coefficient [-]
- Tension capacity [N]
- Line length [m]
- Number of elements

The mass coefficient are the in-air weight of the line. The external cross-section area are made a function of the relative submerged weight in order to get the correct submerged weight. The relative submerged weight for the chain and nylon rope are 0.87 and 0.1, respectively.

The hydrodynamic diameter is the diameter used to calculate forces in Morison's equation. These values are sett equal to the chain- and fibre rope diameter.

The axial stiffness of the towlines are defined by the elasticity of the material, E, and the cross-section are of the line, A, $k = EA$. The material elasticity of steel chain and nylon rope are for the simulations taken as:

- $E_{steel} = 3.5 * 10^7$ [KN/m^2]
- $E_{Nylon} = 6.0 * 10^6$ [KN/m^2]

The elasticity of a synthetic nylon rope are calculated from Hooke's law, assuming a linearised force/elongation relation given in figure 2.5.

The drag coefficients are taken according to DNVGL 2015b:

Table 3.1: Towline drag coefficients DNVGL 2015b

Table 2 Drag coefficients

Mooring component	*Transverse*	*Longitudinal*
Stud chain	2.6	1.4
Stud less chain	2.4	1.15
Stranded rope	1.8	*
Spiral rope without plastic sheathing	1.6	*
Spiral rope with plastic sheathing	1.2	*
Fibre rope	1.6	*
(*) Longitudinal forces may often be neglected in these cases or the expressions from DNV-RP-C205 may be applied.		

2.7.2 Other drag coefficients may be accepted provided they are properly documented.

Added mass coefficients are taken equal to 1.0.

Tension capacity are taken equal to the towline MBL.

Tether

The tether model is a simplified model of the main body tether for the Heidrun platform described in section 2, with clamp-on weights at the ends. The tether is modelled as a steel pipe, consisting of three segments and two different axisymmetric cross-sections.

The middle section, section 2, represent the plain main body tether. This section is modelled with a constant outer diameter of $D_O = 1.118$ m and properties according to table 2.1. The value of the drag and added mass coefficients, C_D and C_A, are sett equal to one.

The end segments of the tether, segment 1 and 3, represents tether segments with added clamp-on weights. These segments are modelled the same way as segment 2, with an additional pipe coating representing the added weight and volume of the clamp-on weights. The added weight sections are assumed to have a length of 10 meters on each end, and having the same properties as steel. The thickness of the added steel coating are modelled after the principle of vertical force equilibrium, being a function of the tug hold-back tension, submerged weight of the tether with clamp-on weights and also towline length, -weight and -vertical angle.

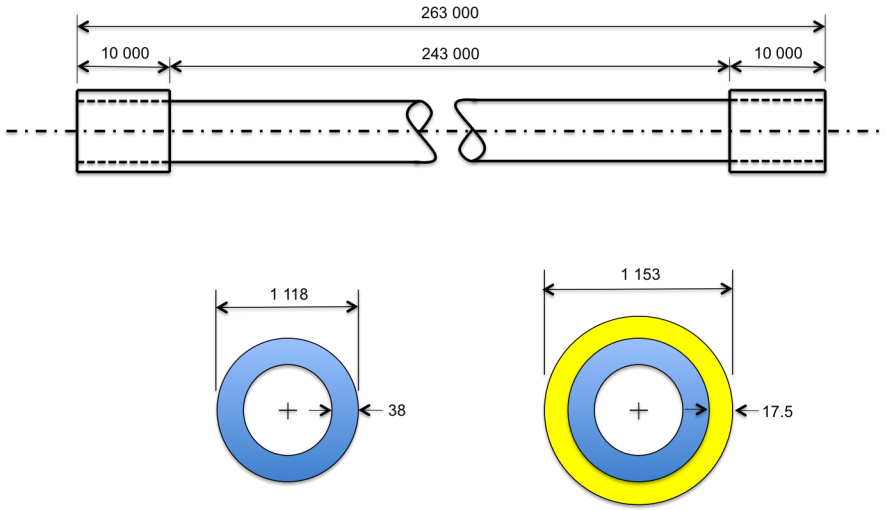

Figure 3.2: SIMA simulation tether model(base case)

The plain tether section (section 2) is divided into 100 elements, each 2.43 meters. The added weight sections (section 1 and 3) are divided into five elements, each of 2 meters.

The weight specifications for the tether without clamp-on weights are as following:

Table 3.2: Tether weight specifications, no clamp-on weights

Thether weight spesifications		
Weight in-air per unit length	W_{air} $[kg/m]$	1012.1
Submerged weight per unit length	W_{subm} $[kg/m]$	5.87
Weight in-air	W_{air} $[kg]$	266 182.3
Submerged weight	W_{subm} $[kg]$	1543.9

Forces

The environmental forces modelled in the simulation model are wave-, current- and ship induced forces. Even though the model offers the ability for different current- and wave heading, it is assumed that the they are of the same direction, as this would be the most critical condition for most situations.

Wave forces

The wave environment is modelled as a time realization of irregular Airly linear waves, following a 3-parameter JONSWAP spectrum. The wave spectrum is defined by user input of H_S and T_P and a default value of $\gamma = 3.3$. It may be argued that a two peak

wave spectrum gives a better representation, but for the case of this thesis a JONSWAP spectrum is assumed to be satisfying.

For the kinematic model of the wave forces, integration to mean water level method is chosen (method 1 in figure 3.4).

No low frequency motions induced by waves are accounted for.

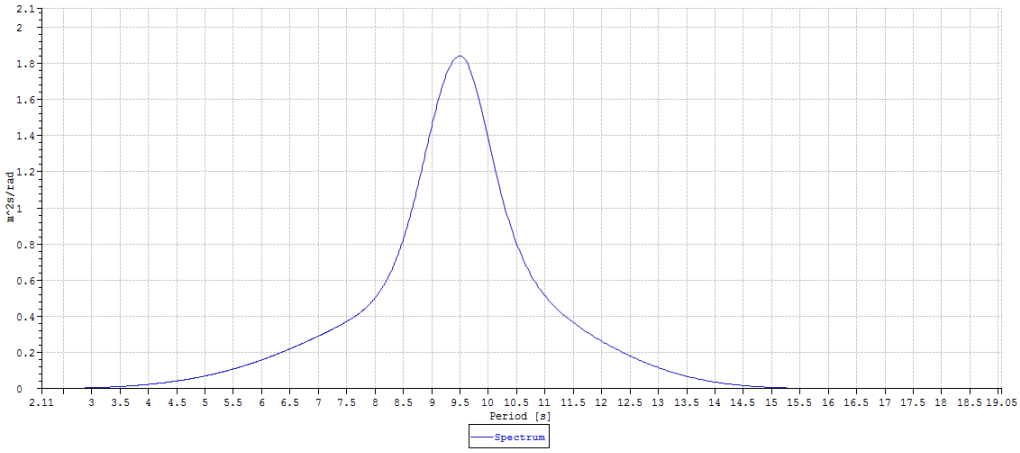

Figure 3.3: SIMA simulation wave spectrum

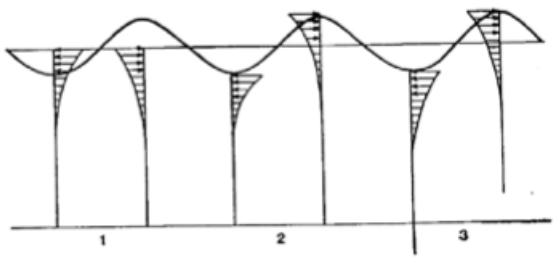

Figure 3.4: SIMA simulation wave potential model (MARINTEK)

Current forces

The simulations are modelled to include both tidal- and wind induced currents. It is assumed that both current contributions are of the same heading. The vertical current profile is modelled according to the theory described in section 1.4.4.

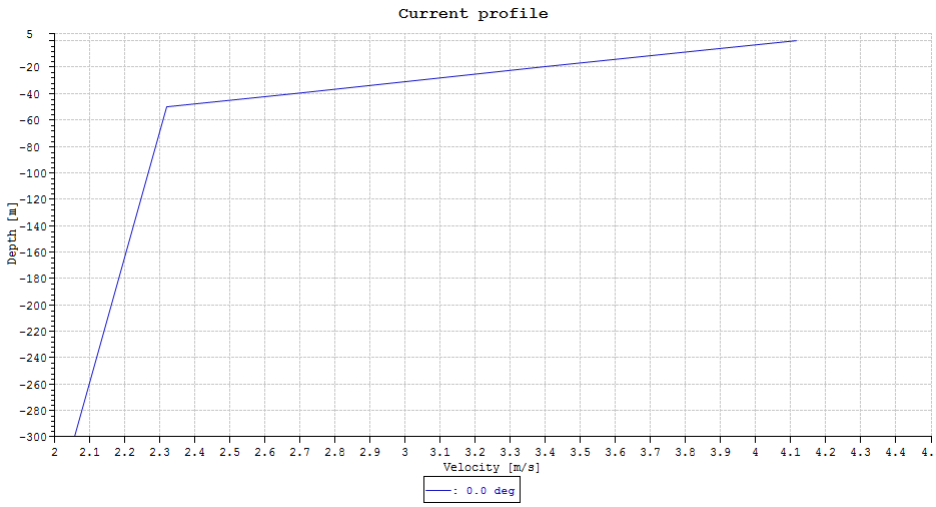

Figure 3.5: SIMA simulation current profile (Base-Case)

Vessel motions

The vessel induced loads on the tow system are dependent on the forces motion of the connection points on the support vessel. As Riflex do not account for the forces acting on the support vessels from the towed system, as mentioned earlier, the motion of the ship is based on the input file of the ship's RAO and the incoming waves only.

As Riflex cannot simulate a forward moving system, the effect of wave encounter frequency is not taken into consideration, as it is not a straightforward task. This is a limitation in the model that can be improved. However this only affects the frequency of the forces and not the force amplitude and since loading from VIV (which is dependent on load frequency) is not simulated by Riflex it can be argued that this simplification will not greatly affect the end result (taken from pre.project).

The effect of a forward moving tow is included in the current model, which encounters for the static loading from a forward moving system. This is done by adding a current contribution in head direction and velocity equal to the vessel speed.

Base-Case model

In order to evaluate a tow configuration and compare the affect of different parameters, a base-case model is established. The input parameters for the base-case are:

Table 3.3: Base-case input-parameters

Input parameters: Base-Case

Name	Value	Description
$H_S\ [m]$	2.5	Significant wave height
$T_P\ [s]$	9.5	Peak period
$DirWave\ [deg]$	0	Wave heading
$DirCurrent\ [deg]$	0	Current heading
$V_{cw}\ [m/s]$	1.8	Velocity of wind induced current in surface
$C_D\ [-]$	1.0	Tether drag coefficient
$h\ [m]$	7	Tow depth
$L_{tl}\ [m]$	22	Towline length
$D_{tl}\ [m]$	0.112	Towline diameter
$Mass_{tl}\ [kg/m]$	7.5	Weight of towline
$K_{tl}\ [N]$	5.911e+07	Towline stiffness (EA)
$MBL_{tl}\ [N]$	1.854e+06	Minimum breaking load of towline
$W_{rel}\ [-]$	0.1	Relative submerged weight of towline
$V_S\ [m/s]$	2.0577	Ship speed
$T_{tug}\ [kg]$	10 000	Tug hold-back tension

Here, the 112mm nylon fibre rope from KTL, table 2.4 are used. With the tow depth and towline length chosen, the vertical towline angle equals 22°. The towline for the base-case is divided into 10 elements, each 2.2 meters.

The thickness of the tether coating, representing the added weight and buoyancy of the clamp-on weights, are calculated by a vertical force equilibrium. The weight and size of the tether ends will thereby be a function of the towline and the tow configuration, as mentioned in the previous section. For the base-case, the thickness is calculated to be 17.5 mm. This gives the following tether weight specifications:

Table 3.4: Tether weight specifications, with clamp-on weights

Thether weight spesifications, with clamp-on weights

Tether weight in-air	$W_{Tet-air}\ [kg]$	266 182
Tether submerged weight	$W_{Tet-subm}\ [kg]$	1 544
Clamp-on weight in-air (per end)	$W_{CO-air}\ [kg]$	4 900
Clamp-on submerged weight (per end)	$W_{CO-subm}\ [kg]$	4 261
Total weight in-air	$W_{Tot-air}\ [kg]$	275 980
Total submerged weight	$W_{Tot-subm}\ [kg]$	10 065

Simulation parameters

The length of the tow operation simulations follows the recommended length of three hours, given by DNV 2014a.

The time increment of each response calculations is sett to 0.015 seconds. The Riflex manual (MARINTEK) recommends a time increment of 70 - 200 time steps per avarage load period. For a base-case of $T_P = 9.5$ sec, this equals a time step of 0.14 - 0.048. How ever, for low tension problems and problems where snap-loads may occur, a finer time step is required.

During the simulation, Riflex is sett to store the following data:

- Displacements of supernodes (connection points)
- Displacement of mid-tether
- Forces in all elements of tether and towlines
- Envelope curves for tether and towlines

3.3.2 Upending model

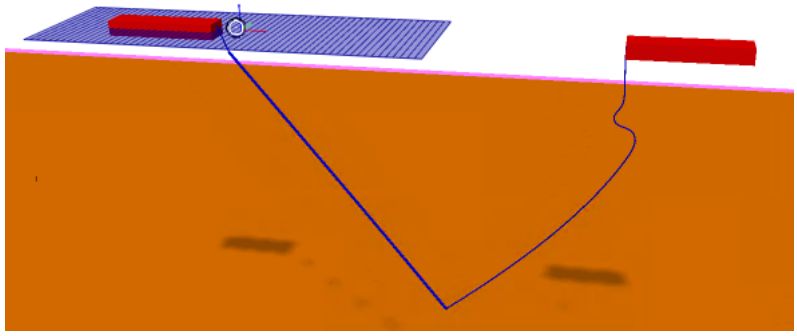

Figure 3.6: SIMA simulation model, upending operation

Model

In order to simulate an upending operation, a separate models are made, adapted from the towing model. For the upending operation, both vessels are kept in the same position during the whole time period, still including wave induced motions, while the tailing vessel releases more towline.

The upending model is made with the same input parameters as the towing model with some additional options:

- Removal of clamp-on weights at tailing end
- Removal of tailing towline in order to simulate ”free-drop”
- Varying towline feed rate

The feeding of towline is simulated by increasing the segment length of the tailing towline. Because of the large length of towline needed during the upending, the number of elements in the tailing towline is increased to 100.

Forces

The wave model is the same as for the towing simulations. The current model are simplified to a uniform current of constant velocity.

During a horizontal to vertical upending of a long slender structure, the vertical current variations may be of great importance. However it is difficult to measure and also to make a good profile representation as there are many different current contributions (section 1.4). The current model is therefore a simplification related to some uncertainty. The current model will be applicable for a brief study of the importance of the current in one direction.

Simulation parameters

Simulating the upending operations, the duration of the simulations will be dependent on the upending speed. The duration of the simulations are therefore adapted to each case till the tether has reached a stable vertical orientation.

The time increment of the simulation calculations is reduced to 0.001 seconds in order to get a stable solution.

For the ”free-drop” simulations, the tailing towline is removed. The tailing end of the tether is then fixed for the first 20 seconds of the simulation, before it is instantly realised.

During the upending simulations, the following data is logged:

- Displacements of supernodes (connection points/ end points)
- Displacement of mid-tether
- Forces in all elements of tether and towlines
- Envelope curves for tether and towlines

Base-Case model

In order to evaluate a upending operation and compare the affect of different parameters, a upending base-case model is established.

Simulating the base-case scenario, no environmental wave or current forces are present.

The upending base-case simulates a ”free-drop” of the tailing tether end, with clamp-on weights from base-case tow operation. Also the same base-case towline from the towing simulations are used.

The input parameters for the base-case are:

Table 3.5: Upending base-case input-parameters

Input parameters: Upending Base-Case

Name	Value	Description
$H_S\ [m]$	-	Significant wave height
$T_P\ [s]$	-	Peak period
$DirWave\ [deg]$	-	Wave heading
$DirCurrent\ [deg]$	-	Current heading
$V_{cw}\ [m/s]$	-	Velocity of wind induced current in surface
$C_D\ [-]$	1.0	Tether drag coefficient
$h\ [m]$	7	Tow depth
$L_{tl}\ [m]$	22	Towline length (start)
$D_{tl}\ [m]$	0.112	Towline diameter
$Mass_{tl}\ [kg/m]$	7.5	Weight of towline
$K_{tl}\ [N]$	5.911e+07	Towline stiffness (EA)
$MBL_{tl}\ [N]$	1.854e+06	Minimum breaking load of towline
$W_{rel}\ [-]$	0.1	Relative submerged weight of towline
$V_S\ [m/s]$	0.0	Ship speed
$T_{tug}\ [kg]$	10 000	Tug hold-back tension

3.4 Post processing of simulation results

The post processing of the simulation data are mainly handled in SIMA's post processor and in Microsoft excel. The presentation of the post processing will be divided into SIMA- and excel post processing of tow- and upending simulations.

SIMA's post processor is a user-friendly, module based data processor. The system makes it easy to get an overview for the post processing and is very flexible. SIMA post processor is great for visualization and statistic analysis of large amount of simulation data.

Microsoft excel is used in order to store and compare relevant simulation results and in order to preform post processing which cannot be done in SIMA, or is more easily pre-formed in excel. Simple calculations used to check the simulation results, or check data against requirements are also handled in excel.

3.4.1 Towing post processing

From the towing simulations, it is of interest to study the characteristic behaviour of the induced forces and loads, in both towlines and the tether, throughout the different simulations.

SIMA post processor

For the analysis of the towing simulation, a SIMA post processor task is made (figure 3.9) with the option of the following output:

- Axial forces, bending moments and pipe stress
- Time series
- Cumulative distribution (Rayleigh or Weibull)
- Spectrum, relating the frequency dependence of the induced loads
- Statistics (Maximum, mean and standard deviation)
- Envelope curves, illustrating the highest value over the lines/tether
- Fatigue damage

The pipe stress in the tether are calculated in eight points for each tether element, and are a product of axial-, bending-, and hoop stress are described in section 1.6.1.

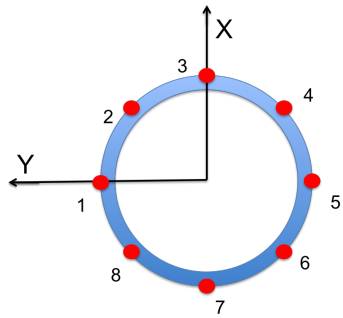

Figure 3.7: Cross-section stress calculation points

The fatigue damage are estimated using rainflow counting method and calculating Miner's sum damage. The SN-curve for the fatigue calculation is taken from DNV 2011b, choosing the F3 curve (figure 1.31) in seawater, with cathodic protection, correcting for thickness factor. The stress concentration factor (SCF) for the welds are calculated according to DNV 2011b:

$$SCF = 1 + \frac{3\delta_m}{t} e^{-\sqrt{t/D}} = 1.2 \tag{3.1}$$

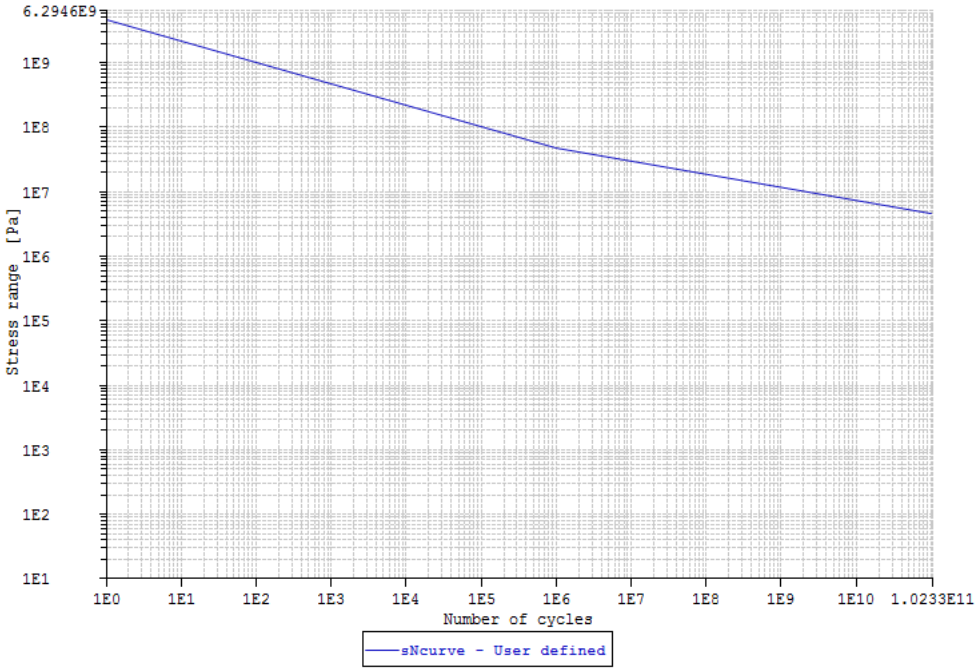

Figure 3.8: SN curve for tether

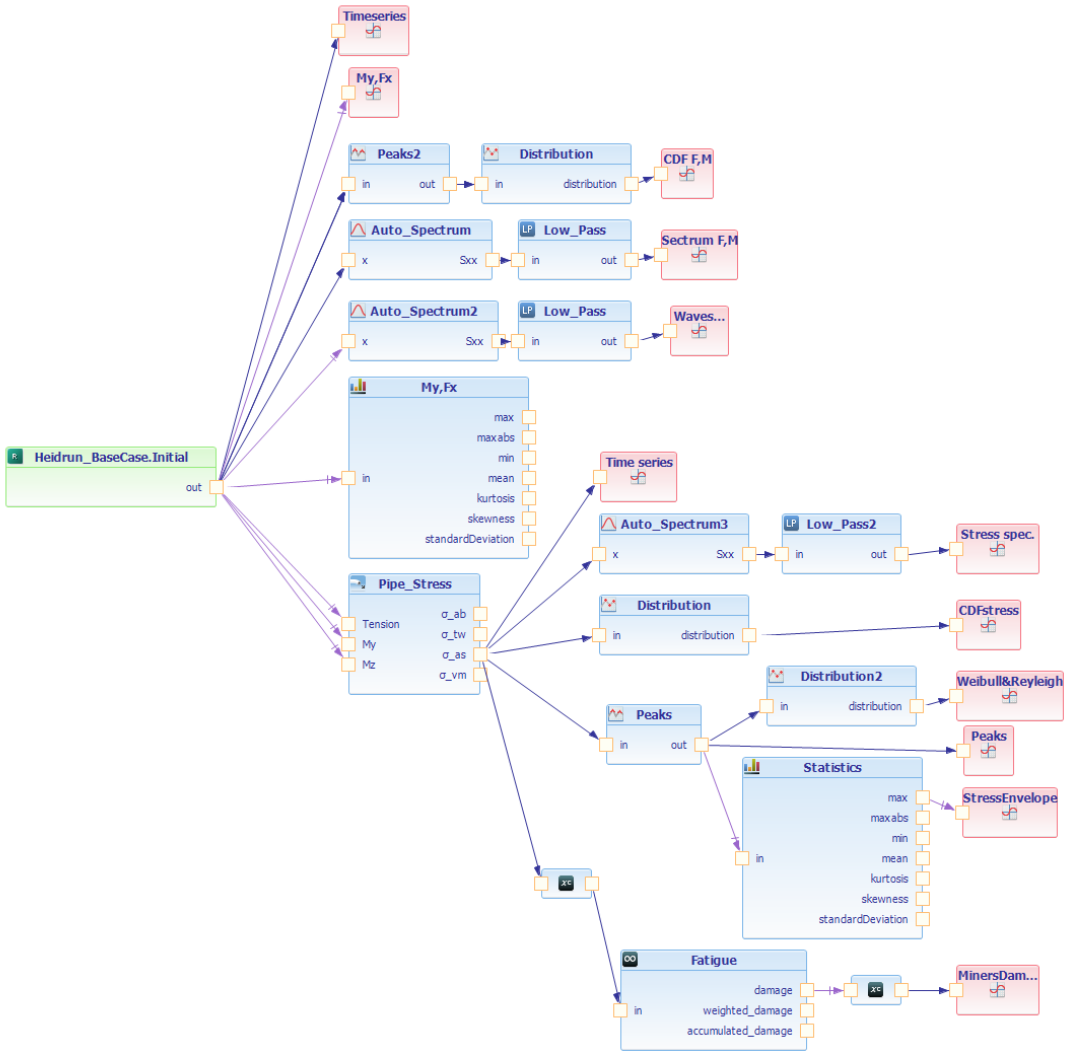

Figure 3.9: SIMA post processor, towing model

Excel post processing

As previously mentioned, excel is used in order to store and post process simulation data in order to easily evaluate and compare the results. The main data which are calculated and evaluated in excel are:

- Stress in towlines and tether
- Maximum induced stress: value, time and position
- Axial-, bending-, and hoop stress contribution [%]
- Static and dynamic stress contribution [%]
- Design resistance, -stress, -hot-spot stress and -utilization (LRDF)
- Total fatigue damage of offshore tow
- Vortex shedding frequency

From the simulations, data of the maximum induced stress in both towlines and tether are collected in form of stress magnitude, time and position. With these data, the induced forces at the time and positions are gathered in order to calculate the value of the different stress contributions. These data are then evaluated and used to calculate the design stress and resistance according to the LRDF-method (section 1.4)

The estimates of fatigue damage are calculated based on a reference period (T_R) of the offshore tow stretch and the hourly fatigue damage from SIMA. The contingency period of the offshore tow operation are taken as 50% of T_{POP}. This is based on the premise that the towing operation is thoroughly planed and the tow speed has been properly assessed (Section 1.3).

$$T_R = T_{POP} + T_C = 1.5 * \frac{96[nm]}{4[knots]} = 36[hrs] \tag{3.2}$$

The fatigue damage are estimates based on the assumptions of constant environmental conditions throughout the offshore tow. The assumption of fatigue damage during the offshore stretch only, is justified by the general calm waters inside the fjords. The validity of this simplification may be discussed.

3.4.2 Upending post processing

A SIMA post processor task and a excel sheet has also been developed for the upending simulation analysis. As the upending operation has a much shorter duration than the tow operation, the fatigue damage during the upending is neglected.

SIMA post processor

The SIMA post processor for the upending simulations is illustrated in figure 3.10, and offers the following outputs:

- Forces and stresses related to tether and towlines
- Plot of time series
- Peaks of time series
- Statistics (maximum, mean and standard deviation)
- Envelope curves

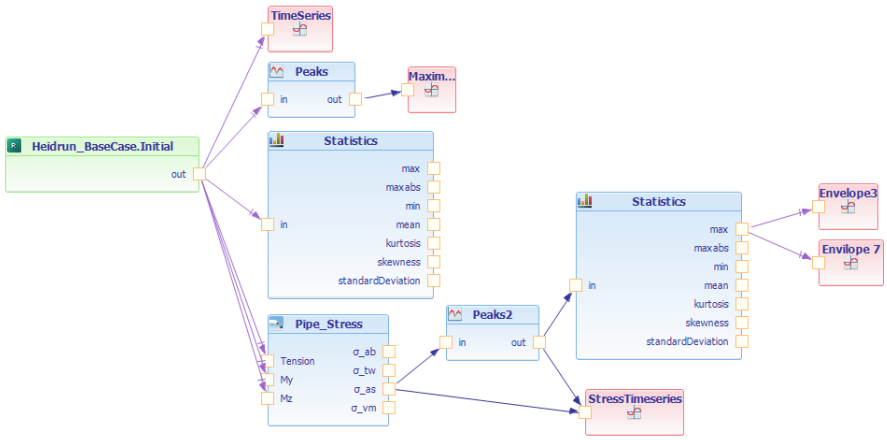

Figure 3.10: SIMA post processor, upending model

Excel post processing

In the excel post processor for the upending simulations, the following data are stored and calculated:

- Maximum induces stress in tether and towlines: value, time and position
- Axial- and bending induced stress
- Utilization of design- and hot-spot design stress
- Total time of upending

As the static induced stresses from weights and hydrostatic pressure changes with time during the upending, the design stress is calculated using only the environmental load factor. This is a conservative simplification.

Chapter 4

Results and discussion

During the thesis work, several Riflex simulations have been preformed of both a tow- and upending operation in order to study and evaluate different solutions and configurations. Results and discussion of the simulations will be presented in the following chapter.

The locations of the tether stresses corresponds to the element number of the model, where 1 is the front-most element and 110 the last element.

The calculated design stress, design resistance and utilization of design are calculated accordign to LRDF method described in section 1.6.

4.1 Towing

Analysing the tow operation, a parametric study have been preformed in order to increase the understanding of different load effects, locate critical areas/hot-spots and establish operational limitations in terms of H_S and T_P. A more detailed description of the analysis approach and results are presented in the following sections.

As a short recap, the following simulation have been conducted:

Table 4.1: Towing simulations

Towing simulations

Number	Name	Description
1	Base-Case (B.C.)	Base-case scenario, described in section 3.3.1
2	Seed 2	Base-case with different wave seed
3	Seed 3	Base-case with a third wave seed
4	T_P = 15	Increase wave peak period
5	T_P = 6	Decrease wave peak period
6	H_S = 3.5	Increase significant wave height to 3.5m, same T_P
7	H_S = 4.5, T_P = 8	Increase significant wave height to 4.5m, 5% bottom T_P value
8	H_S = 5.5, T_P = 9	Increase significant wave height to 5.5m, 5% bottom T_P value
9	90 deg, T_P = 6	Base-case with beam weather
10	Long line	Increase length of towline to 66 meters, same tow depth
11	Chain	Base-case with chain towlines
12	No Vessels (N.V.)	Base-case with no towing vessels, upper towline ends fixed
13	N.V. T_P = 15	No vessels, increased peak period
14	N.V. T_P = 6	No vessel, decreased peak period
15	N.V. H_S = 3.5	No vessel, increased wave height

The key results of these simulations are:

Table 4.2: Simulation results: towing

Key results: Towing simulations

Case	Position of max		Design stress [MPa]			Utilization of design [%]			Fatigue damage
	Stress	Fatigue	Tether	Welds	Towline	Tether	Welds	Towline	Tether
1	82	77	140	173	52	33.51	41.44	34.21	0.1332
2	87	77	144	178	56	34.39	42.66	36.78	0.1296
3	88	77	140	173	52	33.53	41.48	33.91	0.1296
4	71	68	152	188	48	36.45	45.14	31.65	0.1152
5	90	24	232	286	99	55.68	68.45	66.38	0.4320
6	79	56	189	234	88	45.39	56.07	59.32	0.3276
7	88	56	255	310	108	61.01	74.16	73.33	0.7056
8	88	42	281	341	135	67.36	81.77	91.56	1.0044
9	10	39	289	351	107	69.26	84.02	72.07	0.7740
10	57	57	128	157	49	30.56	37.65	32.36	0.1260
11	81	43	161	201	171	38.58	48.09	62.23	0.1663
12	75	78	56	73	19	13.36	17.39	11.23	0.0028
13	73	77	80	102	21	19.23	24.32	12.80	0.0126
14	24	24	37	50	16	8.89	11.91	9.26	0.0003
15	75	79	74	95	25	17.76	22.55	15.46	0.0100
Design resistance tether			417 MPa						
Design resistance fibre rope			188 MPa						
Design resistance chain			347.5 MPa						

*Tether positions corresponds to element number, 1 - 110

The weather conditions for the simulations may be divided into six conditions from the wave statistics for the operation area (A - F):

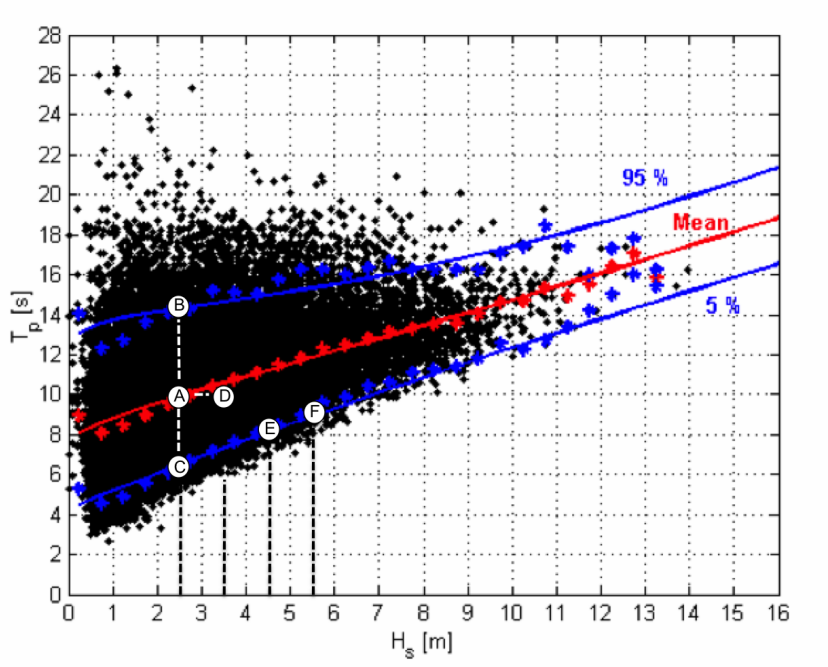

Figure 4.1: Simulation weather conditions

4.1.1 Eigen frequencies

In order to evaluate if resonance behaviour are in risk of being induced, the eigenfrequencies are established using Riflex and compared against environmental loads. As Riflex do not have the ability to simulate the effects of vortex shedding, the eigenfrequencies are also checked against calculations of vortex related drag and lift forces.

The eigenfrequencies are also compared against RAO curves of the connection points on the vessels.

Simulation method

The eigenfrequencies of the tow system are determined by a Riflex eigenvalue analysis.

The simulation model used for the eigenvalue simulation are a base-case tow configuration, where the vessels are removed and the towline end points are fixed in all degrees of freedom.

The first 10 eigenfrequencies are evaluated as the more high frequent eigenfrequencies are in general related to low response.

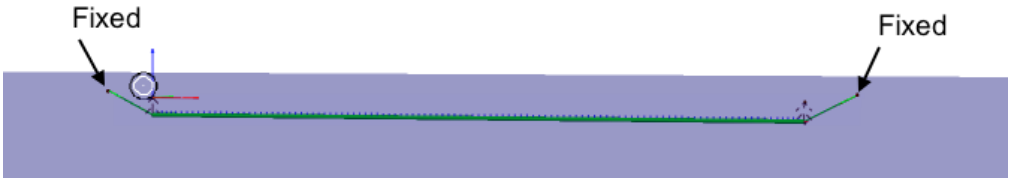

Figure 4.2: Base-case configuration model, no vessels

The frequencies of vortex induced lift and drag forces are calculated as described in section 1.4. The case of vortex induced lift and drag forces are related to beam weather ($DirWave = DirCurrent = 90$).

The RAO of the vessel attachment points are calculated from known ROA values for the centre of gravity, using theory described in section 1.4, equation 1.24.

Results

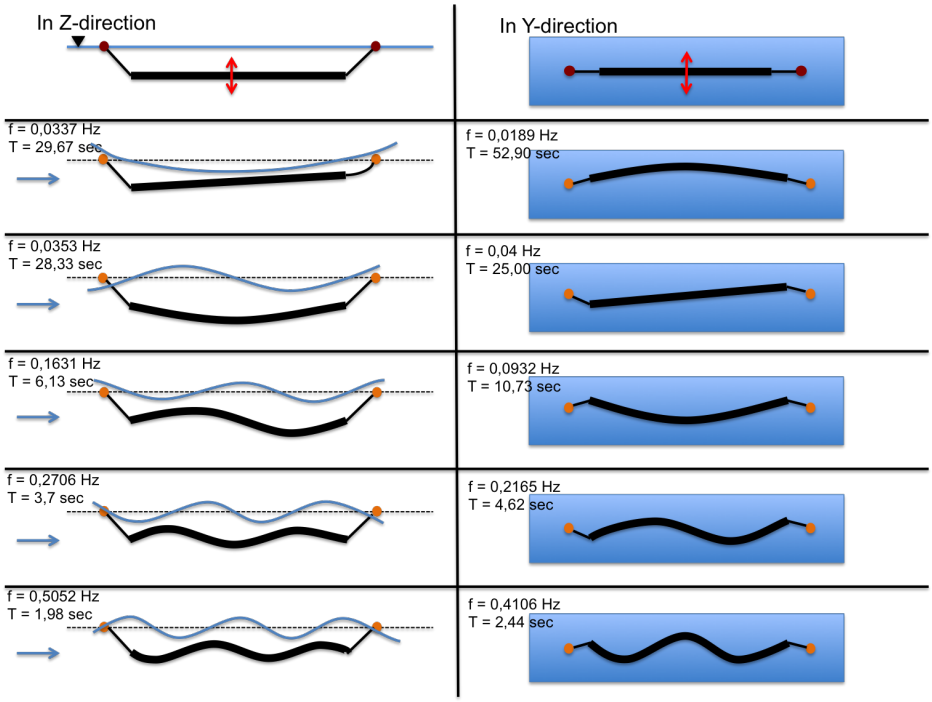

Figure 4.3: System eigenfrequencies

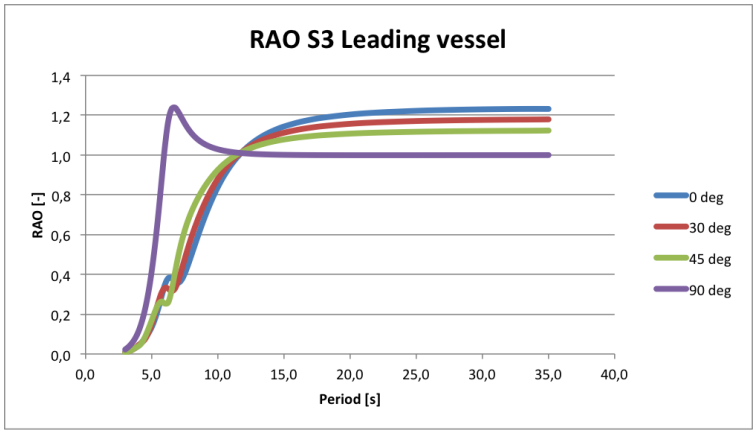

Figure 4.4: Coupled heave motion RAO for leading vessel attachment point

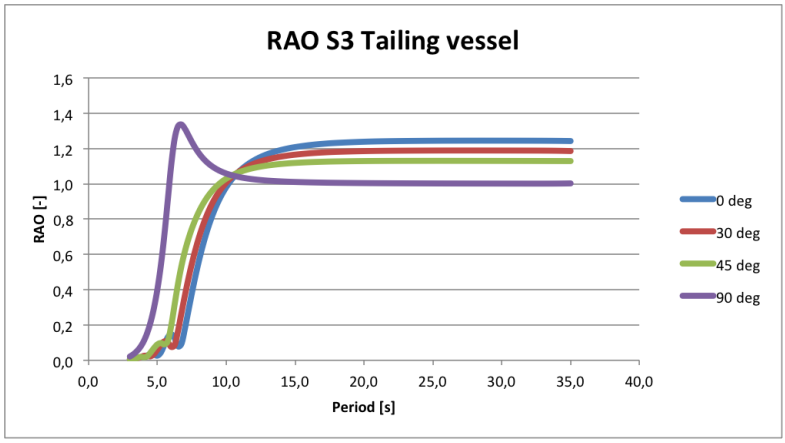

Figure 4.5: Coupled heave motion RAO for tailing vessel attachment point

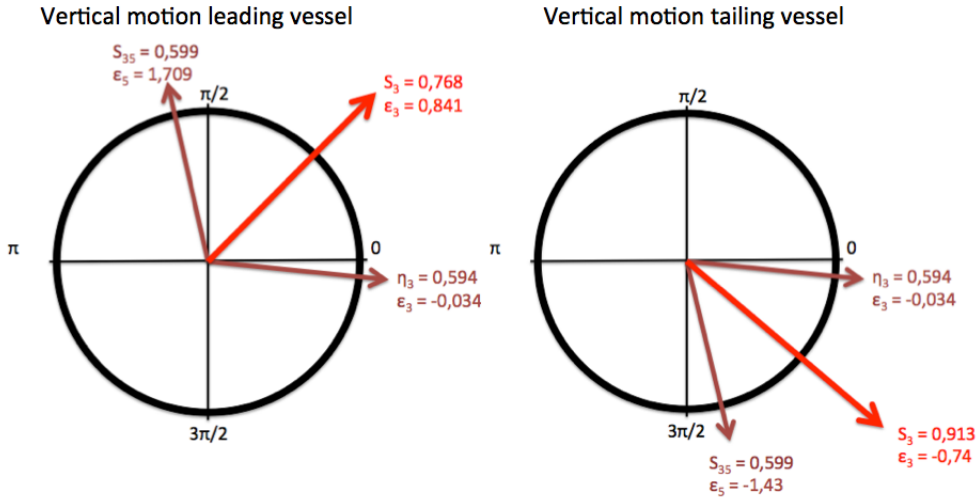

Figure 4.6: Heave and pich contribution of coupled motion, $T = T_P^{BC} = 9.5sec$

Vortex related lift- and drag force frequencies:

Table 4.3: Vortex related force frequencies

Frequency of vortex induced forces, Base-case weather conditions		
Force	**Unit**	**Period**
Lift force period, T_{Fl}	$[s]$	1.86
Drag force period, T_{Fd}	$[s]$	0.54

Discussion

Analysing the result presented above, it is observed that the system eigenfrequency in z-direction for mode 3 almost coincide with the frequency of maximum response for the attachment points $90°$, with $T_{m3} = 6.1sec$ and $T_{S3} = 7sec$, respectively. Comparing with the wave scatter diagram for the area in figure 2.5, wave periods of $T_P = 6 - 7sec$ are a common range for $H_S < 3m$. The similarity of frequencies are unfortunate and suggest a large system response in beam waves $T_P = 6 - 7$ sec. Altering vessel heading, RAO curves indicate a significant reduction of ship motions. Altering the vessel heading, large response may still occur as a result of the system eigenfrequency and vertical wave forces, that is if wave forces are of importance.

Comparing the calculated frequency of vortex induced lift force in table 4.3 with the heave eigenfrequency of mode 5, the frequencies are $T_{Fl} = 1.86$ and $T_{m5} = 1.98$, respectively. The similar frequencies suggests that resonance VIV behaviour may occur for base-case weather conditions of beam heading. Resonant VIV behaviour are however not expected, as the wave induced velocity will vary significantly over time, altering the shedding frequencies. The vortex shedding will however contribute with a force. The magnitude of this force and the induced response are not assessed and have to be further investigated.

Figure 4.6 illustrates the contribution of vessel heave and pitch motion to the total coupled heave motion of the towline attachment points, at base-case weather condition $T_P = 9.5$. The figure illustrates that the heave and pitch motion are around $90°$ out of phase, leading to no cancellation effects of motions. The heave and pitch motions appears to be of almost equal importance. The illustrations suggests that the attachment point in the tailing vessel will experience somewhat larger motions, compared to the leading vessel.

4.1.2 Critical areas and ”hot-spots”

By identifying potential critical stress locations on the tether it is possible to change the tow configuration, or make other improvements in order to reduce the risk of structural damage.

Analysing the ultimate- and fatigue distribution over tether will also give a better understanding of the response behaviour of the system.

Simulation method

The critical areas for both ultimate stress and fatigue damage are assessed by analysing envelope curves from several simulations and conditions. A brief description of the simulations are described in table 4.12. The envelope curves describes the distribution of ultimate stress and fatigue damage over the tether throughout the simulation. Eight points around the tether cross-section are evaluated (see figure 3.7).

”Hot-spot” stress in the tether will occur in the welds connecting the tether segments (22 meter segments, section 2.2.1). The added stress in the welds are estimated by a stress

concentration factor (SCF), which for the tether is calculated using equation 4.1, from DNV 2011b as described in section 3.4.

The envelope curves for all simulations are analysed. Some key results are presented below.

Results

Location for maximum stress and fatigue damage for simulations:

Table 4.4: Simulation results: critical locations

Key results: critical locations		
Case	**Position of max**	
	Stress	**Fatigue**
1	82	77
2	87	77
3	88	77
4	71	68
5	90	24
6	79	56
7	88	56
8	88	42
9	10	39
10	57	57
11	81	43
12	75	78
13	73	77
14	24	24
15	75	79
*Tether positions corresponds to element number, 1 - 110		

Envelope curves illustrate the distribution over the mid tether segment, without clamp-on weights only. The locations represent segment element numbers 1 - 100, front to back location.

Values in envelope curves corresponds to characteristic stress in tether and not design stress or weld stress.

Fatigue damages are given in Miner's sum damage per hour.

Stress and fatigue envelope curves for base-case (case 1) and beam weather (case 9):

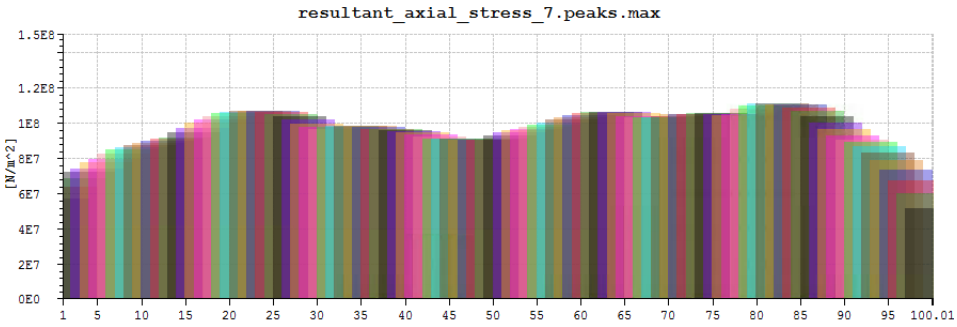

Figure 4.7: Stress envelope curve: Base-case

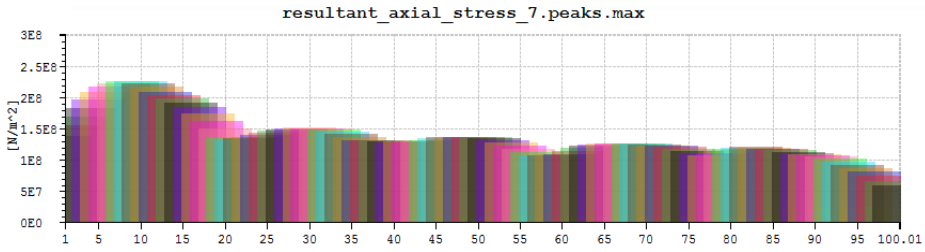

Figure 4.8: Stress envelope curve: Beam weather (case 9)

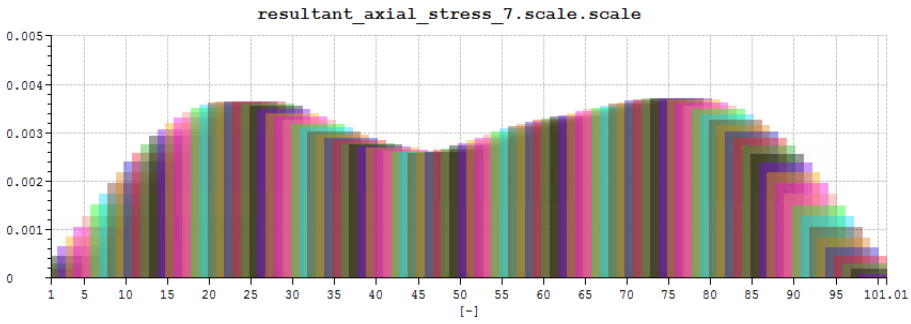

Figure 4.9: Fatigue envelope curve: Base-case

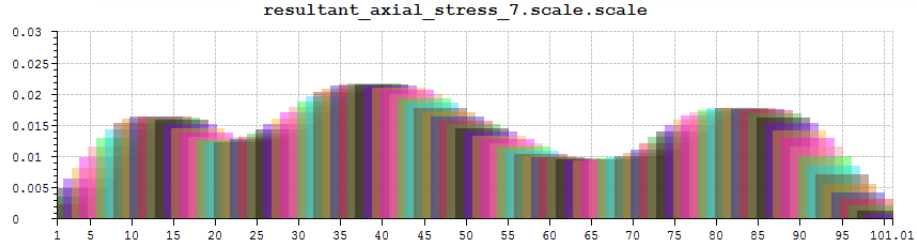

Figure 4.10: Fatigue envelope curve: Beam weather

Fatigue envelope curve for $T_P = 15$ (case 4):

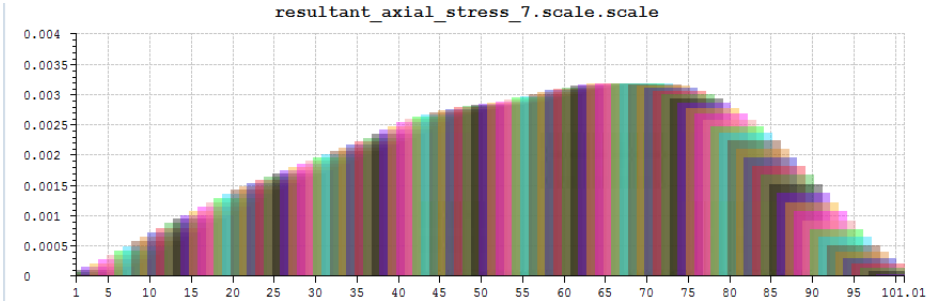

Figure 4.11: Fatigue envelope curve: Inceased T_P (case 4)

Stress concentration factor are calculated as previously described in section 3.4:

$$SCF = 1 + \frac{3\delta_m}{t} e^{-\sqrt{t/D}} = 1.2 \tag{4.1}$$

Discussion

The base-case stress envelope curve (figure 4.7 indicate little variation in the area ≈ 15 - ≈ 93. This indicate that no particular eigenmode are excited and no significant critical area, which is fortunate. If one were to analyse the envelope curves for simulation case 2 - 11, one would find similar results.

From table 4.4 it is observed that absolute maximum are in general found in the area of ≈ 70 - ≈ 95. This may be explained by the slightly higher motions in the connection point of the tailing vessel as described in the previous section.

The results from beam weather simulation (case 9) differs from the base-case in the manner of a slight increase of stress in the area of ≈ 9. No explanation to this result were found, but may be related to unidentified coupled motions between the vessels.

Analysing the envelope curves of fatigue damage for the different simulations, a more clear pattern, indicating excitement of eigenmodes, occurs. Illustrated by fatigue damage for case 1, 9 and 4, figure 4.9 - 4.11, a pattern similar to eigenmodes 3, 5 and 1 (see figure 1.26) occur, respectively. The eigenfrequencies related to these modes do not match the frequencies of the simulation wave environment, and therefore do not indicate excitation of eigenmodes. However, by calculating the wave length λ related to the different wave peak periods $T_P = 6, 9.5$ and 12 seconds, the wave lenghts may be compared to the length of the tether:

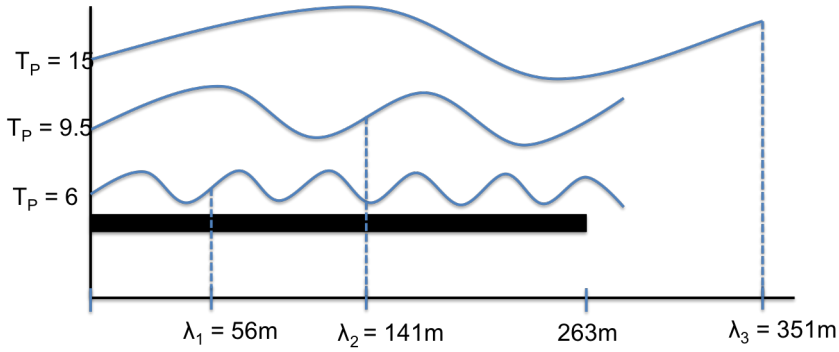

Figure 4.12: Wave lenghts and tether length

The figure above illustrates a wave propagation over the tether, which for $T_P = 9.5$ and 15 are close to both mode shape 3 and 1 (figure 1.26) and the fatigue envelope curves in figure 4.17b and 4.11, respectively. This suggests that wave lengths corresponding to a mode shape will excite fatigue damage in critical areas.

The similarity between fatigue envelope curve and mode shape 5 for beam weather are not determined. As beam waves will not directly contribute to any lengthwise force variation, it is suspected that the fatigue damage mostly will be related to the ship motions.

As for the remaining cases, the distribution varies, with different degree of clear peaks. Most critical fatigue areas are located between areas ≈ 15 - ≈ 90.

The variation of fatigue damage over the tether are in some cases significant and therefore have to be taken into consideration.

For all simulations, ultimate stress and maximum fatigue damage occur at the bottom side of the tether, point 7 in figure 3.7. This is explained by the fact that the upward acceleration of the tether end-point (when towlines tightens) will be greater than the downwards acceleration (slack towlines), due to ship motions and viscous drag and damping.

The stress concentration factor indicate approximate 20% higher stress in the welds. This is in many cases significant and have to be taken into consideration.

4.1.3 Importance of different load effects

In order to better understand the behaviour of the system and make improvements with respect to safety and operability, it is of interest to determine the effect of different loads. By analysing the simulation results, the different loads are classified and compared with respect to:

- Static VS. Dynamic
- Axial- VS. Bending- VS. Hoop stress
- Wave forces: Drag VS. Inertia
- Vessel motion VS. Direct wave loads

Simulation method

The comparison of the different load contributions are conducted, analysing the simulation results from the cases described in table 4.12.

For the three first comparisons both the maximum and standard deviation stress values are considered. The standard deviation stress refers to the upper standard deviation level, $S^{mean} + \sigma$ figure 4.14. The stress utilized in the calculations are the tether stress, stress in welds will be higher, as previously described.

The stress contribution from axial forces and bending moments are based on theory described in section 1.6.1, equation 1.46 - 1.48.

Evaluating the induced stress contributions from ship motions and direct wave loads the simulation results from the two simulation models, with and with out vessels, in identical weather conditions are analysed. The results are studied with respect to envelope curves, maximum and standard deviation value of stress and also ship RAOs versus load spectra. The analysis include a comparison of both stress and fatigue damage on the tether.

The importance of wave induced drag- and inertia forces are evaluated based on theory described in section 1.4, and illustrated based on figure 1.7.

Results

Static versus Dynamic:

Table 4.5: Static VS. Dynamic loads

Static VS. Dynamic load comparison

	Max stress			Standard dev. stress		
Case	**Static**	**Dynamic**	**Utilization**	**Static**	**Dynamic**	**Utilization**
Base-Case (B.C.)	13.4%	87.1%	33.5%	39.0%	61.0%	14.3%
Seed 2	11.9%	88.6%	34.4%	39.3%	60.7%	12.8%
Seed 3	11.9%	88.5%	33.5%	39.4%	60.6%	12.5%
$T_P = 15$	14.0%	86.0%	36.5%	36.4%	63.6%	17.0%
$T_P = 6$	6.9%	93.0%	55.7%	30.8%	69.2%	14.3%
$H_S = 3.5$	10.4%	89.6%	45.4%	34.3%	65.7%	16.7%
$H_S = 4.5, T_P = 8$	6.6%	93.3%	61.0%	28.5%	71.5%	16.3%
$H_S = 5.5, T_P = 9$	6.0%	94.0%	67.4%	28.6%	71.4%	16.9%
90 deg, $T_P = 6$	5.3%	94.7%	69.3%	30.1%	70.0%	14.5%
Long line	13.45%	86.6%	30.6%	33.5%	66.5%	15.7%
Chain	10.7%	89.3%	38.6%	37.6%	62.8%	13.5%
No Vessels (N.V.)	35.0%	66.1%	13.7%	65.2%	34.9%	11.0%
N.V. $T_P = 15$	25.4%	74.6%	19.2%	53.4%	46.6%	12.81%
N.V. $T_P = 6$	48.8%	51.2%	8.9%	76.2%	23.8%	9.7%
N.V. $H_S = 3.5$	26.8%	73.2%	17.8%	58.8%	43.2%	12.0%

Contributions of calculated stress (not design stress)
Utilization given in total utilization of design stress

Axial VS. Bending VS. Hoop:

Time series, base-case:

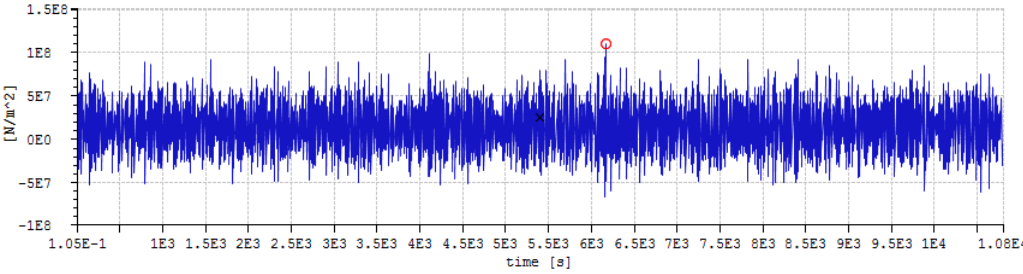

Figure 4.13: Time series Stress, point of maximum response base-case

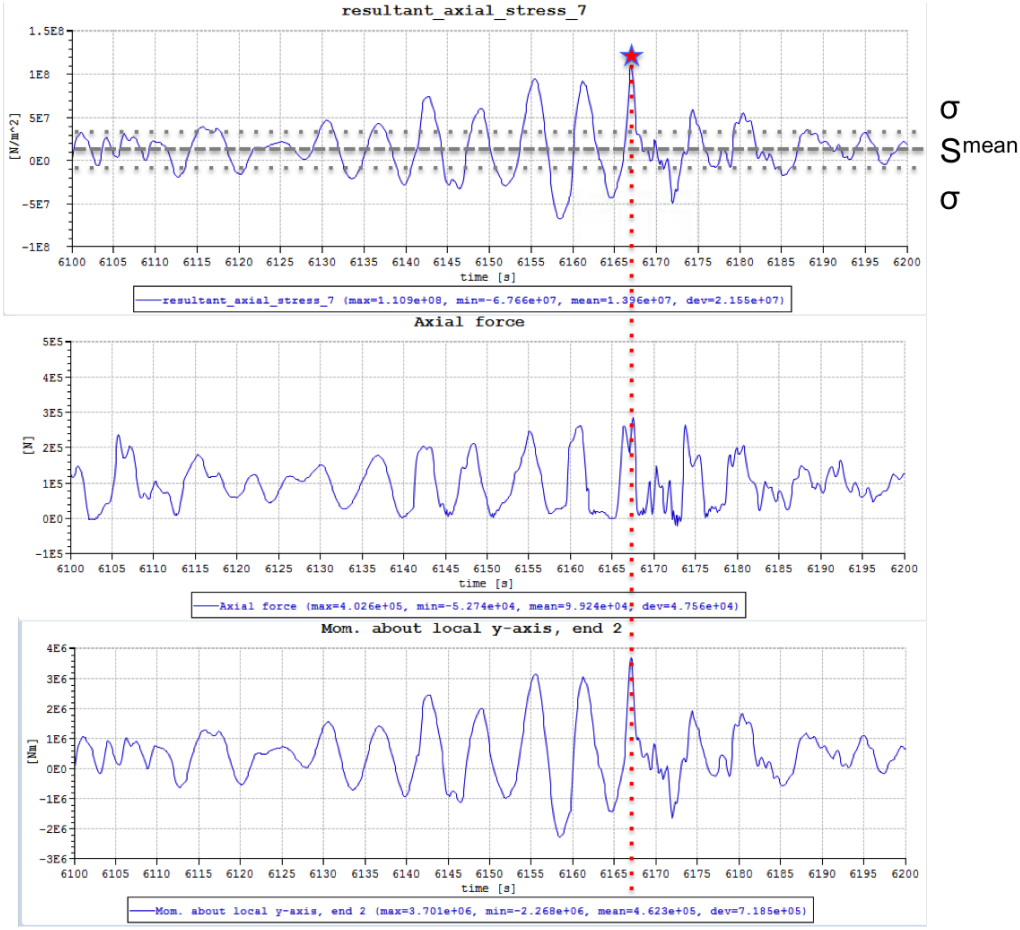

Figure 4.14: Time series window, Stress, axial force and bending moment: Base-Case, extreme value

Table 4.6: Axial- VS. Bending VS. Hoop stress

Axial- VS. Bending VS. Hoop stress

	Max stress			Standard dev. stress		
Case	**Axial**	**Bending**	**Hoop**	**Axial**	**Bending**	**Hoop**
Base-Case (B.C.)	1.3%	99.1%	-0.4%	1.5%	100.9%	-2.4%
Seed 2	1.3%	99.1%	-0.4%	2.2%	99.6%	-1.8%
Seed 3	1.9%	98.6%	-0.4%	2.2%	99.4%	-1.6%
$T_P = 15$	1.5%	98.9%	-0.4%	1.1%	99.3%	-1.9%
$T_P = 6$	2.7%	97.6%	-0.3%	2.7%	98.8%	-1.5%
$H_S = 3.5$	1.3%	99.0%	-0.3%	1.9%	99.3%	-1.2%
$H_S = 4.5, T_P = 8$	1.9%	98.3%	-0.2%	2.6%	98.5%	-1.1%
$H_S = 5.5, T_P = 9$	1.7%	98.5%	-0.2%	2.9%	98.3%	-1.2%
90 deg, $T_P = 6$	2.4%	97.8%	-0.2%	2.8%	98.5%	-1.3%
Long line	0.4%	99.8%	-0.2%	2.1%	99.9%	-2.0%
Chain	1.5%	98.9%	-0.4%	1.9%	99.7%	-1.6%
No Vessels (N.V.)	2.5%	98.7%	-1.2%	1.7%	98.9%	-0.6%
N.V. $T_P = 15$	2.4%	98.0%	-0.4%	1.4%	99.5%	-0.9%
N.V. $T_P = 6$	2.4%	98.0%	-0.4%	1.5%	99.4%	-1.9%
N.V. $H_S = 3.5$	2.7%	97.7%	-0.4%	1.9%	98.8%	-0.7%

Wave forces - Drag VS. Inertia:

Considering the scatter outline and the weather conditions in figure 4.1:

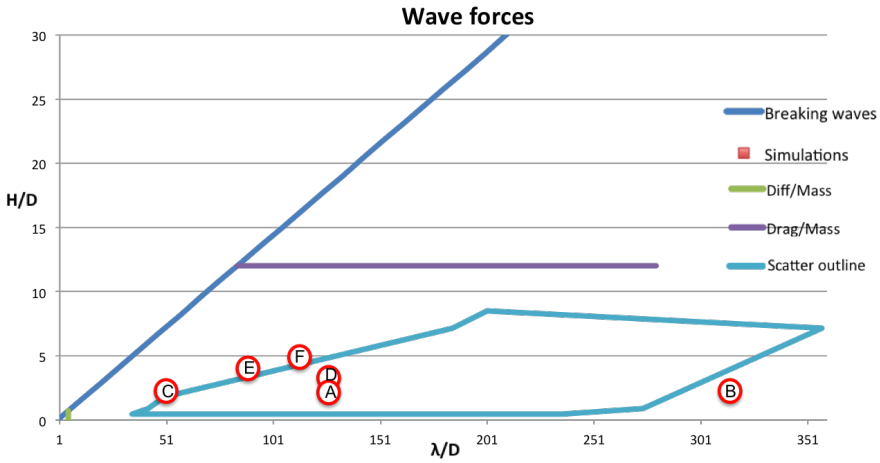

Figure 4.15: Drag V.S. Inertia - direct wave forces only

Ship motions VS. Direct wave loads:

Table 4.7: Ship motions VS. Direct wave loads

Ship motions VS. Direct wave loads

	Wave				Vessel motion			
Case	S_σ	S_{Max}	$Fatigue$	$\frac{S_{MAX}-S_{Mean}}{\sigma}$	S_σ	S_{Max}	$Fatigue$	$\frac{S_{MAX}-S_{Mean}}{\sigma}$
Base-Case (B.C.)	11.0%	13.4%	0.28%	3.76	14.3%	33.5%	13.32%	4.58
T_P = 15	12.8%	19.2%	1.26%	3.62	17.0%	36.5%	11.52%	3.93
T_P = 6	09.7%	08.9%	0.03%	3.48	14.3%	55.7%	43.20%	6.73
H_S = 3.5	12.0%	17.8%	1.00%	3.85	16.7%	45.4%	32.76%	4.91
90 deg, T_P = 6					14.5%	69.3%	77.40%	8.00

S_σ - Standard deviation stress given in total utilization of design stress
S_{MAX} - Standard deviation stress given in total utilization of design stress
$Fatigue$ - Utilization of total fatigue life during the tow operation (T_R)
$\frac{S_{MAX}-S_{Mean}}{\sigma}$ - Indication of Gaussian ($\sqrt{2ln(N)} = 3.6 - 3.9$)

Envelope curves of base-case: No vessel/Vessel, stress and fatigue:

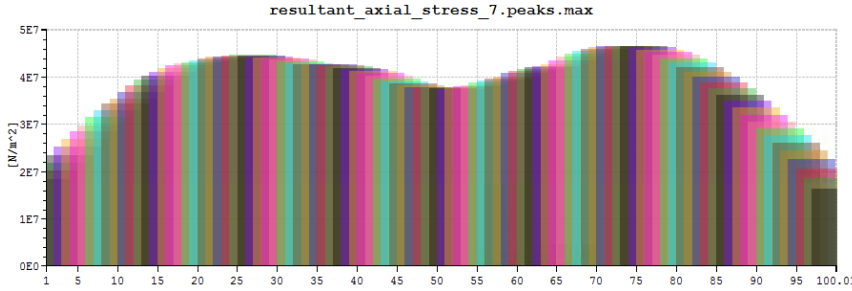

(a) Stress envelope: case 12

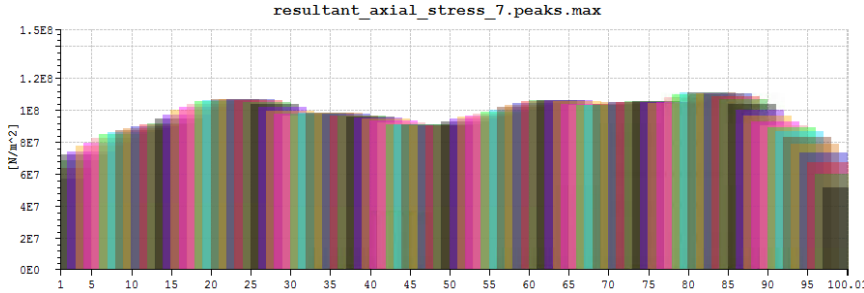

(b) Stress envelope: case 1

Figure 4.16: Stress envelope curves (NB! y-axis in different scales)

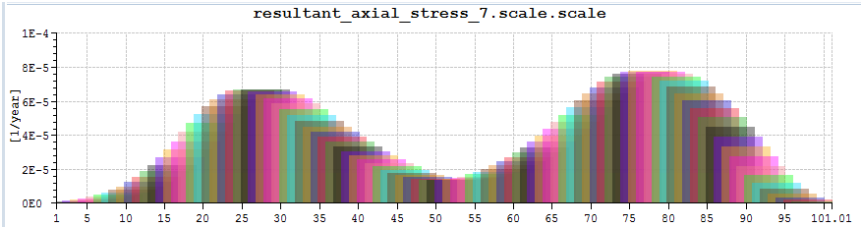

(a) Fatigue envelope: case 12

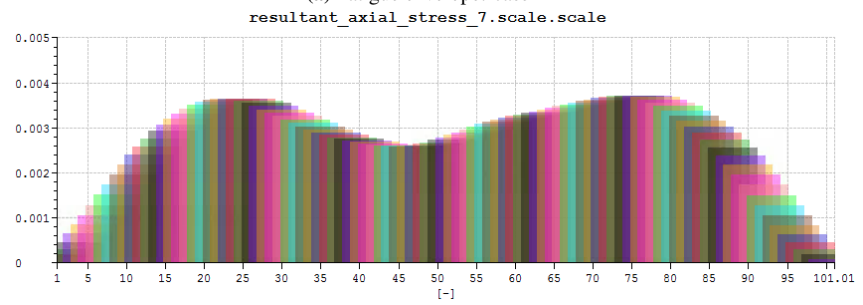

(b) Fatigue envelope: case 1

Figure 4.17: Fatigue envelope curves (NB! y-axis in different scales)

Force and response spectra: No vessel/ Vessel: (Response spectra for point of maximum response)

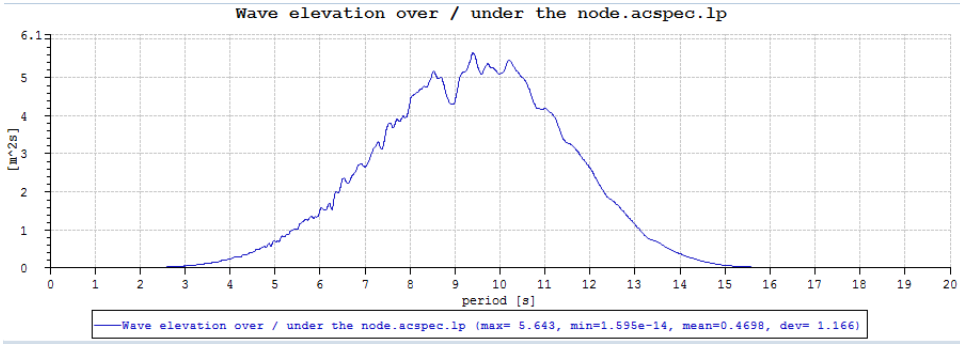

Figure 4.18: Wave surface distribution - wave spectrum

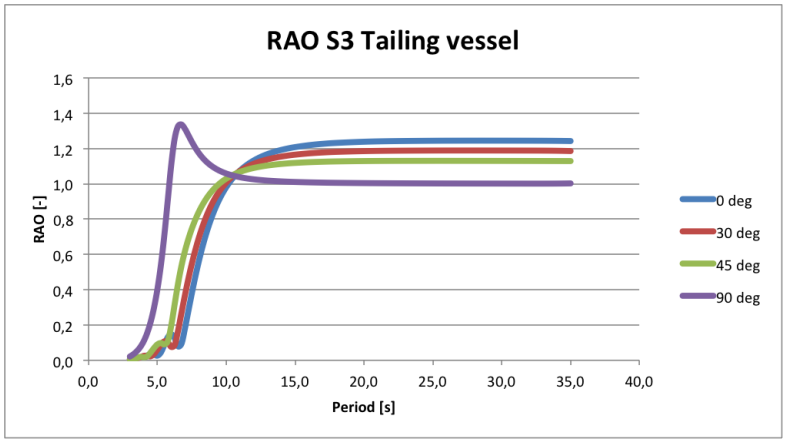

Figure 4.19: Heave RAO, attachment point tailing vessel

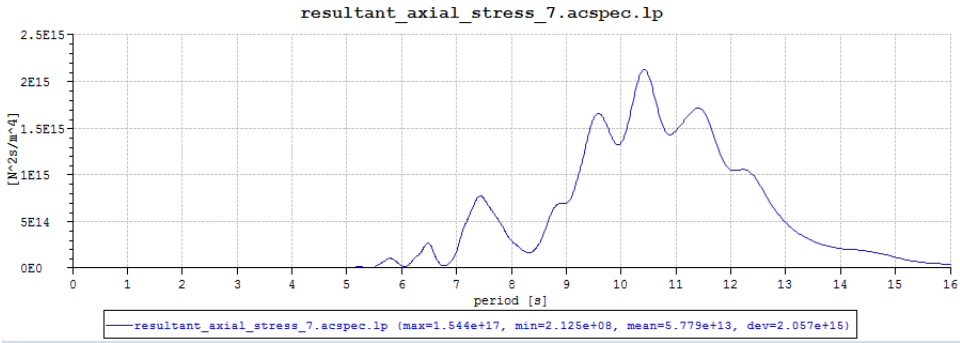

Figure 4.20: Response spectre: case 12

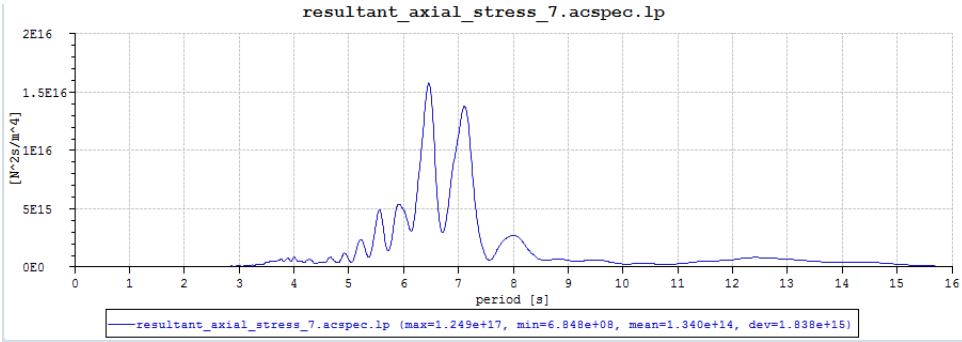

Figure 4.21: Response spectre: case 1

Stress time series, beam sea:

Figure 4.22: Stress time series beam sea

Discussion

Static VS. Dynamic:

Analysing the results for case 1 - 11 (with vessel motion) in table 4.5, it is observed that the dynamic induced stress are the dominating contribution for the case simulations. The dynamic loads contribute with 86 - 95% of the total maximum induced stress and between 60 - 72% of the upper standard deviation level.

Pure static loads are calculated over the tether to have a utilization of design resistance of $\approx 3\%$

For the cases of wave loads and no vessel motions (case 12 - 15), the total induces stress are lower, and thereby the static contribution higher.

Axial VS. Bending VS. Hoop:

Analysing the data in table 4.6 it is clear that the bending moment induced stress are the dominating contribution with 97 - 100 % of the total stress.

The hoop stress as a result of hydrostatic pressure will help to reduce the effective stress.

Wave forces: Drag- VS. Inertia forces:

The direct wave forces on a slander structure can, as discussed in this thesis, be estimated using Morison's equation. Wave forces are divided into drag- and inertia force.

Relating the outline of the wave scatter diagram for the area, and the weather condition simulated in figure 4.1 (A - F), the wave force dominance can be illustrated in figure 4.15. Comparing to the theory earlier described, and figure 1.7, the illustration clearly indicates an inertia dominated system.

Introducing a forced motion to the system, for example induced by the vessels, the relation between drag- and mass forces may change.

Direct wave loads VS. Vessel motion:

A comparison of the induced stress from direct wave loads and the loads from vessel motions plus wave loads are presented in table 4.7. It is observed that the vessel motions will contribute with a significant increase in both response stress and fatigue damage. From the base-case condition, the following observations are made:

- Standard deviation stress: Utilization 11.0% $\rightarrow$ 14.3%, corresponding to design stress 47.5 MPa $\rightarrow$ 61.4 MPa, +29%
- Maximum stress: Utilization 13.4% $\rightarrow$ 33.5%, corresponding to design stress 55.8 MPa $\rightarrow$ 140 MPa, +151%
- Total fatigue damage: 0.28% $\rightarrow$ 13.32%

This indicated that the vessel motions are very important, especially for the fatigue damage.

Comparing the stress response spectra; without and with vessel motions (figure 4.20 and 4.21) it is observed that the spectra have little similarities. This also suggest that the loading induced by the vessel motions are of great importance.

The response spectrum for the case with vessel motions implemented, illustrate large response in the area of 6 to 7.5 seconds, with two clear peaks. No explanation for these two clear peaks at period 6.5 and 7 sec were concluded, but as there are little wave energy in this area, the origin may be related to the motion response of the two ships.

The envelope curves, illustrating the distribution of maximum stress and fatigue damage over the pipe are illustrated in figure 4.16a to 4.17b. The figures illustrates that both fatigue and stress envelope curves in the case of direct wave loads, $T_P = 9.5$, will follow a clear pattern. The shape of the envelope curve are similar to mode shape 3 and also the wave elevation corresponding to T_P, as previously discussed (figure 4.12). For the case of the combined wave loads and ship motions, the stress envelope curves are all over significantly higher. The stress envelope curve for the combined loads also do not follow a clear mode shape pattern.

The value of $\frac{S_{MAX}-S_{Mean}}{\sigma}$ describes the relation between the maximum induced stress and to the standard deviation of the dynamic loads. Comparing this value to the most probable maxima (S_{MPM}) for a Gaussian distribution, the relation can give an indication of the probability area of the simulation extreme value. For the cases of pure wave loads, the wave elevation and the wave induced forces are assumed to be Gaussian. For these cases it is observed that the induced stress are similar to the most probable stress.

Introducing vessel motions to the system, the tether will experience oscillating forces at the ends. As the vessel motions only will contribute with an upwards force component, and not a downward, it is expected that for large vessel motions the induced stress will no longer be a Gaussian process. This means that the formula for most probable stress will no longer be valid.

The simulated case where the vessel induced loads are assumed to be largest is the beam weather conditions (case 9). Analysing the stress time series for this case (figure 4.22, large

peak values and non-symmetry about mean clearly indicate a non-Gaussian process. The result of this ia a $\frac{S_{MAX}-S_{Mean}}{\sigma}$ significantly larger than what is expected for a Gaussian process.

4.1.4 Operational Imitation

An important part of the planning a marine operation like a tow and installation operation is the establishment of operational limits. The operational limits shall ensure a safe operation during realistic conditions. The work of this thesis mainly focus on the operability with respect to structural response (FLS and ULS), while other possible limitations are only briefly discussed.

The operational limitation with respect to structural response, will be determined based on the most critical area. For the tether, this will correspond to the induced stress in the welds.

Simulation method

During the work of this thesis, several simulations of the tow model in different wave conditions have been conducted in order to evaluate the response and effect of H_S and T_P. A total of eight simulations (case 1 - 8), with six different combinations of H_S and T_P (A - F) have been simulated(described in table 4.12, and figure 4.1). The operational limits will be defined by values of H_S and T_P, based on structural response with respect to FLS and ULS in the welds.

The acceptable structural response of the tether are limited to 100 % of the design resistance (ULS) and 10% of the total fatigue life (FLS). The ULS limit correspond to the structural limitation of the structure according to the LRDF method. The FLS limit are according to supervisor recommendation.

The assessments of fatigue damage are based on a calculated reference period of 36 hours for the offshore stretch, as decried in section 3.4, equation 1.1.

The peak distribution and variability of extreme value stress will be assessed.

The distribution of the individual stress peaks are presented in form of a probability density function (made in Matlab), and a cumulative distribution function describing the probability of non-exceedance. A Rayleigh and a Weibull cumulative distribution are evaluated in order to find the best fit.

For the extreme value variation, a SIMA workflow model was made, simulating a total of 20 seed numbers and plotting the maximum stress value as a Gumbel distribution. The Gumbel distribution illustrates the maximum stress variation for a specific point on the tether. For the simulations in this thesis, the point of maximum stress for wave seed 1, element 85 was chosen. (PP = post-processor)

Gumbel workflow:

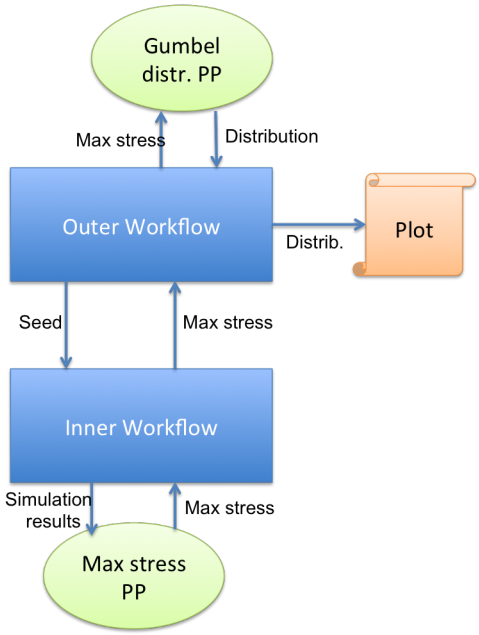

Figure 4.23: Structure of SIMA workflow model

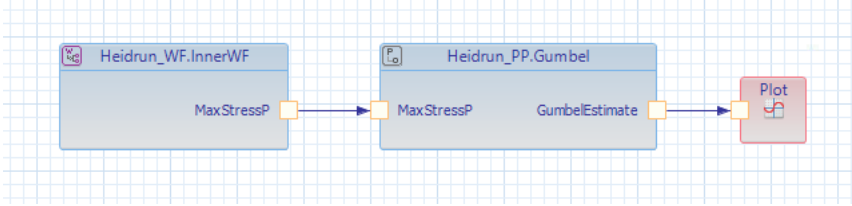

Figure 4.24: Outer forkflow

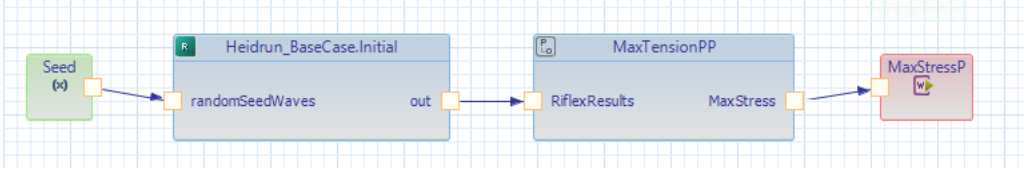

Figure 4.25: Inner workflow

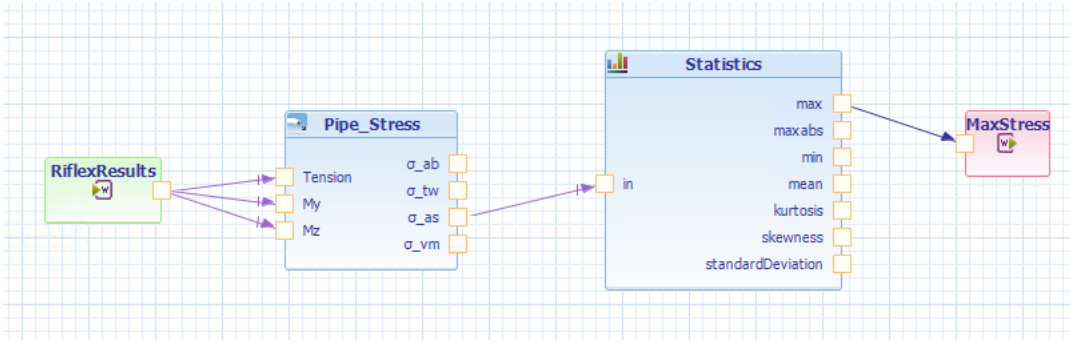

Figure 4.26: Maximum tether stress post-processor

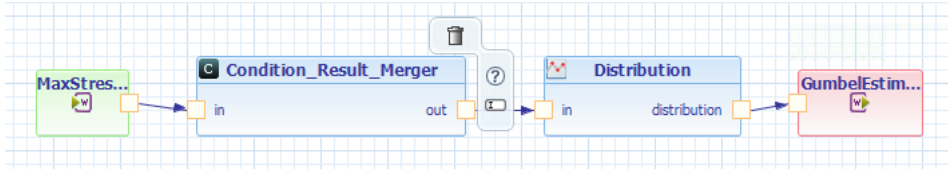

Figure 4.27: Gumbel distribution post-processor

Results

Simulation results:

Table 4.8: Results ULS and FLS

Ship motions VS. Direct wave loads

Case		$MaxStress$	$Fatigue$	$\frac{S_{MAX}-S_{Mean}}{\sigma}$
Base-Case (B.C.)	A	41.4%	13.32%	4.58
Seed 2	A	42.7%	12.96%	5.31
Seed 3	A	41.5%	12.96%	5.29
T_P = 15	B	45.1%	11.52%	3.93
T_P = 6	C	68.5%	43.20%	6.73
H_S = 3.5	D	56.1%	32.76%	4.91
$H_S = 4.5, T_P = 8$	E	74.1%	70.56%	6.12
$H_S = 5.5, T_P = 9$	F	81.8%	100.44%	6.50
90 deg, T_P = 6	C	84.0%	77.40%	8.00

$Maxstress$ - Weld stress, utilization of design resistance
$Fatigue$ - Utilization of total fatigue life during the tow operation (T_R)
$\frac{S_{MAX}-S_{Mean}}{\sigma}$ - Indication of Gaussian ($\sqrt{2ln(N)} = 3.6 - 3.9$)

Peak stress distributions, base-case:

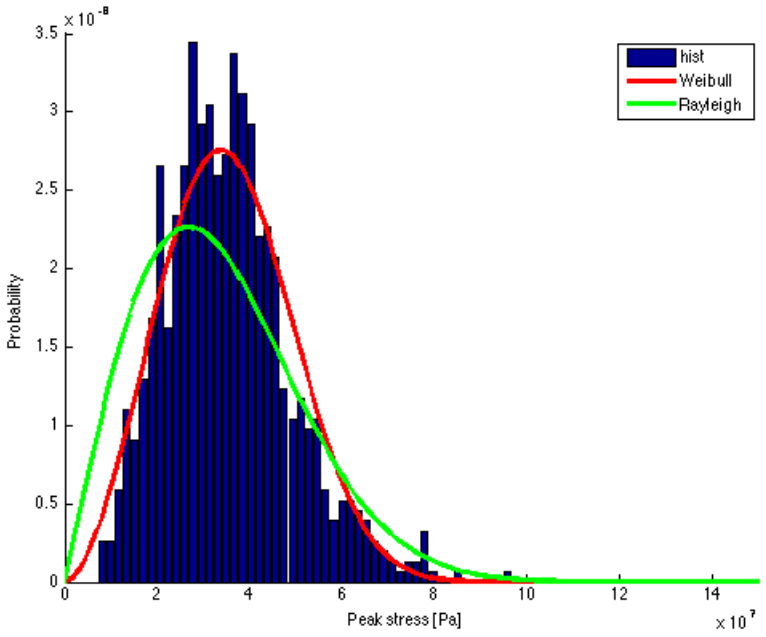

Figure 4.28: Probability density function of stress peaks

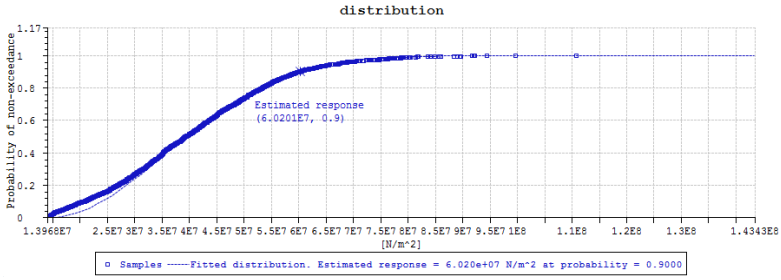

(a) Cumulative Rayleigh distribution of stress peaks

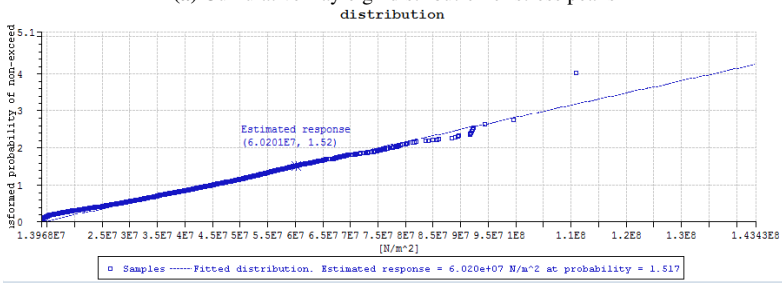

(b) Cumulative Rayleigh distribution of stress peaks, linear presentation

Figure 4.29: Rayleigh stress distribution

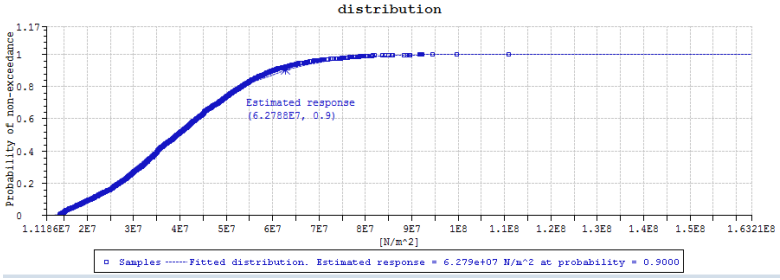

(a)

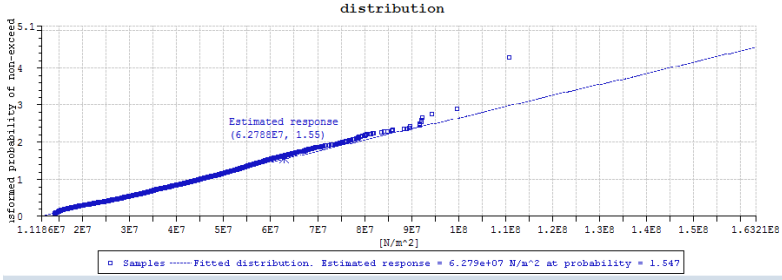

(b) Linear presentation

Figure 4.30: Cumulative Weibull distribution of stress peaks

Beam sea:

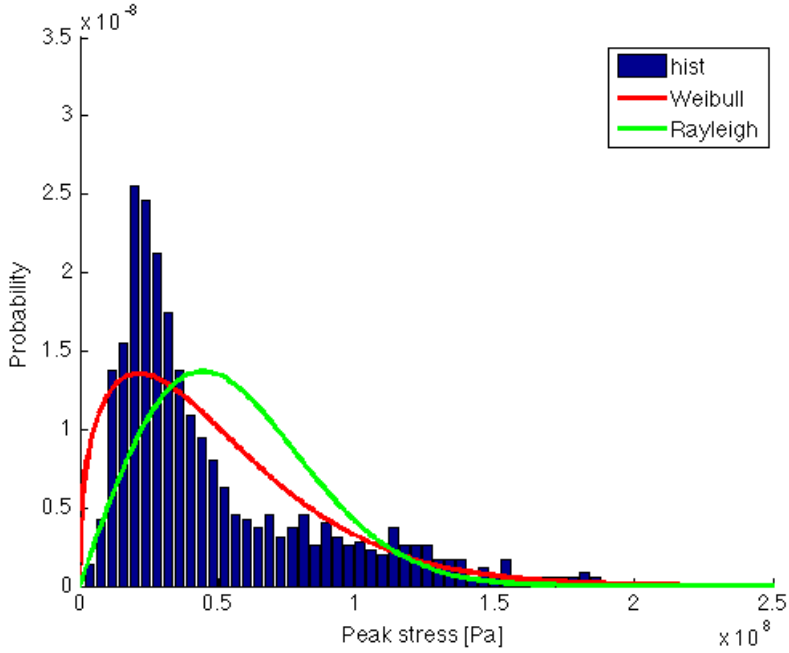

Figure 4.31: Probability density function of stress peaks, beam sea

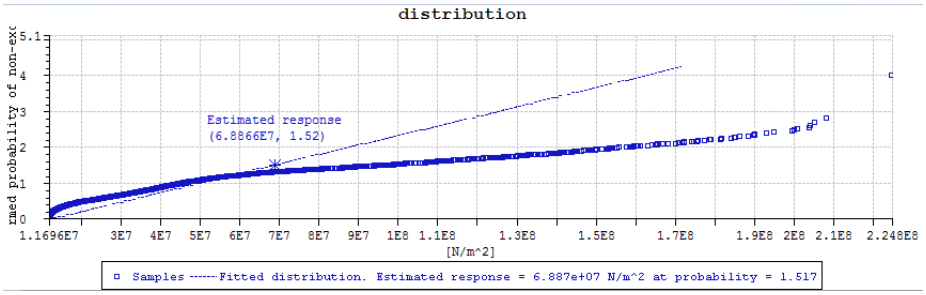

Figure 4.32: Cumulative probability density function of stress peaks, beam sea, linear presentation

Extreme value distribution, base-case:

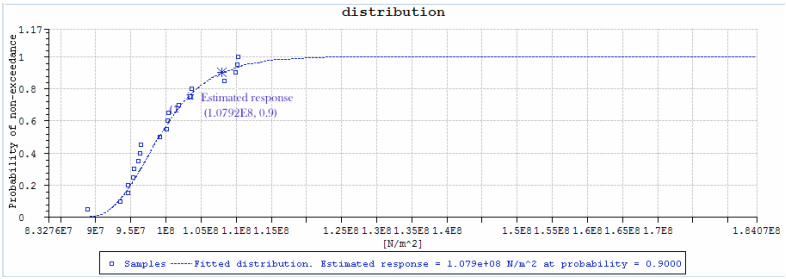

(a)

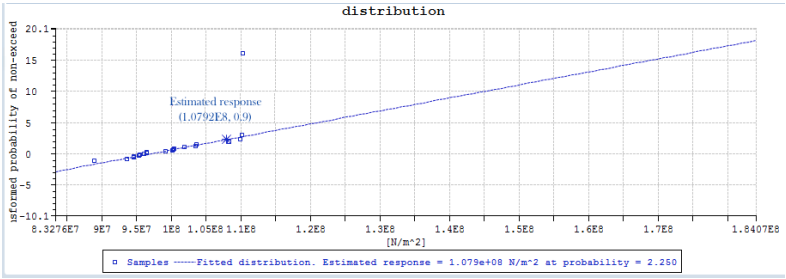

(b) Linear presentation

Figure 4.33: Extreme value Gumbel distribution

Discussion

Analysing the results from the three first weather conditions in table 4.8, it is observed that it is the more high frequent waves that are the most critical with respect to both ULS and FLS. This is due to large response related to eigenfrequencies in both the system and vessels. As a result of this observation, the following simulation were based on wave conditions corresponding to the lower T_P limit in the wave scatter diagram, figure 2.5 (condition E and F).

Table 4.8 indicate that the ULS for the simulated cases are well within the limits. However, none of the simulation results are within the fatigue limitation of $> 10\%$ fatigue damage. These results suggests that the fatigue damage will be the limiting factor for the operation.

As a result of the high level of stress contribution induced by the vessel motions and the RAOs of vessel attachment points, an additional simulation was carried out in conditions where large vessel motions and large response are expected. The additional simulation simulates a beam wave condition with $H_S = 2.5m$ and $T_P = 6s$ (condition C), where the wave periods are close to both the natural period of the system ($\approx 6.1s$) and a natural ship heave period ($\approx 7s$)(figure 4.19). The result is an increase in both stress and fatigue damage compared to the same conditions in head sea direction. These results sug-

gests that it is the beam weather conditions that are the most critical. However, the heave RAO curves indicates that a change of heading will reduce the vessel and tether response significantly.

The beam weather condition simulates similar conditions to the incident where one of the original tethers were lost during the tow. The simulation results shows large vessel motion, similar to what was reported in advance of the failure of the buoyancy element. The incident report Norwegian Contractors 1995 concluded that the cause of the incident was not due to overloading, but rather due to a failure of a lashing strap on the buoyancy element.

Figure 4.28 - 4.30b illustrates the probability density function and the cumulative density function of different stress amplitudes, for base-case conditions. The PDF plot illustrates which stress ranges that most dominating. Comparing the actual measured data, represented by the histogram, to a Weibull and a Rayleigh model, the Weibull seems like a better model for the lower stress ranges. Which of the models that best represents the higher stresses are hard to determine based on the plot. A Rayleigh distribution model will be the most conservative alternative with respect to the higher stresses. This is better illustrated by the CDF graphs.

Analysing the PDF and CDF curves for the beam weather conditions (figure 4.32 - 4.32), neither the Rayleigh nor the Weibull model seems to represent a good model for the induced stress peaks. The peak histogram shows to have a long tail, representing the occurrence of several high peak values. This represent a undesirable situation with several high stress peaks, which may be hard to predict, at least with a Rayleigh or Weibull model.

In order to verify whether the results are representative, the variability of extreme load values are analysed for the base-case and checked against most probable maxima. The Gumbel distribution illustrated the variability of the extreme values of 20 different seeds. Analysing the results, the induced stress vary within the rage of 90 - 110 MPa, corresponding to a weld utilization of 34 - 41%. The 0.9 probable extreme value are calculated to 107.9 MPa, corresponding to a utilization of 41.11 %. These results indicate that the simulation results of case 1 - 3 are representative, slightly on the conservative side.

Analysing results in the linear CDF peak and extreme value figures, one sample point deviating from the rest is detected. This points is consequently found in all linear presentations and not found in the equivalent non-linear plot. This point was discussed with thesis supervisor, which showed to appear for several other students. This indicate that these points are due to a bug in SIMA, and may be neglected.

Results with respect to structural loading and ULS in head seas suggests a operational limitation (OP_{lim}) of $H_S = 5.5m$ (82% utilization). Further, the simulation results indicate a critical weather heading of $90°$, reducing the operability to $H_S = 2.5m$ (84% utilization). Classifying the tow operation to either a level A or B (section 1.3) and introducing the most conservative alternative α-factor = 0.72 (table 1.3) the operational weather forecast limits (OP_{WF}) are estimated to $H_S = 4.0$ and 1.8, respectively.

Evaluating the tow operation with respect to fatigue damage (FLS), the results suggest that

the tow operation is not feasible for any of the simulated weather conditions. The large fatigue damage are previously related to vessel motion induced loading. This will result in an operational limit of $OP_{lim} = H_S < 2.5m$, $OP_{WF} = H_S < 1.8m$.

In addition to the structural limitations of the operation, it is also important to assess other limiting factors that might further restrict the operability of the operation. For a three hour time period in wave conditions $H_S = 5.5$, the most probable largest wave height are calculated to $H_{Max} = 10.4$m (equation 1.56). Comparing this wave height to the RAO of the ship, these wave heights will most probable not corresponding to safe on-deck working conditions.

Using the wave scatter diagram (figure 2.5), these conditions corresponds to wave lengths of $\lambda = 141 - 351$m. With a tow depth of 7 meters and a distance between the two vessels of 305 meters the risk of the tether breaking the wave surface during the largest wave are present. This suggest that a operational limitation of $H_S = 5.5m$ are not feasible.

An operational limitation regarding tether surface piercing may be determined for the worst case scenario, where vessels are located at neighbouring wave crests. For a 7 meter submerged tow, the operational limitation may be addressed as the significant wave height corresponding to a most probable maximum wave height of 6 meters (equation 1.56). This limit, corresponding to the operation reference period of 36 hours, suggests a operational limit of $H_S = 2.6$m.

4.1.5 Towline properties

In order to further analyse the system, the effect of different towline properties are also briefly assessed. The properties of the towline will affect both the maximum stress in the towline and the transferred loading and response of the tether.

Simulation method:

For the simulation analysis of the towline properties, three different configurations are considered: Base-case nylon fibre rope, base-case chain and increased length of fibre rope. As the added clamp-on wieghts are modelled as a function of vertical forces, the weights will also change with the modelled towlines. The properties of the three lines are as following:

Table 4.9: Towline properties

Towline properties					
Case	**Vertical angle**	**Length [m]**	**Stiffness EA [KN]**	**In-air clamp-on weights [Kg]**	k_z **[N/m]**
Base-Case: Nylon	27°	22	59	4900	1217.5
Long line	8.7°	66	59	663	150.6
Chain	27°	22	160	3460	3301.7
Design resistance fibre rope		188 MPa			
Design resistance chain		347.5 MPa			

The change in vertical tow angle, length of towline and the material stiffness will all contribute to change the vertical stiffness of the system and thereby changing the natural frequency and the response behaviour of the system.

The vertical part of the stiffness for the towlines, k_z (table 4.9) are calculated as:

$$k_z = \frac{EA}{L} sin(\alpha) \tag{4.2}$$

The towline study will include the following aspects:

- Maximum induced stress in tether and towlines for the three different towlines
- Stress in base-case fibre rope in different weather conditions
- Static V.S. Dynamic induced stress in towlines, base-case
- Change in system properties

Results:

Table 4.10: Results: towline properties

Results: towline properties

	Utilization of design		**Fatigue damage**
Case	**Tether**	**Towline**	**Tether**
Base-Case (B.C.)	**33.51%**	**34.21%**	**13.32%**
T_P = 15	36.45%	31.65%	11.52%
T_P = 6	55.68%	66.38%	43.20%
H_S = 3.5	45.39%	59.32%	32.76%
$H_S = 4.5, T_P = 8$	61.01%	73.33%	70.56%
$H_S = 5.5, T_P = 9$	67.36%	91.56%	100.44%
90 deg, T_P = 6	69.26%	72.07%	77.40%
Long line	**30.56%**	**32.36%**	**12.60%**
Chain	**38.58%**	**62.23%**	**16.63%**
Design resistance tether		417 MPa	
Design resistance fibre rope		188 MPa	
Design resistance chain		347.5 MPa	

Table 4.11: Results: towline static V.S. Dynamic

Results: towline static V.S. Dynamic

	Standard deviation		Maximum	
Case	**Static**	**Dynamic**	**Static**	**Dynamic**
Base-Case (B.C.)	56.7%	43.3%	10.7%	89.3%
T_P = 15	64.9%	35.1%	12.8%	87.2%
T_P = 6	51.7%	48.3%	6.9%	93.1%
H_S = 3.5	47.5%	52.5%	6.5%	93.5%
$H_S = 4.5, T_P = 8$	39.5%	60.5%	5.1%	94.9%
$H_S = 5.5, T_P = 9$	36.0%	64.0%	4.2%	95.8%
90 deg, T_P = 6	44.4%	55.6%	6.4%	93.6%
Long line	45.6%	54.4%	9.0%	91.0%
Chain	52.9%	47.1%	6.4%	93.6%

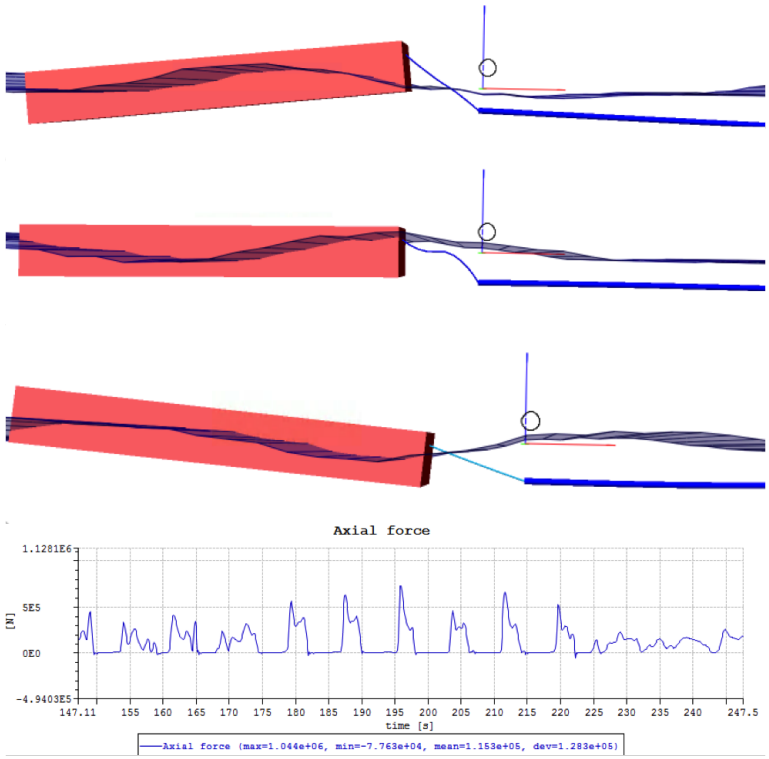

Figure 4.34: Snapping loads (Case 7 example)

Discussion

A comparison between the different towlines are conducted by analysing maximum induces tether stress and fatigue damage in table 4.10 (**Bold**).

The comparison of the two fibre lines, base-case and long line, will start by analysing how the system properties changes. By increasing the line length and reducing the vertical line angle, both the axial stiffness in the towline and the vertical stiffness component will be reduced. This suggests that the load contribution from the vessel heave motion will be reduced, while the vessel surge contribution will increase. Because of the reduced axial stiffness of the towlines, the total vessel contribution will be reduced as the towlines will absorb more energy. As a result of the reduced added weights and stiffness, the eigen periods of the system will be increased as well as the system inertia forces will be reduced. This may result in larger induced motions at the tether ends, resulting in larger bending moments. Analysing the results in table 4.10, for the base-case weather condition, the result of the increased length is a slight reduction in the response of system. The results suggests that the change in towlines are not crucial for the simulated case, indicating that a further comparison of the towlines may be beneficial. This evaluation may including other weather conditions, evaluation of eigenfrequencies, manoeuvrability and cost.

Increasing the length of the towlines, the manoeuvrability of the tow will be reduced, while the reduction of clamp-on weights will ease the handling of the weights. Reducing the weights will reduce the cost, but have to be compared against the increased line lengths.

For the case of the chain lines, also here the clamp-on weights are reduced as a result of the weight of the chain, increasing the eigenperiod and reducing the inertia resistance forces. Changing towlines from nylon rope to steel chain will also result in an increased towline- and system stiffness. The increased stiffness indicate that less energy will be absorbed by the towlines, increasing the vessel motion induced loads. From the results in table 4.10 it is observed an increased load in both the tether and the towlines, as expected. The biggest affect of the chain line are the induced stress in the towlines itself. These results suggests that the fibre lines are preferred for the simulated cases.

By comparing the utilization of the towlines with the utilization of tether stress it is observed that the towline stress to a large extent follow the induces tether stress. For the more severe weather conditions, the utilizatoin of the towlines are higher than for the tether, sill within the limits. This indicates that the selected fibre towlines are feasible for the operation, not restricting the operation operability.

Comparing the static- and dynamic induced stress in the towlines it is observed that the static contribution in the towlines are significantly higher than in the tether, using the upper standard deviation stress value. The static induced loadings corresponds to 36 - 65% of the total loading.

Comparing the contributions for the maximum stresses, the dynamic contributions are much higher. This suggests high stress peaks in the towlines. Further analysing the stress time series and simulation animations for the towline (example values from case 7) it is

observed that the high towline dynamic stress are related to snapping loads (figure 4.34). The snapping loads are related to large vessel motions in combination with inertia in the tether system. The snapp loadings are illustrated in the tension time series as zero tension (slack line) followed by a steep peak as the towline rapidly tightens.

The small negative tension values in the time series suggests compression in the towlines. This will not be realistic for a fibre rope and may be a result of numerical unsuitability in the simulation calculations. In attempt of removing the negative tension values, a simulation trail, introducing a small bending stiffness to the towline, was carried out. The towline bending stiffness did not affect the result significantly as negative tension values still occurred. As the negative values does not affect the result, they were ignored.

Tension snapping loads are related to large and rapid loads. The snapping loads are more crucial for chain lines than for fibre ropes as it is related to the towline stiffness. This is also observed by a high towline utilization for the chain line in table 4.10. As the calculated tension in towlines from Rieflex are strongly dependent of the calculation time step, it would be recommended to verify the maximum tension related to snapping.

4.2 Upending

In order to make a feasible proposal for a upending operation, several different simulation analysis have been conducted in order to determine the response behaviour and compare the different solutions. It is desirable to make the operation as safe and cost efficient as possible. This may be done by minimizing the duration and structural behaviour of the tether whilst ensuring a high level of operability and control of the operation. The parameters used to evaluate the towing methods are therefore established as:

- Maximum induced stress in tether
- Duration of upending (horizontal to vertical position)
- Operability with respect to weather conditions (effect of waves and current)
- Response motion behaviour of tether

Simulation method

For the case of this thesis, three possible upending methods are evaluated:

- Free-drop, with clamp-on weights still attached (Upending base-case)
- Free-drop, without clamp-on weights
- Line feed, with clamp-on weights

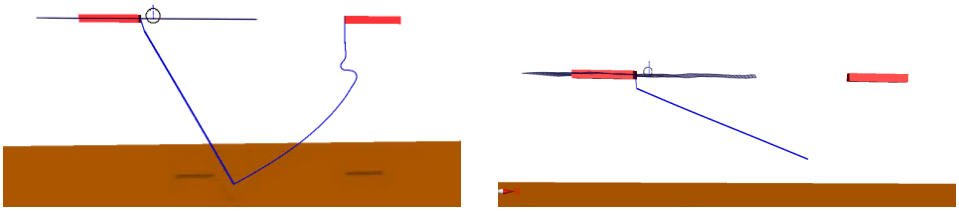

(a) Line assisted upending **(b)** Free drop upending

Figure 4.35: Upending models

All three simulation models are based on the base-case configuration of the towing, as previously described. This implies an original tow depth of 7 meters and the usage of 22 meter long nylon fibre ropes. The upending base-case scenario are previously described in section 3.3.2.

In addition to a calm water simulation, the different upending methods are simulated in different weather conditions in order to evaluate the effect of waves and current on the various solutions.

For the upending analysis, the following simulations have been conducted:

Table 4.12: Towing simulations

Towing simulations

Number	Name	Description
1	Base-Case (B.C)	Base-case scenario, free-drop with calmp on weights, calm water
2	B.C. current	Base-case in uniform head current 1 m/s
3	B.C. waves	Base-case in head waves $H_S = 2.5$ $T_P = 9.5$
4	B.C. current waves	Base-case, waves and current
5	No Weights (N.W.)	Free-drop without clamp-on weights, calm water
6	N.W. current	No weights, current
7	N.W. waves	No weights, waves
8	N.W. current waves	No weights, waves and current
9	Line feed (L.F.)	Line feed 1 m/s, calm water
10	L.F. current waves	Line feed 1 m/s, waves and current
11	L.F. 0.5	Line feed 0.5 m/s, calm water
12	L.F. 0.5 current waves	Line feed 0.5 m/s, waves and current

Results

Key results:

Table 4.13: Key results: Upending

Key results upending stress and time

Case	Time [min]	Hot-spot utilization
Base-Case (B.C.)	10.0	29.0%
B.C. current	10.0	29.2%
B.C. waves	14.2	54.8%
B.C. current waves	15.7	54.8%
No weights (N.W.)	24.2	8.8%
N.W. current	24.2	8.8%
N.W. waves	53.3	72.4%
N.W. current waves	57.4	72.3%
Line feed (L.F.)	14.4	30.4%
*L.F. current waves**	25.4	52.9%
L.F. 0.5 m/s	17.5	18.5%
*L.F. 0.5 m/s current waves**	33.0	136.9%
Design resistance tether		417 MPa
Design resistance fibre rope		188 MPa

*Numerical unsuitability, see discussion

Time series - Tether stress, axial tension and bending moment:

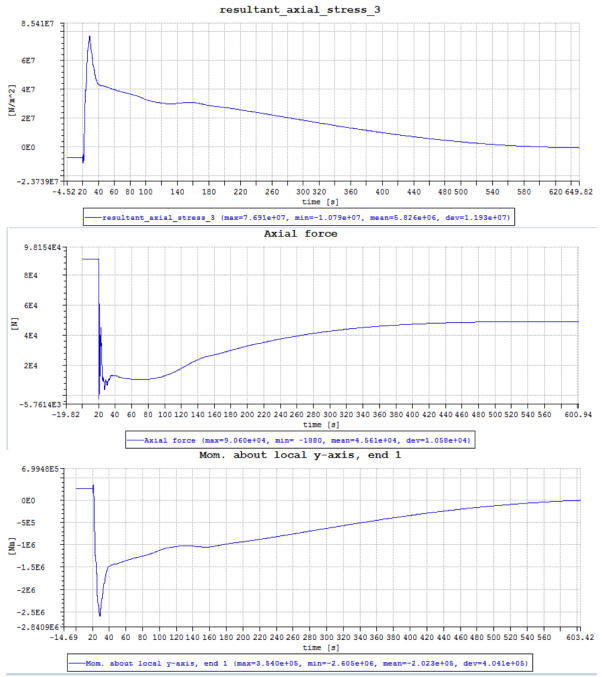

(a) Time series: Base-case

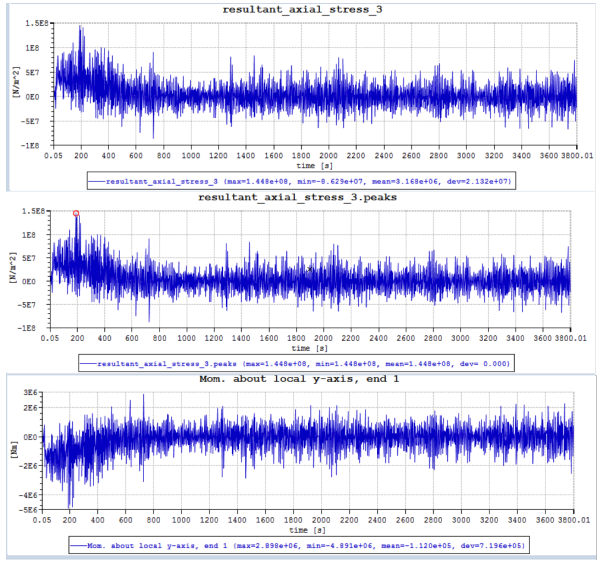

(b) Time series: B.C. waves and current

Figure 4.36: Time series - stress contributions upending

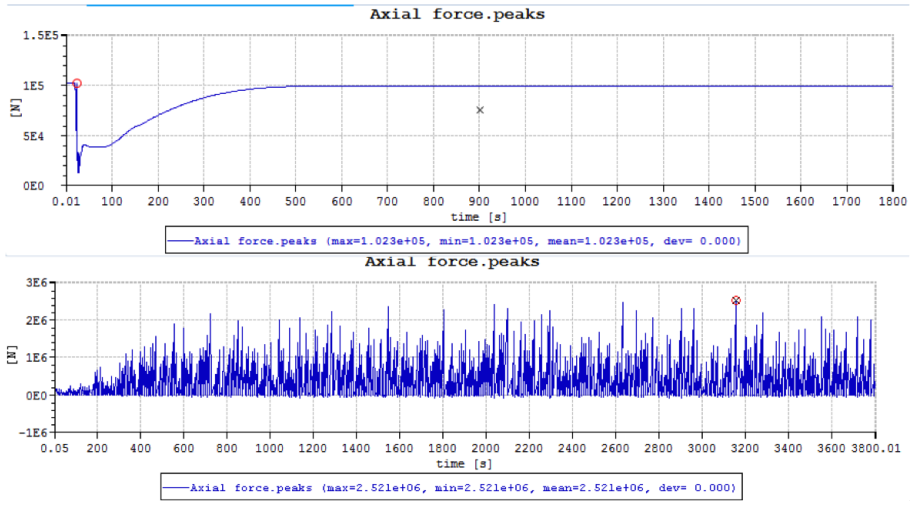

Figure 4.37: Tension time series of front towline, base-case - no weather and waves + current

Axial V.S. Bending loads:

Table 4.14: Results: Axial V.S. Bending load

Results: Axial- V.S. Bending load

Case	Axial [%]	Bending [%]
Base-Case (B.C.)	0.1%	99.9%
B.C. current	0.1%	99.9%
B.C. waves	0.1%	99.9%
B.C. current waves	0.1%	99.9%
No weights (N.W.)	0.6%	99.4%
N.W. current	0.6%	99.4%
N.W. waves	4.3%	95.7%
N.W. current waves	4.3%	95.7%
Line feed (L.F.)	0.1%	99.9%
L.F. current waves	1.5%	98.5%
L.F. 0.5 m/s	0.9%	99.1%
L.F. 0.5 m/s current waves	1.0%	99.0%

Critical areas:

Table 4.15: Results: Critical load area

Results: Critical load area

Case	Element nr.	Circular point
Base-Case (B.C.)	54	3
B.C. current	54	3
B.C. waves	83	3
B.C. current waves	83	3
No weights (N.W.)	56	3
N.W. current	56	3
N.W. waves	20	7
N.W. current waves	20	7
Line feed (L.F.)	54	3
L.F. current waves	93	7
L.F. 0.5 m/s	49	3
L.F. 0.5 m/s current waves	89	7

Element number in main body tether model, 1 - 100
Circular cross-section point in figure 3.7

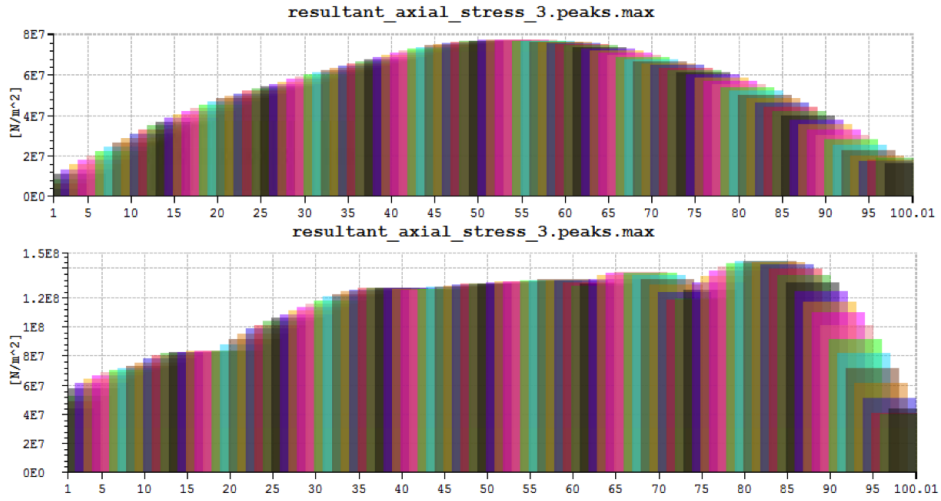

Figure 4.38: Envelope curves: Base-case, calm seas and waves + current

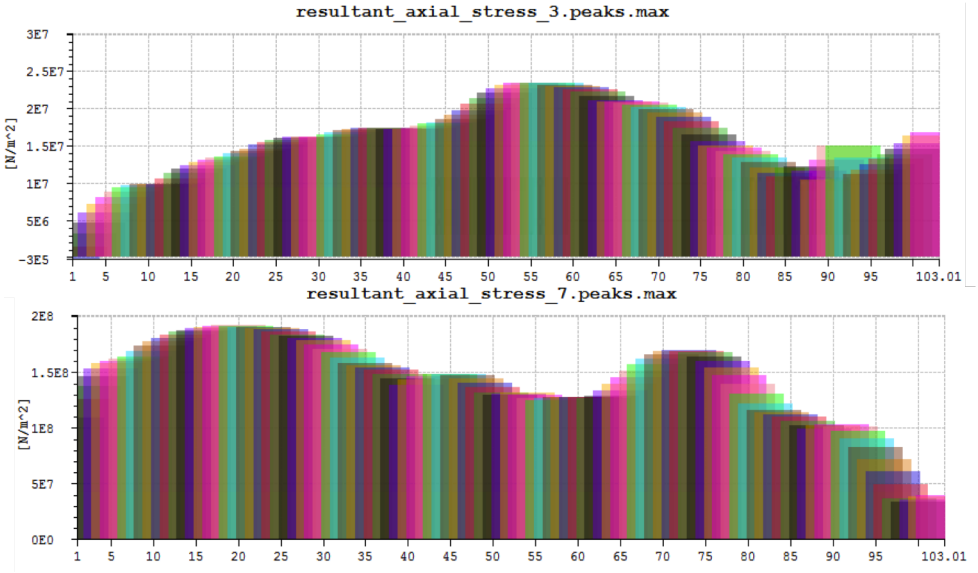

Figure 4.39: Envelope curves: No clamp-on weights, calm seas and waves + current

Snapping loads:

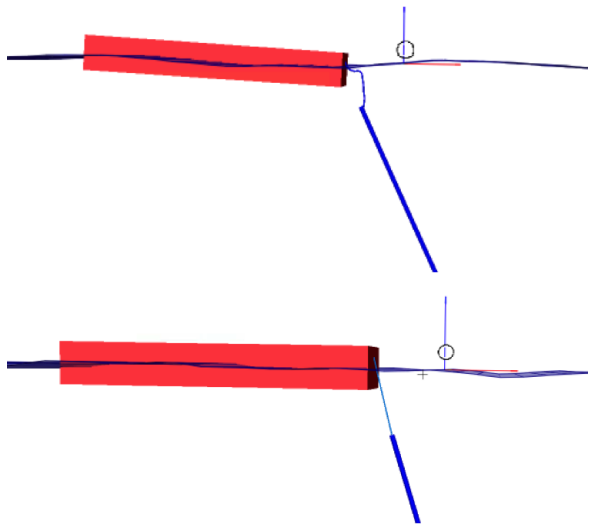

Figure 4.40: Snaping loads in towlines: Base-case waves + current

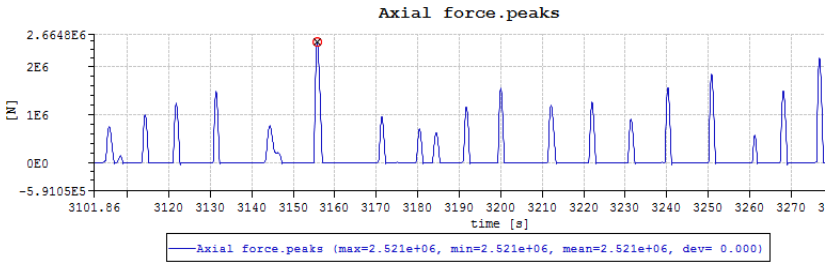

Figure 4.41: Time series: Snapping loads in towlines

Maximum towline stress: 0.1 - 1.7% of design

Discussion

For the simulations of towline assisted upending in waves and current (case 10 and 12) non-realistic behaviour of the upper sections of the towline being fed are observed (figure 4.42). This behaviour may be due to numerical instability in the event of too high feeding rate relative to upending speed in combination with the motion of the assisting vessel and no towline bending stiffness. These behaviours may compromise the validity of results related to these simulations. A possible solution would be to introduce a bending stiffness to the model of the towlines.

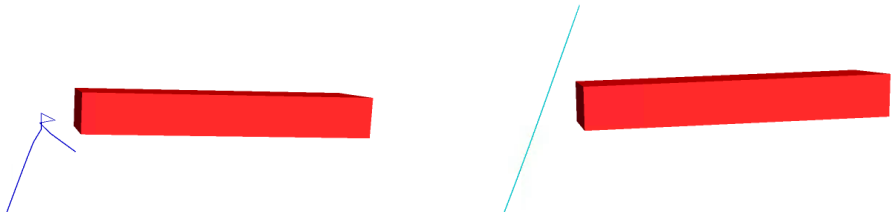

(a) **(b)**

Figure 4.42: Non-realistic towline behaviour

Analysing the visualization of the different simulated operation, the results suggests that all solution are feasible with respect to relative motion between the vessel and the slender structure. That is for the modelled wave condition of $H_S = 2.5$m, $T_P = 9.5$. The tether also behaves in a stable and predictable manner.

By comparing the results in table 4.13 it is observed that removing the bottom clamp-on weight prior to the upending operation will result in a significant increase in the upending time. Introducing waves and currents, the duration of the upending will almost quadruple as a consequence of removing the clamp-on weights.

For the calm water conditions it is observed a significant reduction of tether stress, removing the clamp-on weights. This is due to the reduced upending speed, leading to a reduction in viscous drag forces on the tether. Introducing wave and current loads to the system, the removal of weights will lead to in significantly lager tether stress.

Comparing the simulation results between the base-case free drop method and the towline assisted methods, the towline assisted method will result in an increased operation period. This is result of the towline force reducing the upending speed. Analysing the induced stresses, the towline assisted method with an feeding rate of 1 m/s results in induced tether stress similar to the free drop. This is the result in both calm seas and with waves present. This is a result of the towline not being tight, introducing a geometric stiffness to the system, which will absorb much of the loads from the vessel motions.

Decreasing the rate of line feed to 0.5 m/s will lead to a tight hold-back line, removing the geometric stiffness. As a result, more of the loading from the vessel motions will transfer into the towlines and tether. The result indicate that the reduced feeding rate is not an feasible solution as the induced loading in the tether exceeds the design resistance. However, as a result of the non-realistic behaviour of the towline, the validity of these results have to be questioned (for both feed rates).

The results suggests that the effect of uniform 1 m/s head current are negligible with respect to both upending time and induced tether stress. The effect of the wave environment will however strongly affect the results.

Time series of the base-case simulations in calm weather (figure 4.36a a) and in present of waves and current (figure 4.36b) illustrates the load response affect of the presents of waves and vessel motions. The results show that the dynamic loading from weather conditions will be dominating for the total loading during the upending operation. The same tendencies are also found in the stress time series of the front towline in figure 4.37. From the analysis of the tow operation, it is expected that the vessel motions will be the main contribution to the large stress amplitudes.

Analysing the base-case simulation results in waves and current, the large stress peaks in the front towline are identified as snapping loads (figure 4.40 and 4.41). The maximum stress in the different simulations are calculated to be in the area of 0.1 - 1.7 % of the towline design resistance.

Comparing the axial induced stress in the tether with the bending induced stress, it is observed from table 4.14 that the total stress are almost exclusively a result of bending stress.

From the results in table 4.15, it is observed that the maximum stress in the tether will occur either at the bottom or top point of the circular cross-section 3.7.

A comparison of the maximum stress distribution for the base-case and no clamp-on weight method in both calm water and in waves and current are illustrated in envelope curve 4.38 and 4.39. For the calm water conditions, the forces acting on the tether will mainly consist of viscous drag forces. The drag forces will increase towards the free end as the velocity increase. At the same time, the bottom clamp-on weight will pull the free

end downwards. The result of this, as illustrated by the envelope curves and the critical load are results in table 4.15 is a maximum stress around the middle of the tether.

Introducing wave- and vessel motions induced forces at the top end of the tether, the position of the maximum loaded area will shift. For the upending with the clamp-on weights still attached, envelope curve 4.38 illustrated that the maximum loaded point will be located further down. For the case of the clamp-on weights removed prior to the upending, the maximum loaded point will move upwards. This might be explained by the added inertia in the bottom section of the tether system. This indicated a more mass dominated response behaviour, compared to the upending without weights (more stiffness dominated). This phenomenon are illustrated in figure 4.43.

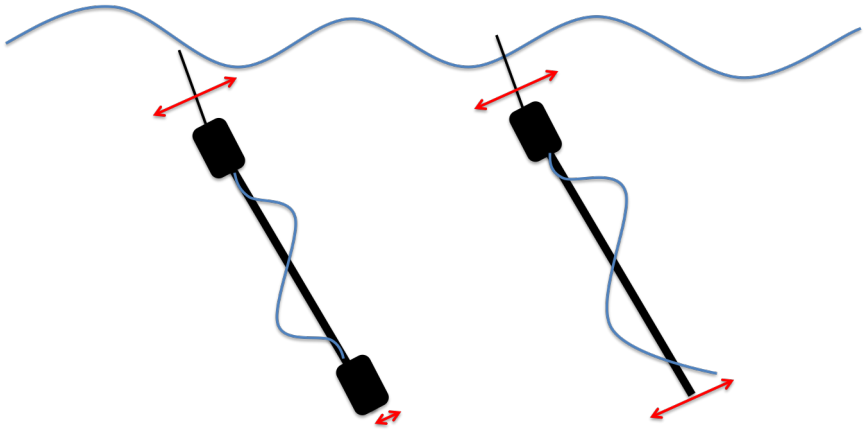

Figure 4.43: Upending in waves, with and without clamp-on weights

The results suggests a free drop upending method with clamp-on weights still attached as the preferred method with respect to time and induced tether loading. The simulation results indicate that this solution is both an efficient and feasible solution. Whether it is practically possible to remove the clamp-on weights after the upending of the tether or not are not assessed in this thesis. A possible alternative method is the towline assisted upending method with a heavy weight element at the end, substituting the mass of the clamp-on weights.

In order to reduce the load effects from the vessel motions, the option of using an active heave compensator on the winch/connection point during the upending might be considered. A further evaluation of this option will not be discussed in this thesis.

It is important to be aware that the tow configuration and the three different upending configurations are all different systems with different properties. The properties of the system will change with the configuration of towlines and weights. As a result of this, the dynamic behaviour characteristics and eigenfrequencies will change.

Chapter 5

Planing of tow and installation operation

Based on the simulation analysis of the different towing- and upending solutions, a brief description of a possible transport and installation operation for the tethers of Heidrun TLP will be presented and discusses.

The intention of this chapter is not a full and detailed operational instruction, but rather a brief recap of the analysis results related to planing of marine operations. This chapter also include reflections of the operational limitations, the feasibility and operability of the operation.

5.1 Operation

Heidrun TLP, located 190 kilometres of the coast of Norway was the first ever concrete tension-leg platform, installed in 1995. As part of a maintenance plan, the 16 steel tethers are scheduled to be replaced within a few years. The transport of the tether are divided into two main phases, towing and installation.

The 263 meter long structures are to be transported individually by a submerged tow method from Gulvica, Narvik to site. The total transport distance is approximately 117 nautical miles, consisting of a 21 nm long in-shore route, followed by a 96 nm long open water off-shore stretch (see figure 2.2a). The planed towing speed for the two route sections are 2 and 4 knots,respectively, corresponding to a planed operation period of 11 and 24 hours.

At site, the tethers are to be installed by upending. A preferred method of choice for the upending operation are not defined prior to the thesis.

The transport and installation operations shall be as safe and efficient as possible, ensuring safety of the crew involved and minimizing the structural loading and environmental impact.

5.2 Tow operation

The preferred method of choice for the towing operation is a near surface/control depth tow. Properties that define this method are good manoeuvrability, reduced loading from oscillating surface forces and excellent adaptive properties.

A base-case tow configuration were established in cooperation with thesis supervisor and analysed thought a series of time domain numerical simulations. The base-case configuration utilize a leading and a tailing platform support vessel and two 22 meter long synthetic nylon towlines in order to tow the structure at a controlled depth of 7 meters. The tether is equipped with a sett of heavy clamp-on weight elements at each end while the tailing vessel provide a relative hold-back tension of 10 tons in order to reduce induced stress by stiffening the system.

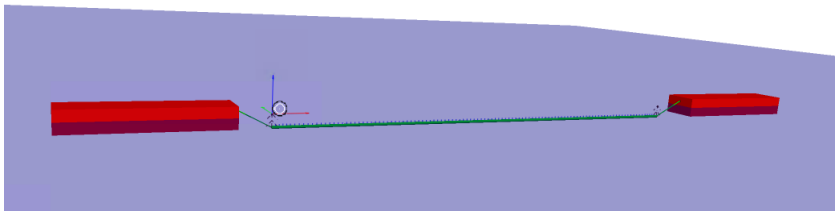

Figure 5.1: Tow method of choice

All simulated cases showed a satisfying clearance between the tether and the vessels throughout the visualized simulation results.

Simulation results indicate that induced tether response are dominated by dynamic loading and that the bending moments are the main contribution to the tether resultant axial stress. Simulation results from where the vessels were kept fixed, showed a significant reduction in induced responce, suggesing that the vessel motion induced loading are of great importance to the total loading.

From the simulation results, both ultimate loading and fatigue damage were assessed (ULS and FLS). Simulation results and post processing suggests that the fatigue damage will be the structural limiting factor with respect to environmental operational limitations.

The simulation results indicate that beam weather are more crucial than head seas, due to the large vessel heave motions.

In attempt of reducing the vessel heave motion loading, simulations were conducted, increasing the fibre line length to 66 meters, keeping the 7 meter tow depth. The result of

these simulations suggests a slight reduction in tether loading. The miner improvement have to be evaluated against other factors, like reduced manoeuvrability and increased towline costs.

5.3 Upending operation

Simulation analysis, including three different upending solutions in calm waters and in wave conditions $H_S = 2.5$m suggests a free drop upending method with clamp-on weights still attached during the upending as the method of choice. The method showed to be the most efficient method while the structure behaved in a stable manner and induced stress values well within the limits.

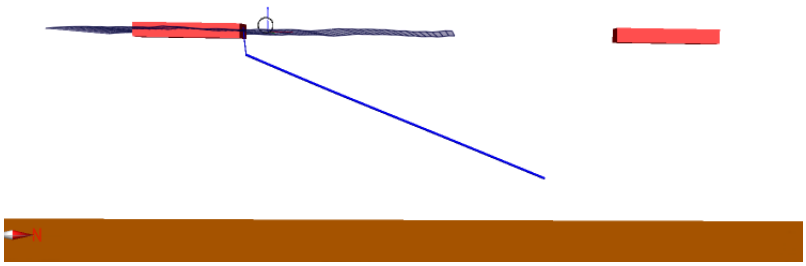

Figure 5.2: Upending method of choice

Dynamic loading due to vessel motions were identified as the main contribution of the maximum induced tether stress. Keeping the clamp-on weights on during the upending helped reducing the operation duration as well as the induced loading in the tether. A possible explanation for the reduced stress using weights is that the added weight introduced added system inertia, reducing the induced motions of the oscillating vessel motions and thus reducing induced stress.

Only head sea were assessed for the upending case, as it is assumed that this is the most favourable condition which the operation will seek upon the execution.

A large uncertainty in the analysis of a upending operation is related to the downward current profile, both with respect to velocity and heading. A uniform head current of 1 m/s in the simulation suggests that the response affect of currents are negligible, indicating that the simulated currents are sufficient.

Bending moments were identified as the strongly dominating stress contribution in the tether, contributing with around 99.9% of the resultant axial stress.

Further assessment have to be addressed regarding the practical feasibility and challenges of removing the clamp-on weights after the upending.

A possible alternative to the free drop method is a towline assisted upending, with clamp-on weights still attached and a feeding rate of 1 m/s. The towline feed rate will for the simulated cases keep the towline partly slack, introducing a geometric stiffness, absorbing a lot of the vessel induced forces from the tailing vessel. These simulations indicate induced stress similar to the base-case free drop case, a slightly longer duration and introduce the ability to regulate the upending speed and otherwise control the tether end. A possible alternative introduced by this method is attaching weights at the bottom end of the towline, replacing the added weight from the clamp-on weights.

Simulation results suggests that both the base-case free drop method and the towline assisted upending (1m/s feed rate) are feasible solutions. Some uncertainty are related to the towline assisted simulation in waves, as unrealistic towline behaviour were identified.

5.4 Operational limitations

As described in earlier in this thesis, the operational limit shall be based on the first of several different possible limiting, mainly related to one of the following issues:

- Weather limitations
- Structural limitations
- Equipment limits
- Limitations for safe working conditions
- Other contractor defined limitations

Through case simulations in different weather conditions, structural limitations are assessed with respect to significant wave height and peak period. The structural evaluation include extreme value loadings (ULS) in tether and towlines, hot-spot stress in welds and fatigue damage in welds.

In addition to the structural limitations form simulation analysis, operational limitations related to tether surface piercing, safe working conditions and repression handling during installation are shortly discussed.

The main results from the operational limitation study are as following:

Table 5.1: Operational limitations

Operational limitations

Restriction	OP_{lim} [H_S]	OP_{wf} [H_S]	α
Tow,Tether ULS	5.5	4.3	0.78
Tether ULS, 90°	2.5	1.8	0.72
Tether FLS*	<2.5	<1.8	0.78
Towline ULS (90°)	2.5	1.8	0.72
Surface piercing	2.6	1.9	0.78
Upending, Tether ULS	2.5	1.9	0.74
Repression handling and safe work	2.5	1.9	0.74

α-factor according to DNV 2011a, weather forecast level B
*Tether fatigue damage exceeds operation design limitation of 10%

Operational limitations are based on the simulated weather conditions and the resultant structural response. For several of the cases, the design stress were not fully utilized, indicating that some of the operational limits might be even higher (e.g. ULS tether during tow = 82% utilization). As the ultimate weather conditions were not addressed in the simulations, due to other limiting factors, the operational limitation are set to the most severe conditions simulated.

Towline limitations are based on the selected towline properties taken from KTL. The results indicate that the towline limitations will be the restricting component with respect to ULS.

As beam weather condition showed to reduce the operation operability, several weather heading conditions should be conducted. As the vessel motion induced loading seems to be the dominating load contribution, it is expected that the beam condition will be the most crucial heading. This is assumed as the simulated condition corresponds to the vessel natural period in heave (figure 4.5). If this is the case, the vessel RAO suggests that a altering direction would significantly reduce the system response.

Fatigue calculations, based on estimated reference period for the offshore tow and a fatigue limitation equal to 10% of fatigue life suggests that the designed operation is not feasible for the wave conditions used in the simulation analysis. This means that that the further simulations have to be conducted in order to establish the operational fatigue limitation, or the fatigue damage during the operation have to be reduced. A weather forecast limit of $OP_{wf} < 1.8$m for the duration of the transport leaves a very limited window of opportunities, indicating that operability have to be improved.

5.5 Operation time schedule

Based on transport and upending time estimates and approximate duration of additional sub-operations by thesis supervisor, an exemplary time table are presented:

Table 5.2: Operation time table

Operation time table					
	Sub operation	T_{POP} $[Hrs]$	T_R $[Hrs]$	OP_{lim} $[H_S, m]$	$OP_{wf}[H_S, m]$
1	Inshore tow	11	16.5	<2.5m	<1.8
2	Off-shore tow	24	36	<2.5m	<1.8
3	Positioning and equipment rig	4	8	2.5	2.5
4	Upending	0.27	1	2.5	2.5
5	Installation	4	8	2.5	2.5
	Total time	43.27	69.5		

The operation is considered compete after the installation, as the tether can be considered to be exposed to normal conditions as it would be under working condition.

The transport duration are calculated based on the route suggestion illustrated in figure 2.2a, and tow speed previously mentioned. The tow contingency, compensating for uncertainty in the time estimates as well as contingency situations are taken as 50% of the planed operation time. This is according to recommendations given by DNV 2011a, assuming the time estimates are well addressed.

The upending duration are taken as four times the planed operation period, thus being on the conservative side.

Remaining contingency are taken as 100% of the planed operation period. This is according to DNV 2011a, stating that the planed reference period should normally be at leased twice the planed operation period.

5.6 Improvement potential

Improving the operability of an operation would mean an increased number of feasible weather windows. For the over all planing of the manufacturing, vessel chartering and other pre-operational processes, a larger flexibility in the execution of the transport operation could mean significant financial savings.

Based on the factors defining the operational limitations, there are four areas that may be addressed in order to improve operability:

- Reduce loading
- Reduce system/structural response
- Reduce reference period
- Improve equipment

As vessel motion induced loading are identified as a crucial contribution of the total tether and towline loading, measurements reducing the vessel motions or reducing the transferred loading to the tether would help increase operability, with respect to bout ULS and FLS. A possible measurement could be changing the tow vessels to vessels with smaller response motions in crucial conditions. This will in general mean larger vessels, which often are more expensive to charter.

Reducing the duration of the offshore transport is also a possible measurement, reducing the total fatigue damage and increasing operability. Increased vessel tow speed from 4 knots would mean new assessment of the operation.

For the upending operation, the option of an active heave compensator (AHP) could be evaluated as an possible measurement of reducing the affect of towline transferred loadings and towline snap loads.

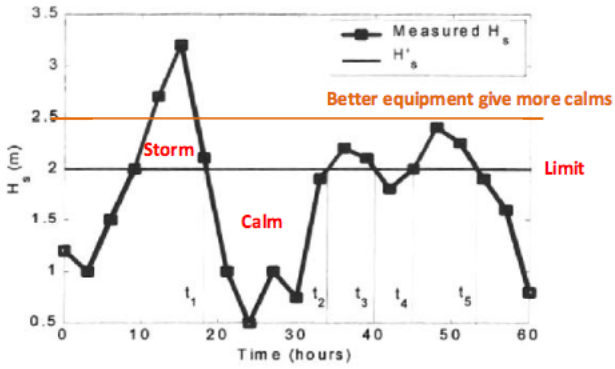

Figure 5.3: Increase operability (Larsen 2015)

Chapter 6

Conclusion

During the work of this master's thesis, the concept a submerged near-surface towing method have been analysed and evaluated for the transportation of a TLP tether for the Heidrun platform. Literature study of the towing method and the hydrodynamic forces involved indicate that the method is a promising solution for the transport of long slender structures. The study also suggests that due to large variation in the system behaviour characteristics, the method have to be evaluated based on case to case studies.

Results from numerical Riflex simulations of a case configuration, it is observed that the tether response will strongly depend on the dynamic loads and that the main stress contribution will be due to bending moments. The results also strongly suggests that the vessel motions are crucial to the response of the system. Beam sea heading are identified as a more severe weather condition compared to a head sea condition. The simulation results and vessel RAOs suggests that this is mainly due to large vessel heave motions.

With respect to ultimate limit state, no critical load area was identified during the simulations. However, hot-spot stress is expected related to the welds between different tether segments.

Based on study of the structural response with respect to both ultimate loading and fatigue damage, the simulation results indicate that fatigue damage will be limiting for the operation. The results suggests that non of the simulated weather conditions are feasible for the tow operation, based on a operation limit of maximum 10% of total fatigue utilization. This corresponds to an operation weather forecast limit of $OP_wf = H_S < 1.8$m. It is recommended that measurements should be taken in order to increase operability.

Following the transportation, an efficient solution of an upending at site of the tether have been suggested, based on numerical simulations and literature study. Case simulation results from four different solutions suggests a free-drop upending solution, with clamp-on weights still attached at the ends. The solution appeared to be the most efficient of the

simulated cases. The tether seemed to behave in a stable manner and with induced stress well within the operational ULS limit for the simulated weather conditions.

A uniform head current of 1 m/s seemed to have minimal affect on the behaviour of the system during the upending. Simulation results suggest that vessel motions and wave loads will be crucial to the duration and structural response during the upending.

Chapter 7

Further Work

The topic considering transportation of slender structures by towing shows to have many interesting challenges to be studied further. As for the case of transportation of tethers for Heidrun TLP, the tow configuration seems to have some room for improvements in order to increase operability.

As the work of this master's thesis is final, no further work or reports by the author regarding the topic are planed. Suggestions for further work may include:

- Verifications of results
- Improve tow operation in order to increase operability
- Further analyse the tow configuration with respect to different weather conditions
- Further analyse the upending operation with respect to system behaviour
- Address other limiting factors
- Analyse alternative/new tow- and upending solutions

Bibliography

Berge, Stig. 2006. *Fatigue Design of Welded Structures*.

Conoco Norway Inc. 1994. *WORLD'S FIRST CONCRETE TLP TAKES SHAPE OFF NORWAY*. Visited on 05/12/2016. http://www.ogj.com/articles/print/volume-92/issue-33/in-this-issue/general-interest/world39s-first-concrete-tlp-takes-shape-off-norway.html.

DNV. 2011a. "DNV-OS-H101 Marine Operations , General", no. October.

— . 2012. *DNV-OS-H102 - Marine Operations, Design and Fabrications*.

— . 2011b. "DNV-RP-C203 - FATIGUE DESIGN OF OFFSHORE STEEL STRUCTURES".

— . 2014a. *DNV RP-H103 Modelling and Analysis of Marine Operations*.

— . 2013. "Offshore Installation Operations". DNV-OS-H20 (November): 37.

— . 2014b. *RP-C205 - Environmental Conditions and Environmental Loads*.

DNVGL. 2015a. *Design of offshore steel structures, general - LRFD method*.

— . 2015b. *DNVGL-OS-E301 Position mooring*.

Faltinsen, O M. 1999. *SEA LOADS ON SHIPS AND OFFSHORE STRUCTURES*.

Greco, Marilena. 2012. *TMR 4215: Sea Loads - Lecture Notes*.

KTL, OFFSHORE. *WIRE ROPE, RIGGING AND MOORING FOR OFFSHORE CONSTRUCTIONS*.

Larsen, Carl M. 2014. "TMR4182 - Marin dynamikk".

Larsen, Kjell. 2015. "TMR4225 Marine Operations - Lecture notes".

MARINTEK. "Riflex manual".

— . "RIFLEX Theory Manual Introduction".

Natskaar, Asle, Torgeir Moan, and Per O. Alvær. 2015. "Uncertainty in forecasted environmental conditions for reliability analyses of marine operations". *Ocean Engineering* 108:636–647. ISSN: 00298018. doi:10.1016/j.oceaneng.2015.08.034. http://dx.doi.org/10.1016/j.oceaneng.2015.08.034.

Nielsen, Finn Gunnar. 2007. “LECTURE NOTES IN MARINE OPERATIONS”.

Norwegian Contractors. 1995. *ACCIDENTAL RELEASE OF TOW BUOYS DURING TOW OF TETHER Q43 ON 3RD MAY 1995*. Tech. rep.

— . 1991. *TETHER TOW AND INSTALLATION PROCEDURE*. Tech. rep.

Nygaard, Eik and. 2004. *Heidrun Metocean Design Basis*. Tech. rep.

oljemuseum, Norsk. 2015. *Heidrun*. Visited on 05/10/2016. `http://www.norskolje.museum.no/heidrun/`.

Pettersen, Bjørnar. 2007. “Kompendium TMR4247 MARIN TEKNIKK 3 HYDRODYNAMIKK”.

— . 2012. “TMR 4182 MARIN DYNAMIKK - Virvelinduserte svigninger”.

Statoil. “Heidrun TLP - Nøkkeltall”.

Appendices

Appendix A

Vessel RAOs

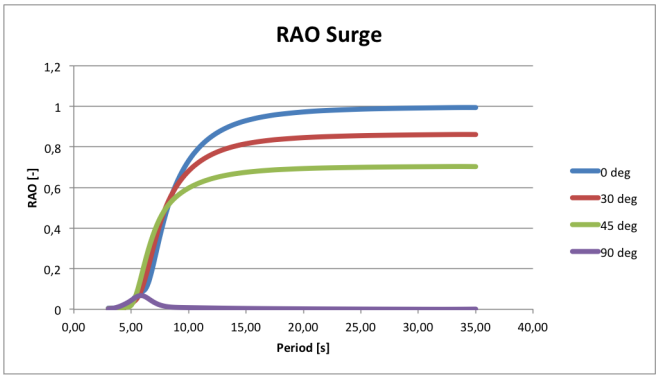

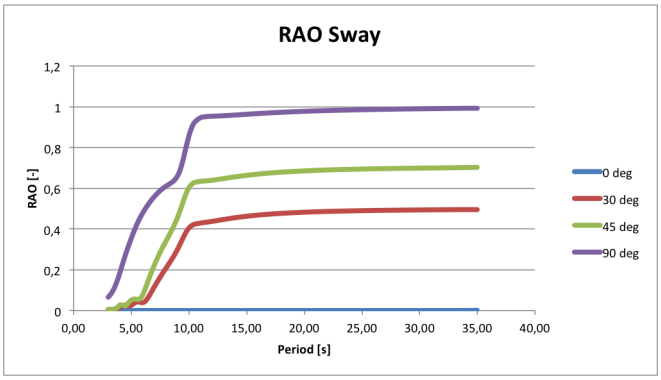

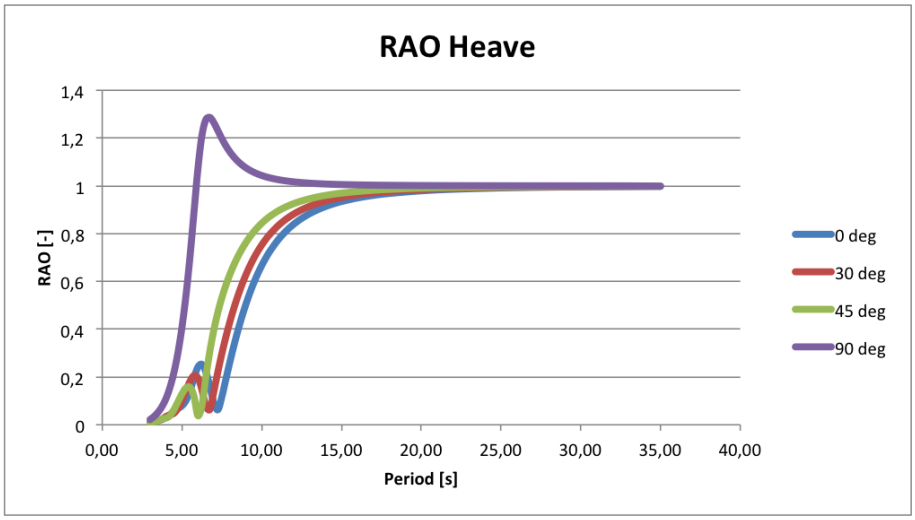
RAO Heave
RAO [-]
1,4
1,2
1
0,8
0,6
0,4
0,2
0
0,00
5,00
10,00
15,00
20,00
25,00
30,00
35,00
40,00
Period [s]
0 deg
30 deg
45 deg
90 deg

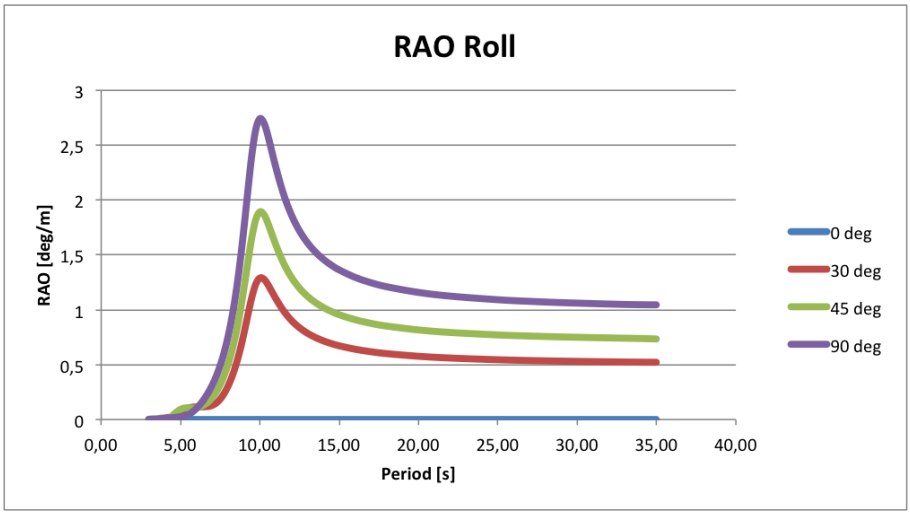
RAO Roll
RAO [deg/m]
3
2,5
2
1,5
1
0,5
0
0,00
5,00
10,00
15,00
20,00
25,00
30,00
35,00
40,00
Period [s]
0 deg
30 deg
45 deg
90 deg

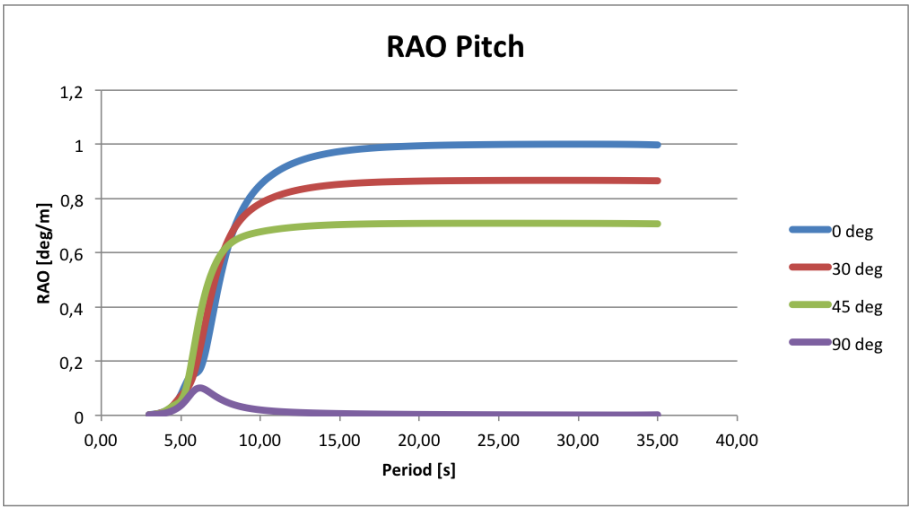
RAO Pitch
RAO [deg/m]
1,2
1
0,8
0,6
0,4
0,2
0
0,00
5,00
10,00
15,00
20,00
25,00
30,00
35,00
40,00
Period [s]
0 deg
30 deg
45 deg
90 deg

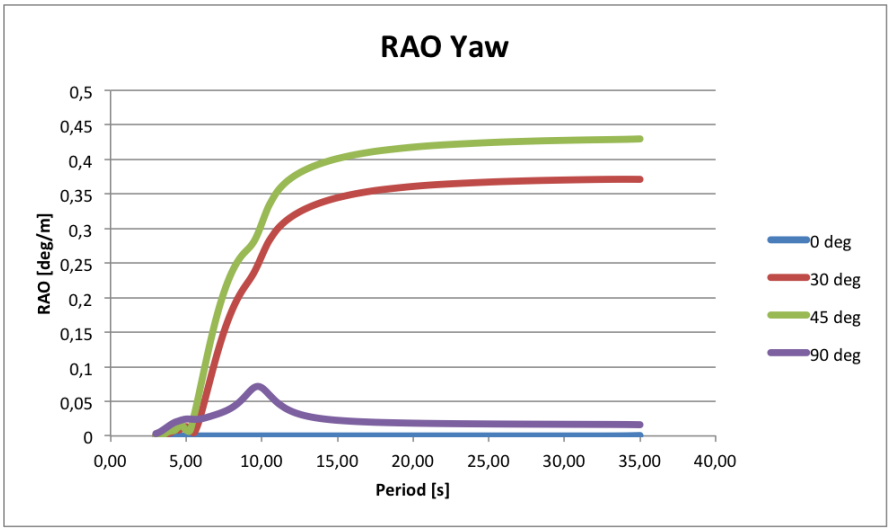
RAO Yaw
RAO [deg/m]
0,5
0,45
0,4
0,35
0,3
0,25
0,2
0,15
0,1
0,05
0
0,00
5,00
10,00
15,00
20,00
25,00
30,00
35,00
40,00
Period [s]
0 deg
30 deg
45 deg
90 deg

Appendix B

Attachment point RAOs

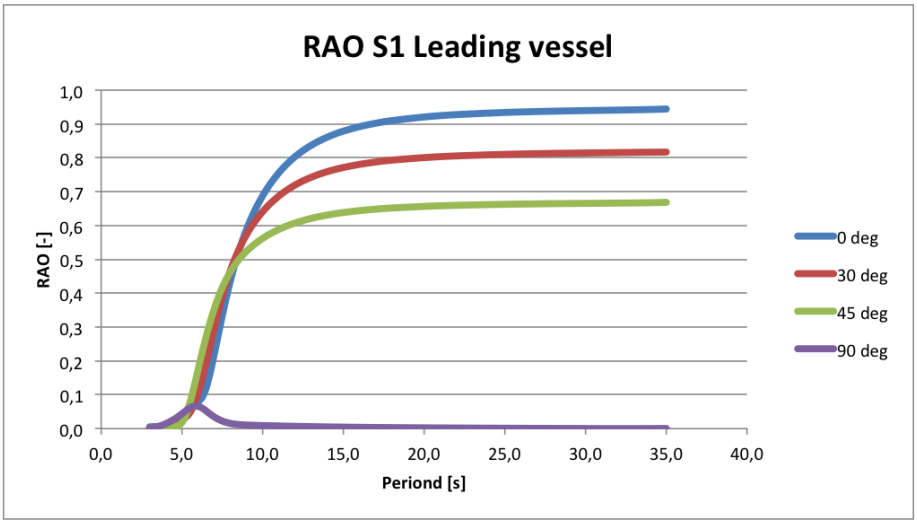

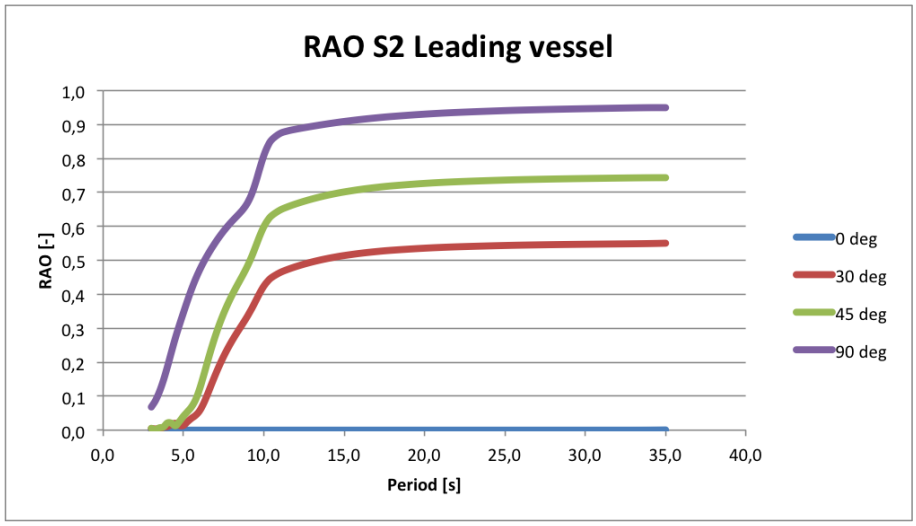
RAO S2 Leading vessel
RAO [-]
1,0
0,9
0,8
0,7
0,6
0,5
0,4
0,3
0,2
0,1
0,0
0,0
5,0
10,0
15,0
20,0
25,0
30,0
35,0
40,0
Period [s]
0 deg
30 deg
45 deg
90 deg

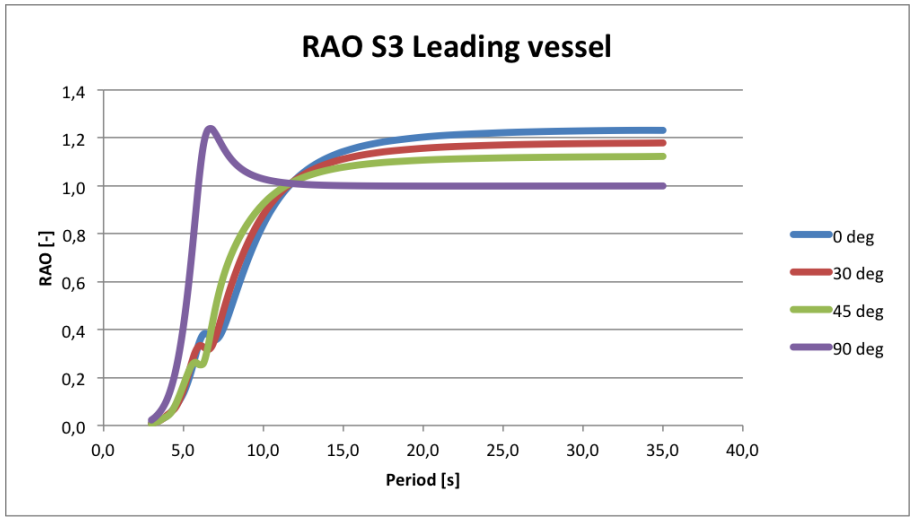
RAO S3 Leading vessel
RAO [-]
1,4
1,2
1,0
0,8
0,6
0,4
0,2
0,0
0,0
5,0
10,0
15,0
20,0
25,0
30,0
35,0
40,0
Period [s]
0 deg
30 deg
45 deg
90 deg

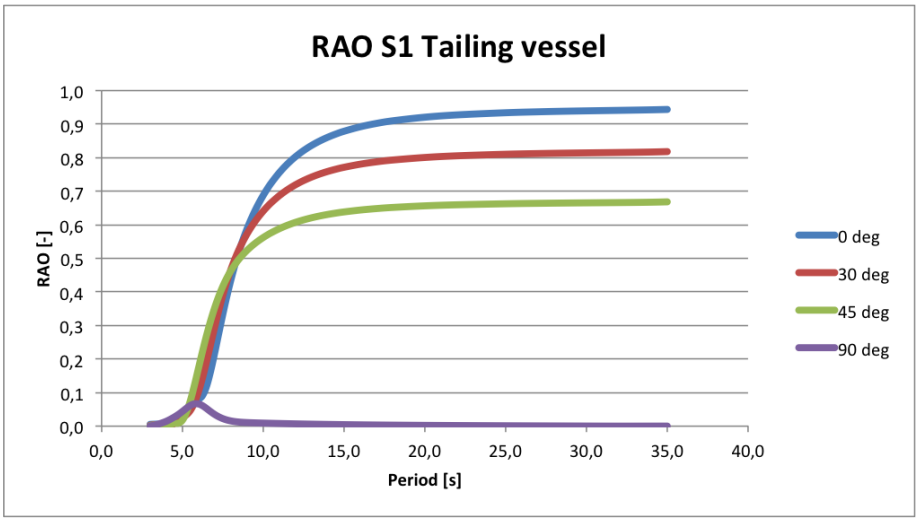
RAO S1 Tailing vessel
RAO [-]
1,0
0,9
0,8
0,7
0,6
0,5
0,4
0,3
0,2
0,1
0,0
0,0
5,0
10,0
15,0
20,0
25,0
30,0
35,0
40,0
Period [s]
0 deg
30 deg
45 deg
90 deg

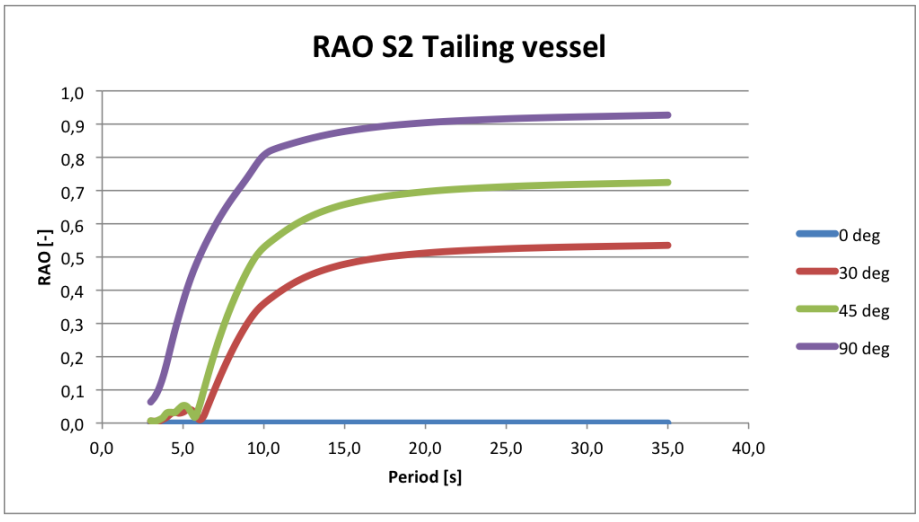
RAO S2 Tailing vessel
RAO [-]
1,0
0,9
0,8
0,7
0,6
0,5
0,4
0,3
0,2
0,1
0,0
0,0
5,0
10,0
15,0
20,0
25,0
30,0
35,0
40,0
Period [s]
0 deg
30 deg
45 deg
90 deg

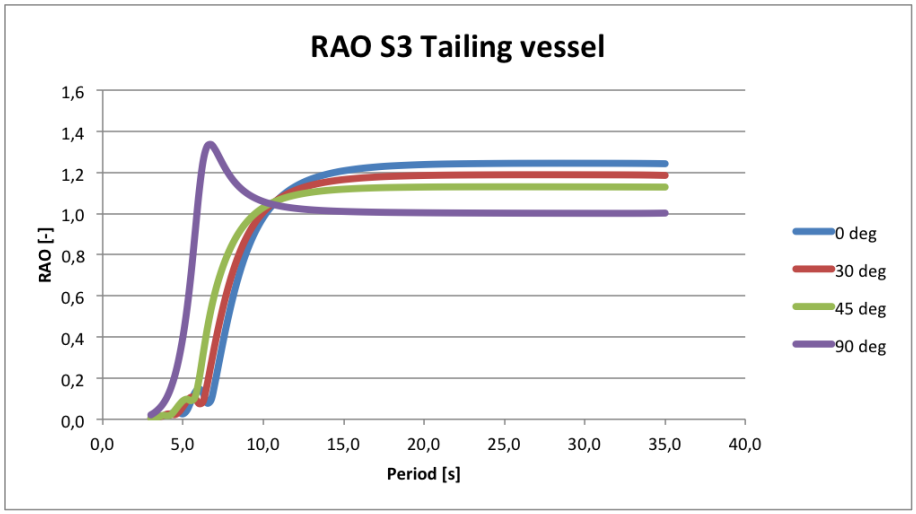
RAO S3 Tailing vessel
RAO [-]
1,6
1,4
1,2
1,0
0,8
0,6
0,4
0,2
0,0
0,0
5,0
10,0
15,0
20,0
25,0
30,0
35,0
40,0
Period [s]
0 deg
30 deg
45 deg
90 deg

Appendix C

Electronic appendices

SIMA/Riflex files attached:

- Heidrun_BaseCase.stask
- Heidrun_BaseCase_noweather.stask
- Heidrun_BaseCase_noline.stask

Rielex '.stask' files containing respectively base-case tow model, towline assisted upending model and free-drop upending model.